Exploring the Effects of Linkage for Ancestry and Temporal Polygenic Adaptation

By

Vincent Scott Buffalo

Dissertation

Submitted in partial satisfaction of the requirements for the degree of

Doctor of Philosophy

in

Population Biology

in the

Office of Graduate Studies

of the

University of California

Davis

Approved:

Graham M. Coop, Chair

Charles H. Langley

Michael Turelli

David J. Begun

Committee in Charge

2019

To my father, Ray Buffalo, who during my childhood worked six days a week, sometimes commuting over 120 miles on weekends to work extra hours, all to pay for my education. I will never forget my father visiting me in San Jose after a long work day in San Francisco just to teach me fractions in café bookstore after I struggled to understand the teacher's explanation. At this time, my love of science grew, in no small part thanks to his dedication, and his occasional gifts like Linus Pauling's General Chemistry *and Richard Feynman's Feynman's* Lost Lecture: The Motion of Planets Around the Sun *for Easter, alongside a few dark chocolate bunnies. I owe you more than you know, Dad.*

Contents

List of Figures

List of Tables

Abstract

Exploring the Effects of Linkage for Ancestry and Temporal Polygenic Adaptation

Since Darwin's characterization, adaptation has often been portrayed as a gradual, plodding process acting over geological timescales to shape organisms' phenotypes to their environment. The masterful theoretical work of early geneticists like R.A. Fisher, Sewall Wright, and J.B.S Haldane developed population genetic models to understand the dynamics of selection, the impact of population structure, and the effects of genetic drift. However, this depiction of adaptation as a slow process has shifted, as numerous researchers have found numerous examples of rapid adaptation in the wild. I have been fascinated by rapid adaptation and models of recent ancestry since starting my PhD, and have developed theory and statistical methods exploring these ideas in my dissertation. Uniting my three chapters is the influence of linkage. Linkage shapes patterns of identity by descent (IBD) sharing between recently related individuals on the X chromosome which I explore in Chapter 1 by developing theoretical expressions for the number and length of IBD segments shared on the X chromosome between recent relatives. Due to the inheritance pattern of the X chromosome and the fact that recombination only occurs along the entire length of the X chromosome in females, IBD segment sharing on the X is rather different than sharing on the autosomes.

In the second chapter of my dissertation, linkage determines the impact heritable fitness variation has in affecting the allele frequency trajectories of neutral sites in the genome. I investigate this in Chapter 2 by developing theoretical expressions for the temporal autocovariance experienced by neutral sites, as they become associated with sites that determine a polygenic trait under selection. I propose that these temporal covariances can be estimated using genome-wide temporal data. In Chapter 3, I develop the statistical methods to accurately estimate temporal covariances, and quantify the impact of linked selection in three experimental evolution populations: two *Drosophila simulans* evolve-and-resequence populations adapting to a lab environment, and one artificial selection

experiment in mice. Overall, we find linked selection has a significant impact on allele frequency changes genome-wide.

Acknowledgments

First and foremost, I am deeply indebted to my advisor Graham Coop for his mentorship and guidance during my PhD. I came into this PhD broadly interested in evolution, statistics, and genetics, with little idea of how to do rigorous science, nor how to become a good biologist and population geneticist. Graham was endlessly patient with me as I explored various sub-disciplines and grew distracted by other projects; ultimately he (correctly) predicted that my interests would solidify around what this dissertation is about. There were times over the course of my PhD program that were extraordinarily difficult on me. As I encountered challenges, Graham was incredibly supportive and understanding. I would always look forward to our scientific discussions during our weekly meetings to rekindle my spirit. Looking back, I learned more about life and myself in this period than at any other point in my life, and I owe Graham an incredible debt for being so patient and supportive. I hope to pay his mentorship efforts forward as my career grows.

I would also like to thank members of the Coop Lab I have had the pleasure of working with and learning from: Simon Aeschbacher, Chenling Antelope, Jeremy Berg, Gideon Bradburd, Yaniv Brandvain, Erin Calfee, Nancy Chen, Doc Edge, Katie Ferris, Emily Josephs, Ivan Juric, Kristin Lee, Matt Osmond, Alisa Sedghifar, Anita To, and Sivan Yair. I owe a debt of gratitude to Jeff Ross-Ibarra for first getting me interested in population genetics through his REHAB journal club, and allowing me to work in his lab before grad school. I am grateful for countless excellent conversations and good advice from members of my qualifying exam and dissertation committees, Chuck Langley, Dave Begun, Jeff Ross-Ibarra, Michael Turelli, Rasmus Nielsen, and Bruce Rannala.

Throughout my PhD, numerous colleagues have collaborated on or provided guidance with particular chapters. I would like to thank our collaborator Steve M. Mount for his ideas and contributions in Chapter 1, as well as Amy Williams, Noah Rosenberg, and two anonymous reviewers for their feedback during the revision process at *Genetics*. I am deeply indebted to Nick Barton for providing extraordinarily helpful feedback for Chapter 2, as well as Enrique Santiago, Aneil Agrawal, Bill Hill, John Kelly, Tyler Kent, Sally

Otto, Jonathan Pritchard, Kevin Thornton, and two anonymous reviewers for feedback on previous versions of the manuscript. Finally, for providing assistance with the datasets we reanalyzed and/or helpful feedback on Chapter 3, I would like to thank Christian Schlötterer, John Kelly, Kimberly Hughes, Frank Chan, Campbell Rolian, Nick Barton, Alan Bergland, and Dmitri Petrov. My research has been supported by an NSF Graduate Research Fellowship (1148897); I would like to thank the NSF for the opportunity to conduct this research.

I owe my family for their patience and encouragement during this process: Mom, Dad, Anne, Lisa, Violet, Lauren, Dalilah, Grammy and Papa, and Grandma and Grandpa Lamb. Lastly, I would like to thank my partner Sarah Friedman for endless support and being a lovely dissertation-bae. I promise you I'll make up for the lost backpacking trips this season.

Chapter 1

A Genealogical Look at Shared Ancestry on the X Chromosome

Close relatives are expected to share large contiguous segments of their genome due to the limited number of crossovers per chromosome each generation (Donnelly 1983; Fisher et al. 1949, 1954). These large identical by descent (IBD) segments shared among close relatives leave a conspicuous footprint in population genomic data, and identifying and understanding this sharing is key to many applications in biology (Thompson 2013). For example, in human genetics, evidence of recent shared ancestry is an integral part of detecting cryptic relatedness in genome-wide association studies (Gusev et al. 2009), discovering mis-specified relationships in pedigrees (Sun et al. 2002), inferring pairwise relationships (Epstein et al. 2000; Glaubitz et al. 2003; Huff et al. 2011), and localizing disease traits in pedigrees (Thomas et al. 2008). In forensics, recent ancestry is crucial for both accounting for population-level relatedness (Balding and Nichols 1994) and in familial DNA database searches (Belin et al. 1997; Sjerps and Kloosterman 1999). Additionally, recent ancestry detection methods have a range of applications in anthropology and ancient DNA to understand the familial relationships among sets of individuals (Baca et al. 2012; Fu et al. 2015; Haak et al. 2008; Keyser-Tracqui et al. 2003). In population genomics, recent ancestry has been used to learn about recent migrations and other demographic events (Palamara et al. 2012; Ralph and Coop 2013). An understanding of recent ancestry also plays a large role in understanding recently admixed populations,

where individuals draw ancestry from multiple distinct populations (Gravel 2012; Liang and Nielsen 2014; Pool and Nielsen 2009). Finally, relative finding through recent genetic ancestry is increasingly a key feature of direct-to-consumer personal genomics products and an important source of information for genealogists (Durand et al. 2014; Royal et al. 2010).

Approaches to infer recent ancestry among humans have often used only the autosomes, as the recombining autosomes offer more opportunity to detect a range of relationships than the Y chromosome, mitochondria, or X chromosome. However, the nature of X chromosome inheritance means that it can clarify details of the relationships among individuals and be informative about sex-specific demography and admixture histories in ways that autosomes cannot (Bryc et al. 2010; Bustamante and Ramachandran 2009; Goldberg and Rosenberg 2015; Pool and Nielsen 2007; Ramachandran et al. 2008, 2004; Rosenberg 2016; Shringarpure et al. 2016).

In this paper, we look at the inheritance of chromosomal segments on the X chromosome among closely related individuals. Our genetic ancestry models are structured around biparental genealogies back in time, an approach used by many previous authors (e.g., Barton and Etheridge 2011; Chang 1999; Donnelly 1983; Rohde et al. 2004). If we ignore pedigree collapse, the genealogy of a present-day individual encodes all biparental relationships back in time; e.g. the two parents, four grandparents, eight great-grandparents, 2^k great^{k-2} grandparents, and in general the 2^k ancestors k generations back; we refer to these individuals as one's *genealogical ancestors*. Note that throughout this paper, k^{th} generation *ancestors* refers to the ancestors within generation k, not the total number of ancestors from generations 1 to k. A genealogical ancestor of a present-day individual is said to also be a *genetic ancestor* if the present-day individual shares genetic material by descent from this ancestor. We refer to these segments of shared genetic material as being identical by descent, and in doing so we ignore the possibility of mutation in the limited number of generations separating our individuals. Throughout this paper, we will ignore the pseudo-autosomal (PAR) region(s) of the X chromosome, which undergoes crossing over with the Y chromosome in males (Koller and Darlington

1934) to ensure proper disjunction in meiosis I (Hassold et al. 1991). We also ignore gene conversion which is known to occur on the X (Rosser et al. 2009).

Here, we are concerned with inheritance through the *X genealogy* embedded inside an individual's genealogy, which includes only the subset of one's genealogical ancestors who could have possibly contributed to one's non-PAR X chromosome. We refer to the individuals in this X genealogy as *X ancestors*. Since males receive an X only from their mothers, a male's father cannot be an X ancestor. Consequently, a male's father and all of his ancestors are excluded from the X genealogy (Figure 1.1). Therefore, females are overrepresented in the X genealogy, and as we go back in one's genealogy, the fraction of individuals who are possible X ancestors shrinks. This property means that genetic relationships differ on the X compared to the autosomes, a fact that changes the calculation of kinship coefficients on the X (Pinto et al. 2011, 2012) and also has interesting implications for kin-selection models involving the X chromosome (Fox et al. 2009; Rice et al. 2008).

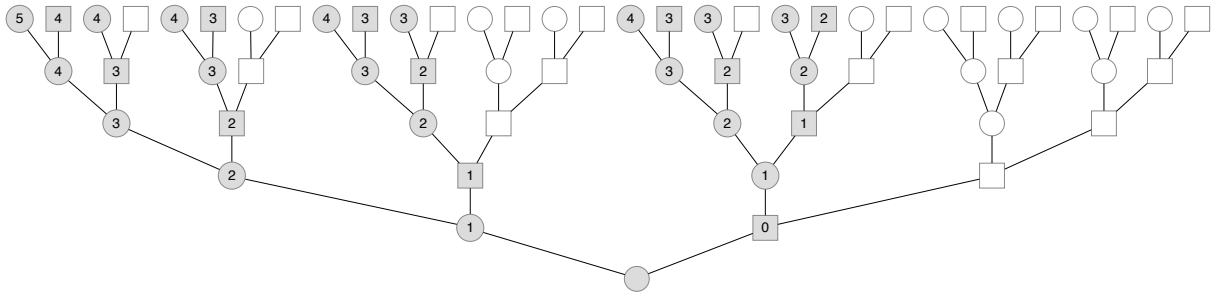

Figure 1.1: A genealogy back five generations with the embedded X genealogy. Males are depicted as squares and females as circles. Individuals in the X genealogy are shaded gray while unshaded individuals are ancestors that are not X ancestors. Each X ancestor is labeled with the number of recombinational meioses to the present-day female.

In Section 1.1 (and in Appendix 1.7) we review models of autosomal identity by descent among relatives, on which we base our models of X genetic ancestry. Then, in Section 1.2 we look at X genealogies, as their properties affect the transmission of X genetic material from X ancestors to a present-day individual. We develop simple approximations to the probability distributions of the number and length of X chromosome segments that will be shared IBD between a present-day female and one of her X ancestors a known number of generations back. These models provide a set of results for the X chromosome equivalent

to those already known for the autosomes (Donnelly 1983; Thomas et al. 1994). Then, in Section 1.3, we look at shared X ancestry—when two present-day cousins share an X ancestor a known number of generations back. We calculate the probabilities that genealogical half- and full-cousins are also connected through their X genealogy, and thus can potentially share genetic material on their X. We then extend our models of IBD segment length and number to segments shared between half- and full-cousins. Finally, in Section 1.4 we show that shared X genetic ancestry contains additional information (compared to genetic autosomal ancestry) for inferring relationships among individuals, and explore the limits of this information.

1.1 Autosomal Ancestry

To facilitate comparison with our X chromosome results, we first briefly review analogous autosomal segment number and segment length distributions (Donnelly 1983; Huff et al. 2011; Thomas et al. 1994). Throughout this paper, we assume that one's genealogical ancestors k generations back are distinct (e.g. there is no inbreeding), i.e. there is no pedigree collapse due to inbreeding (see Appendix 1.10 for a model of how this assumption breaks down with increasing k). Thus, an individual has 2^k *distinct* genealogical ancestors. Assuming no selection and fair meiosis, a present-day individual's autosomal genetic material is spread across these 2^k ancestors with equal probability, having been transmitted to the present-day individual solely through recombination and segregation.

We model the process of crossing over during meiosis as a continuous time Markov process along the chromosome, as in Thomas et al. (1994) and Huff et al. (2011), and described by Donnelly (1983). In doing so we assume no crossover interference, such that in each generation b recombinational breakpoints occur as a Poisson process running with a uniform rate equal to the total length of the genetic map (in Morgans), ν. Within a single chromosome, b breaks create a mosaic of $b + 1$ alternating maternal and paternal segments. This alternation between maternal and paternal haplotypes creates long-run dependency between segments (Liang and Nielsen 2014). We ignore these dependencies in our analytic models by assuming that each chromosomal segment survives segregation

independently with probability $1/2$ per generation. For d independent meioses separating two individuals, we imagine the Poisson recombination process running at rate νd, and for a segment to be shared IBD between the two ancestors it must survive $1/2^d$ segregations. Consequently, the expected number of segments shared IBD between two individuals d meioses apart in a genome with c chromosomes is approximated as (Thomas et al. 1994):

$$\mathbb{E}[N] = \frac{1}{2^d}(\nu d + c) \tag{1.1}$$

Intuitively, we can understand the $1/2^d$ factor as the coefficient of kinship (or path coefficient; Wright 1922, 1934) of two individuals d meioses apart, which gives the probability that two alleles are shared IBD between these two individuals. Then, the expected number of IBD segments $\mathbb{E}[N]$ can be thought of as the average number of alleles shared between two individuals in a genome with $\nu d + c$ loci total. Under this approximation, recombination increases the number of independent loci linearly each generation (by a factor of the total genetic length). A fraction $1/2^d$ of parental alleles at these loci survive the d meioses to be IBD with the present-day individual.

By convention, we count the number of contiguous IBD segments N in the present-day individual, not the number of contiguous segments in the ancestor. For example, an individual will share exactly one block per chromosome with each parent if we count the contiguous segments in the offspring, even though these segments may be spread across the parent's two homologues. This convention, which we use throughout the paper, is identical to counting the number of IBD segments that occur in $d - 1$ meioses rather than d meioses. This convention only impacts models of segments shared IBD between an individual and one of their ancestors; neither the distribution of segment lengths nor the distributions for segment number shared IBD between cousins are affected by this convention.

1.1.1 The distribution of IBD segments between a present-day individual and an ancestor

Given that a present-day individual and an ancestor in the k^{th} generation are separated by k meioses, the number of IBD segments can be modeled with what we call the *Poisson-Binomial* approximation. Over $d = k$ meioses, $B = b \sim \text{Pois}(\nu k)$ recombinational breakpoints fall on c independently assorting chromosomes, creating $b + c$ segments. Ignoring long-range dependencies, we assume all of these $b + c$ segments have an independent chance of surviving the k segregations to the present-day individual, and thus the probability that n segments survive given $b + c$ trials is Binomially distributed with probability $1/2^k$. Marginalizing over the unobserved number of recombinational breakpoints b, and replacing k with $k - 1$ to following the convention described above:

$$\begin{aligned} P(N = n|k) = \sum_{b=0}^{\infty} &\text{Bin}(N = n \mid l = b + c, p = 1/2^{k-1}) \\ &\times \text{Pois}(B = b \mid \lambda = \nu(k-1)) \end{aligned} \tag{1.2}$$

The expected value of the Poisson-Binomial model is given by equation (1.1) with $d = k - 1$ and this model is similar to those of Donnelly (1983) and Thomas et al. (1994). We can further approximate this by assuming that we have a Poisson total number of segments with mean $(c + \nu(k - 1))$ and these segments are shared with probability $1/2^{k-1}$ as in Huff et al. (2011). This gives us a thinned Poisson distribution of shared segments:

$$\begin{aligned} P(N = n|k, \nu, c) &= \text{Pois}(N = n|\lambda = (c + \nu(k-1))/2^{k-1}) \\ &= \frac{((c + \nu(k-1))/2^{k-1})^n e^{-(c+\nu(k-1))/2^{k-1}}}{n!} \end{aligned} \tag{1.3}$$

This thinned Poisson model also has an expectation given by equation (1.1) but compared to the Poisson-Binomial model has a larger variance than the true process. This overdispersion occurs because modeling the number of segments created after b breakpoints involves incorporating the initial number of chromosomes into the Poisson rate. However, this initial number of chromosomes is actually fixed, which the Poisson-Binomial

model captures but the Poisson thinning model does not (i.e. one generation back such that $k = 1$, the thinning model treats the number of segments shared IBD with one's parents is $N \sim \text{Pois}(c)$ rather than c). See Appendix 1.6 for a further comparison of these two models. A more formal description of this approximation as a continuous-time Markov process is given in Thomas et al. (1994). In Appendix 1.7, we describe similar results for the number of autosomal segments shared between cousins and the length distributions of autosomal segments.

We will use similar models as these in modeling the length and number of X chromosome segments shared been relatives. However, the nature of X genealogies (which we cover in the next section) requires we adjust these models. Specifically, while one always has k recombinational meioses between an autosomal ancestor in the k^{th} generation, the number of recombinational meioses varies across the lineages to an X ancestor with the number of females in a lineage, since X homologous recombination only occurs in females (Figure 1.1). This varying number of recombinational meioses across lineages leads to a varying-rate Poisson recombination process, with the rate depending on the specific lineage to the X ancestor. After we take a closer look at X genealogies in the next section, we adapt the models above to handle the varying-rate Poisson process needed to model IBD segments in X genealogies.

1.2 X Ancestry

1.2.1 Number of Genealogical X Ancestors

While a present-day individual can potentially inherit autosomal segments from any of its 2^k genealogical ancestors k generations back, only a fraction of these individuals can possibly share segments on the X chromosome. In contrast to biparental genealogies, males have only one genealogical X ancestor—their mothers—if we ignore the PAR. This constraint (which we refer to throughout as the *no two adjacent males condition*) shapes both the number of X ancestors and the number of females along an X lineage. For example, consider a present-day female's X ancestors one generation back: both her father and mother contribute X chromosome material. Two generations back, she has three X

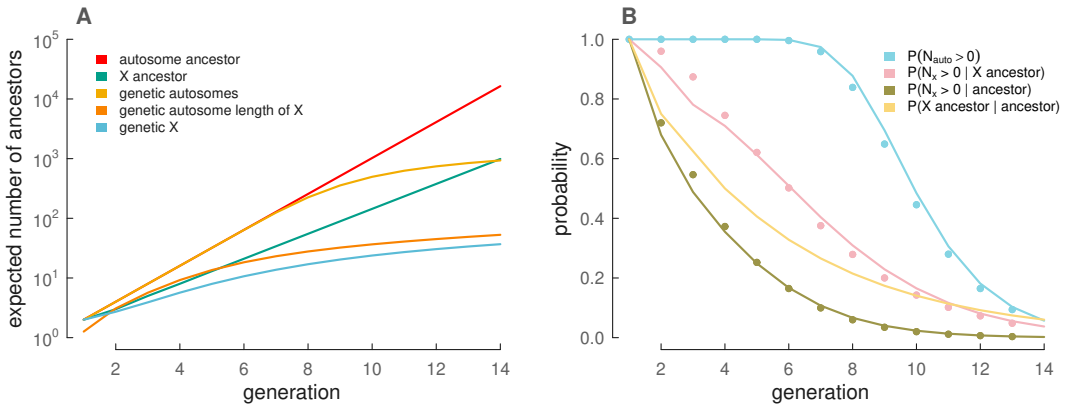

Figure 1.2: How the number of genetic and genealogical ancestors and probabilities of sharing genetic material vary back through the generations for different cases. A: Each line represents a present-day female's expected number of ancestors (y-axis) in the k^{th} generation (x-axis; where $k = 1$ is parental generation), for a variety of cases. The present day female's number of genealogical ancestors in the k^{th} generation is in red, and the expected number of these ancestors that contribute any autosome genetic material is in yellow. Likewise, the present-day female's number genealogical X ancestors is in green, and the expected number of these ancestors that contribute any X genetic material is in blue. For comparison, the number of genetic ancestors of an autosome of length equal to the X is included (orange). B: The probability of genealogical and genetic ancestry (y-axis) from an arbitrary ancestor in the k^{th} generation (x-axis). $P(\text{N}_{\text{auto}} > 0)$ is derived from equation (1.3), $P(\text{N}_{\text{X}} > 0 \mid \text{X ancestor})$ from equation (1.8), $P(\text{N}_{\text{X}} > 0 \mid \text{ancestor})$ from equations (1.8) and (1.4), and $P(\text{X ancestor} \mid \text{ancestor})$ from equation (1.4). Points show simulated results.

genealogical ancestors: her father only inherits an X from her paternal grandmother, while her mother can inherit X material from either of parents. Continuing this process, this individual has five X ancestors three generations back and eight ancestors four generations back (Figure 1.1).

In general, a present-day female's X genealogical ancestors is growing as a Fibonacci series (Basin 1963; Laughlin 1920), such that k generations back she has $\mathcal{F}_{k+2}$ X genealogical ancestors, where $\mathcal{F}_k$ is the k^{th} Fibonacci number (where k is 0-indexed and the series begins $F_0 = 0, F_1 = 1, \ldots$; Online Encyclopedia of Integer Sequences reference A000045; Sloane, 2010). We can demonstrate that one's number of X genealogical ancestors (n_k) grows as a Fibonacci series by encoding the X inheritance rules for the number of males and females (m_k and f_k, respectively) in the k^{th} generation as a set of recurrence relations:

Rearranging these recurrence equations gives us $n_k = n_{k-1} + n_{k-2}$, which is the Fibonacci recurrence. Starting with a female in the $k = 0$ generation, we have initial values

$$f_k = n_{k-1} \qquad \text{every individual receives an X chromosome from his/her mother}$$
$$m_k = f_{k-1} \qquad \text{every female receives an X chromosome from her father}$$
$$n_k = f_k + m_k$$

$n_0 = 1$ and $n_1 = 2$, which gives us the Fibonacci numbers offset by two, $\mathcal{F}_{k+2}$. For a present-day male, his number of X ancestors is $\mathcal{F}_{k+1}$, i.e. offset by one to count the number of X ancestors his mother has. To simplify our expressions, we will assume throughout the paper that all-present day individuals are female since a simple offset can be made to handle males.

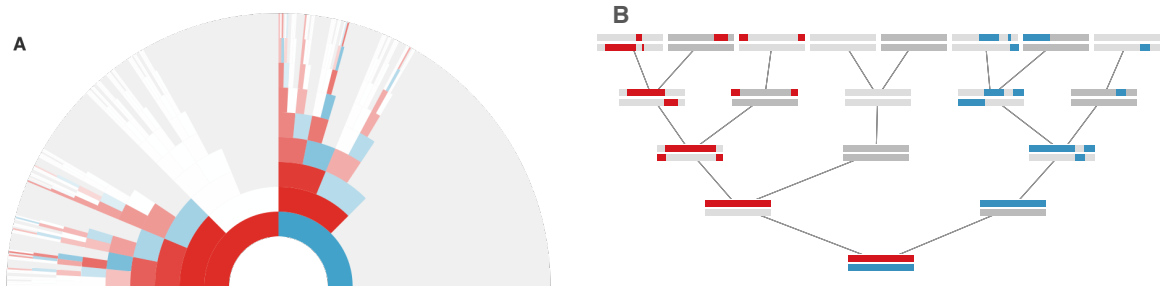

Figure 1.3: Graphical representations of an example X chromosome genealogy. A: Simulated X genealogy of a present-day female, back nine generations. Each arc is an ancestor, with female ancestors colored red, and male ancestors colored blue. The transparency of each arc reflects the genetic contribution of this ancestor to the present-day female. White arcs correspond X genealogical ancestors that share no genetic material with the present-day female, and gray arcs are genealogical ancestors that are not X ancestors. B: The X segments of the simulation in (A), back five generations. The maternal X lineage's segments are colored red, and the paternal X segments are colored blue. A male ancestor's sex chromosomes are colored dark gray (and include the Y) and a female ancestor's sex chromosomes are colored light gray.

In Figure 1.2A we show the increase in the number of X genealogical and genetic ancestors (green and light blue) and compare these to the growth of all of one's genealogical ancestors and autosomal genetic ancestors. The closed-form solution for the k^{th} Fibonacci number is given by Binet's formula ($\mathcal{F}_n = ((1+\sqrt{5})^n - (1-\sqrt{5})^n)/(2^n\sqrt{5})$), which shows that the Fibonacci sequence grows at an exponential rate slower than 2^k.

Consequently, the fraction of ancestors who can contribute to the X chromosome declines with k. Given that a female has $\mathcal{F}_{k+2}$ X ancestors and 2^k genealogical distinct ancestors, her proportion of X ancestors is:

$$P(\text{X ancestor} \mid \text{ancestor}) = \frac{\mathcal{F}_{k+2}}{2^k} \tag{1.4}$$

This fraction can also be interpreted as the probability that a randomly chosen genealogical ancestor k generations ago is also an X genealogical ancestor. We show this probability as a function of generations into the past in Figure 1.2B (yellow line).

From our recurrence equations we can see that a present-day female's $\mathcal{F}_{k+2}$ ancestors in the k^{th} generation are composed of $\mathcal{F}_{k+1}$ females and $\mathcal{F}_k$ males. Likewise for a present-day male, his $\mathcal{F}_{k+1}$ ancestors in the k^{th} generation are composed of $\mathcal{F}_k$ females and $\mathcal{F}_{k-1}$ males. We will use these results when calculating the probability of a shared X ancestor.

1.2.2 Ancestry Simulations

In the next sections, we use stochastic simulations to verify the analytic approximations we derive; here we briefly describe the simulation methods. We have written a C and Python X genealogy simulation procedure (source code available in File S1 and at `https://github.com/vsbuffalo/x-ancestry/`). We simulate a female's X chromosome genetic ancestry back through her X genealogy. Figure 1.3 visualizes the X genetic ancestors of one simulated example X genealogy back nine generations to illustrate this process. Each simulation begins with two present-day female X chromosomes, one of which is passed to her mother and one to her father. Segments transmitted to a male ancestor are simply passed directly back to his mother (without recombination). For segments passed to a female ancestor, we place a Poisson number of recombination breakpoints (with mean ν) on the X chromosome and the segment is broken where it overlaps these recombination events. The first segment along the chromosome is randomly drawn to have been inherited from either her mother/father, and we alternate this choice for subsequent segments. This procedure repeats until the target generation back k is reached. The segments in the k-generation ancestors are then summarized as either counts (number of IBD segments per individual) or lengths. These simulations are necessarily approximate as they ignore crossover interference. However, unlike our analytic approximations, our simulation procedure maintains long-run dependencies created during recombination, allowing us to see the extent to which assuming independent segment survival adversely

impacts our analytic results.

1.2.3 The number of recombinational meioses along an unknown X lineage

If we pick an ancestor at random k generations ago, the probability that they are an X genealogical ancestor is given by equation (1.4). We can now extend this logic and ask: having randomly sampled an X genealogical ancestor, how many recombinational meioses (i.e. females) lie in the lineage between a present day individual and this ancestor? Since IBD segment number and length distributions are parameterized by a rate proportional to the number of recombination events, this quantity is essential to our further derivations. Specifically, if there's uncertainty about the particular lineage between a present-day female and one of her X ancestors k generations back (such that all of the $\mathcal{F}_{k+2}$ lineages to an X ancestor are equally probable), the number of females (thus, recombinational meioses) that occur is a random variable R. By the no two adjacent males condition, the possible number of females R is constrained; R has a lower bound of $\lfloor k/2 \rfloor$, which corresponds to male-female alternation each generation to an ancestor in the k^{th} generation. Similarly, the upper bound of R is k, since it is possible every individual along one X lineage is a female. Noting that an X genealogy extending back k generations enumerates every possible way to arrange r females such that none of the $k - r$ males are adjacent, we find that the number of ways of arranging r such females this way is

$$\binom{r+1}{k-r}. \tag{1.5}$$

For some readers, it may be useful to visualize the relationship between the numbers of recombinational meioses across the generations using Pascal's triangle (Figure 1.4). The sequence of recombinational meioses is related to a known integer sequence; see Online Encyclopedia of Integer Sequences reference A030528 (Sloane 2010) for a description of this sequence and its other applications.

If we pick an X genealogical ancestor at random k generations ago the probability

that there are r female meioses along the lineage leading to this ancestor is

$$P_R(R = r|k) = \frac{\binom{r+1}{k-r}}{\mathcal{F}_{k+2}}. \tag{1.6}$$

In Appendix 1.8, we derive a generating function for the number of recombinational meioses. We can use this generating function to obtain properties of this distribution such as the expected number of recombinational meioses. We can show that the expected number of recombinational meioses converges rapidly to $\mathbb{E}[R] \approx (\varphi/\sqrt{5})\ k$ with increasing k, where φ is the Golden Ratio, $\frac{1+\sqrt{5}}{2}$.

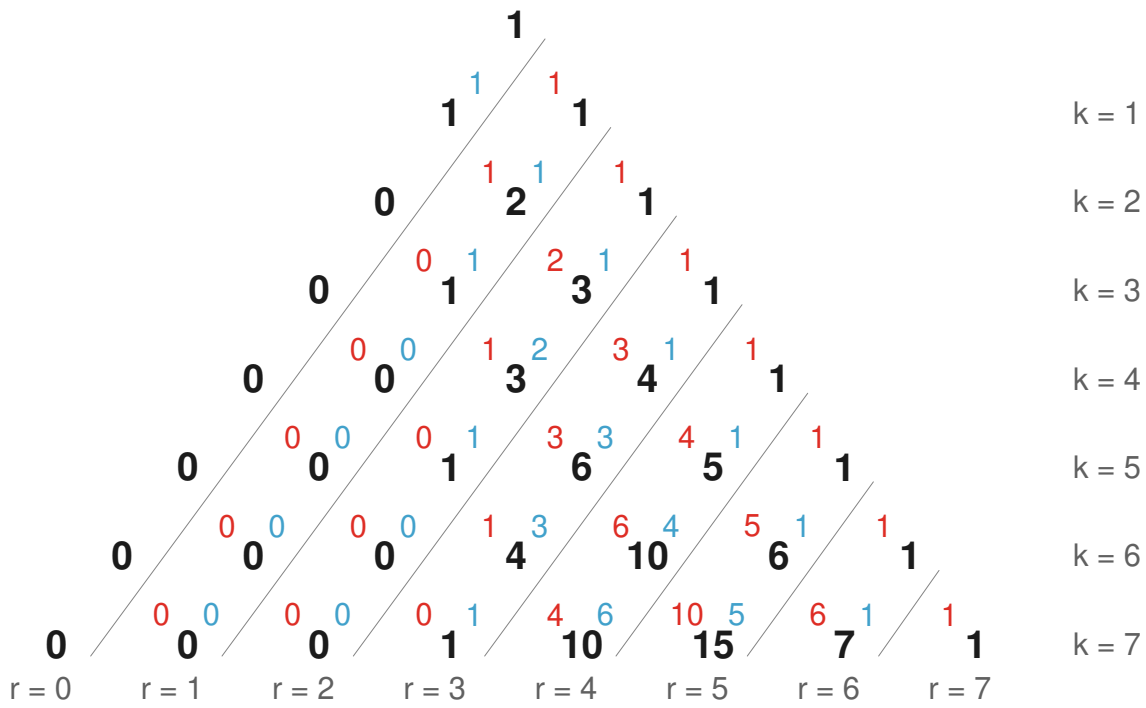

Figure 1.4: The number of individuals (black numbers) with r recombinational meioses (each diagonal, labeled at base of triangle) for a generation k (each row). This encodes the number of recombinational meioses as the binomial coefficient $\binom{r+1}{k-r}$. Each value is further decomposed into the number of recombinational meioses from the female (red value, upper left) and male (blue value, upper right) lineages. Each black value is calculated by adding the black number to the left in the row above (the number of recombinational meioses from the maternal side) and the black number two rows directly above (the number of recombinational meioses from the paternal side). The sum of each row (fixed k) is a Fibonacci number and the values in the diagonal corresponding to a fixed value of r are binomial coefficients. Reading from the top left side to bottom right corner, Pascal's triangle is contained in the red, blue, and black numbers.

1.2.4 The Distribution of Number of Segments Shared with an X Ancestor

Using the distribution of recombinational meioses derived in the last section, we now derive a distribution for the number of IBD segments shared between a present-day individual and an X ancestor in the k^{th} generation. For clarity, we first derive the number of IBD segments counted in the *parents* (i.e. not following the convention described in Section 1.1), but we can adjust this simply by replacing k with $k-1$.

First, we calculate the probability of a present-day individual sharing $N = n$ IBD segments with an X genealogical ancestor k generations in the past, where it is *known* that there are $R = r$ females (and thus recombinational meioses) along the lineage to this ancestor. This probability uses the Poisson-Binomial model described in Section 1.1.1:

$$P(N = n|r, k, \nu) = \sum_{b=0}^{\infty} \text{Bin}(N = n \mid l = b + 1, p = 1/2^r) \times \text{Pois}(B = b \mid \lambda = \nu r) \tag{1.7}$$

Note that once we have conditioned on the number of recombinational meioses r, the lineages to an X ancestor are interchangeable; the specific X lineage affects recombination (and thus the IBD number and length distributions) only through the number of recombinational meioses along the lineage.

If we consider an X genealogical ancestor k generations back, this individual could be any of the present-day female's $\mathcal{F}_{k+2}$ X ancestors. Since the particular lineage to this ancestor is unknown, we marginalize over all possible numbers of recombinational meioses that could occur:

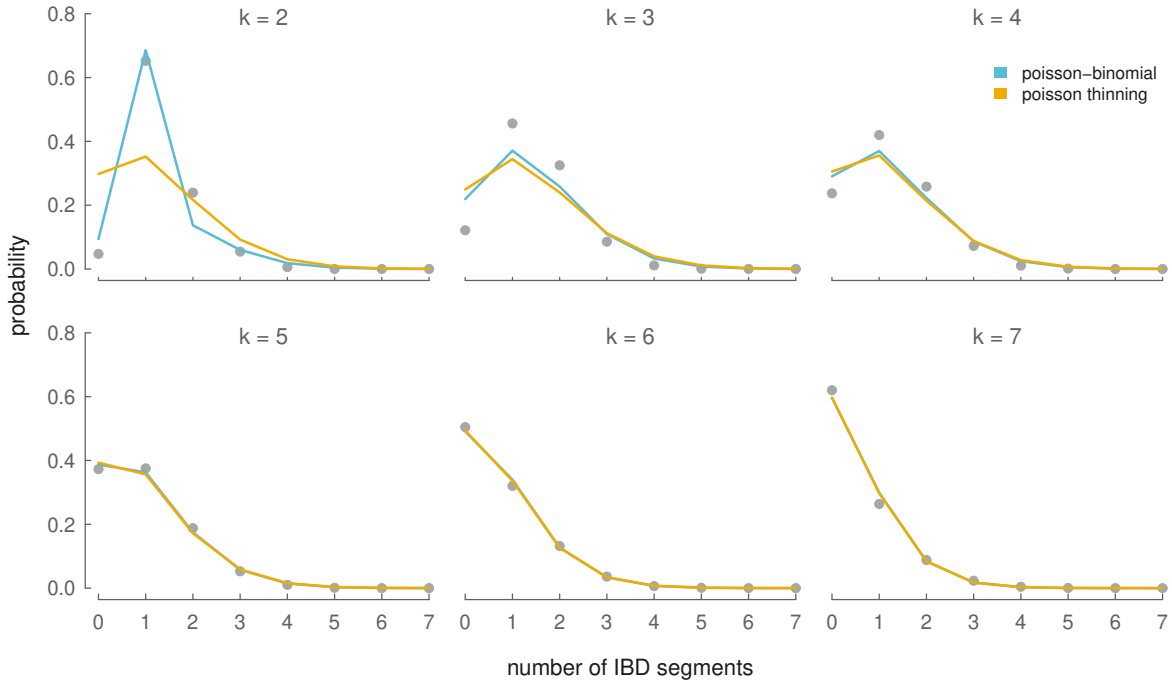

Figure 1.5: The Poisson thinning (yellow lines) and Poisson-Binomial (blue lines) analytic distributions of IBD segment number between an X ancestor in the k^{th} generation (each panel) and a present-day female. Simulation results averaged over 5,000 simulations are the gray points.

$$
\begin{aligned}
& P(N = n | k, \nu) \\
= & \sum_{r=\lfloor k/2 \rfloor}^{k} \sum_{b=0}^{\infty} \quad \mathrm{Bin}(N = n | l = b+1, p = 1/2^r) \\
& \qquad \times \mathrm{Pois}(B = b \mid \lambda = \nu r) \, \frac{\binom{r+1}{k-r}}{\mathcal{F}_{k+2}} \\
= & \sum_{r=\lfloor k/2 \rfloor}^{k} \sum_{b=0}^{\infty} \quad \binom{b+1}{n} 1/2^{rn} (1 - 1/2^r)^{b-n+1} \\
& \qquad \times \frac{(\nu r)^b e^{-\nu r}}{b!} \, \frac{\binom{r+1}{k-r}}{\mathcal{F}_{k+2}}
\end{aligned}
$$

For the distribution of number of IBD segments counted in the offspring, we substitute $k-1$ for k

$$P(N = n \mid k, \nu) = \sum_{r=\lfloor (k-1)/2 \rfloor}^{k-1} \sum_{b=0}^{\infty} \text{Bin}(n \mid l = b+1, p = 1/2^r) \times \text{Pois}(B = b \mid \lambda = \nu r) \times \frac{\binom{r+1}{k-r-1}}{\mathcal{F}_{k+1}}. \quad (1.8)$$

In this formulation, if $k = 1$, $r = 0$. In this case, the lack of recombinational meioses implies $b = 0$, such that a present-day female shares $n = 1$ X chromosomes with each of her two parents in the $k = 1$ generation with certainty. These segment number distributions are visualized in Figure 1.5 (light blue lines) alongside simulated results (gray points).

We can use our equation (1.8) to obtain $P(N > 0)$, the probability that a genealogical X ancestor k generations ago is a *genetic* ancestor. This probability over $k \in \{1, 2, \ldots, 14\}$ generations is shown in Figure 1.2B. For comparison, Figure 1.2B also includes the probability of a genealogical ancestor in the k^{th} generation being an autosomal genetic ancestor and the probability of being a genetic X ancestor unconditional on being an X genealogical ancestor.

We have also assessed the Poisson thinning approach to modeling X IBD segment number. As with the Poisson-Binomial model, we marginalize over R:

$$P(N = n \mid k, \nu) = \sum_{r=r_M}^{k-1} \text{Pois}(B = b \mid \lambda = (1 + \nu r)/2^r) \times \frac{\binom{r+1}{k-r-1}}{\mathcal{F}_{k+1}} \quad (1.9)$$

where $r_M = \lfloor (k-1)/2 \rfloor$.

In Figure 1.5 we have compared the Poisson-Binomial and Poisson-thinning approximations for the number of IBD segments (counted in the offspring) shared between an X-ancestor in the k^{th} generation and a present-day female. Overall, the analytic approximations are close to the simulation results, with the Poisson-Binomial model a closer approximation for small k and both models' accuracy improving quickly with increasing k. For a single chromosome (like the X), the Poisson-thinning model offers a noticeable

worse fit than it does for the autosomes due to overdispersion discussed in Section 1.1.1 (see Appendix 1.6 for details). Throughout the paper, we use the more accurate Poisson-Binomial model rather than this Poisson thinning model. If only X ancestry more than 3 generations back is of interest, the Poisson thinning approach may be used without much loss of accuracy.

1.2.5 The Distribution of IBD Segment Lengths with an X Ancestor

The distribution of IBD segment lengths between a present-day female and an unknown X genealogical ancestor in the k^{th} generation is similar to the autosomal length distribution described in Appendix 1.7 (equation 1.29). However, with uncertainty about the particular lineage to the X ancestor, the number of recombinational meioses can vary between $\lfloor k/2 \rfloor \leq r \leq k$; we marginalize over the unknown number of recombinational meioses using the distribution equation (1.6). Our length density function is:

$$p(U = u|k) = \sum_{r=\lfloor k/2 \rfloor}^{k} re^{-ru} \frac{\binom{r+1}{k-r}}{\mathcal{F}_{k+2}} \tag{1.10}$$

In Figure 1.6, we compare our analytic length density to an empirical density of X segment lengths calculated from 5,000 simulations. As with our IBD segment number distributions, our analytic model is close to the simulated data's empirical density, and converges rapidly with increasing k.

Note that both the IBD segment length and number distributions marginalize over an unobserved number of recombinational meioses (R) that occur along the lineage between individuals. As the IBD segments shared between two individuals is a function of the number breakpoints B, and thus recombinational meioses, the length and number distributions $P(N = n)$ and $p(U = u)$ (which separately marginalize over both R and B) are not independent of one another.

1.3 Shared X Ancestry

Because only a fraction of one's genealogical ancestors are X ancestors (and this fraction rapidly decreases with k; see equation (1.4)), two individuals sharing X segments IBD from

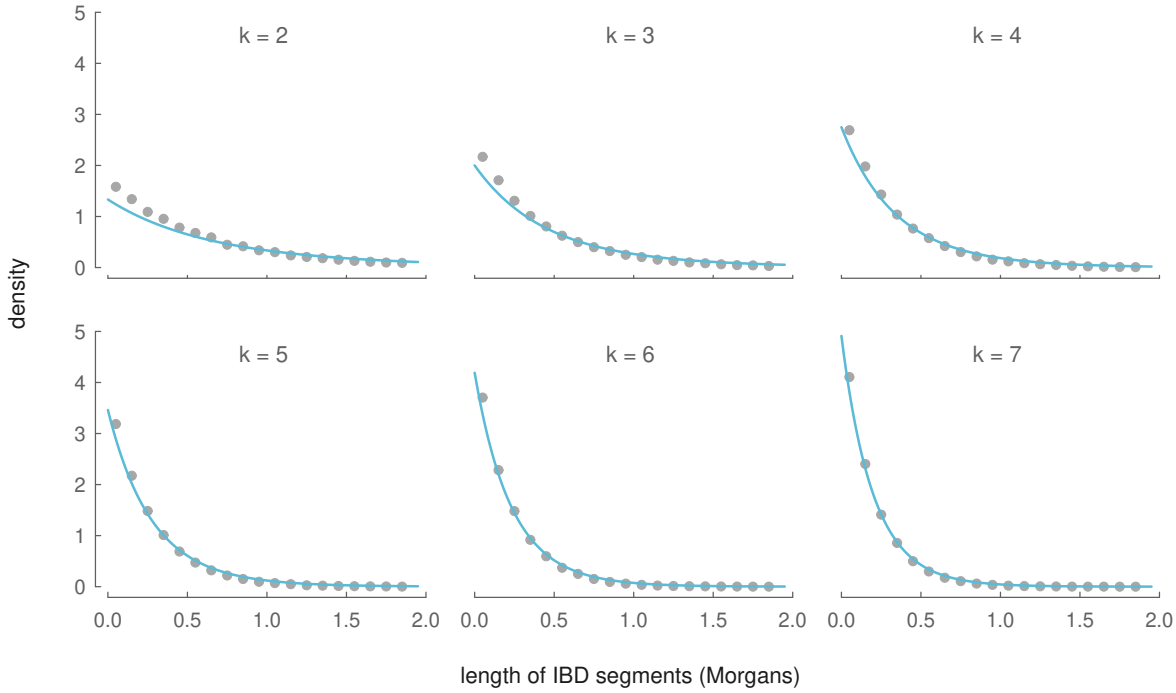

Figure 1.6: The analytic distributions of IBD segment length between an ancestor in the k^{th} generation (for $k \in \{2, \ldots, 7\}$) and a present-day female (blue lines), and the binned average over 5,000 simulations (gray points).

a recent ancestor considerably narrows the possible ancestors they could share. In this section, we describe the probability that a genealogical ancestor is an X ancestor, and the distributions for IBD segment number and length across full- and half-cousin relationships. For simplicity we concentrate on the case where the cousins share a genealogical ancestor k generations ago in both of their pedigrees, i.e. the individuals are $k-1$ degree cousins. The formulae could be generalized to ancestors of unequal generational-depths (e.g. second cousins once removed) but we do not pursue this here.

1.3.1 Probability of a Shared X Ancestor

Two individuals share their first common genealogical ancestor in the k^{th} generation if one of an individual's 2^k ancestors is also one of the other individual's ancestors k generations back. Given this shared ancestor, we can calculate the probability that this single ancestor is also an X genealogical ancestor. Since this shared ancestor must be of the same sex in each of the two present-day individuals' genealogies, we condition on the ancestor's

sex (with probability 1/2 each) and then calculate the probability that this individual is also an X ancestor (with the same sex). Let us define $N_{\female}$ and $N_{\male}$ as the number of genealogical female and male ancestors, and $N_{\female}^X$ and $N_{\male}^X$ as the number of X female and male ancestors of a present-day individual in the k^{th} generation. Then:

$$\begin{aligned} &P(\text{shared X ancestor} \mid \text{shared ancestor } k \text{ generations}) \\ &\quad = \frac{N_{\female}}{2^k}\left(\frac{N_{\female}^X}{N_{\female}}\right)^2 + \frac{N_{\male}}{2^k}\left(\frac{N_{\male}^X}{N_{\male}}\right)^2 \\ &\quad = \frac{1}{2}\left(\frac{\mathcal{F}_{k+1}}{2^{k-1}}\right)^2 + \frac{1}{2}\left(\frac{\mathcal{F}_k}{2^{k-1}}\right)^2 \end{aligned} \tag{1.11}$$

Thus, the probability that a shared genealogical ancestor is also a shared X ancestor is decreasing at an exponential rate. By the 8^{th} generation, a shared genealogical ancestor has less than a five percent chance of being a shared X ancestor of both present-day individuals.

1.3.2 The Sex of Shared Ancestor

Unlike genealogical ancestors—which are equally composed of males and females—recent X genealogical ancestors are predominantly female. Since a present-day female has $\mathcal{F}_{k+1}$ female ancestors and $\mathcal{F}_k$ male ancestors k generations ago, the ratio of female to male X genealogical ancestors converges to the Golden Ratio $\varphi = \frac{1+\sqrt{5}}{2}$ (Simson 1753).

$$\lim_{k\to\infty} \frac{\mathcal{F}_{k+1}}{\mathcal{F}_k} = \varphi \tag{1.12}$$

In modeling the IBD segment number and length distributions between present day individuals, the sex of the shared ancestor k generations ago affects the genetic ancestry process in two ways. First, a female shared ancestor allows the two present-day individuals to share segments on either of her two X chromosomes while descendents of a male shared ancestor share IBD segments only through his single X chromosome. Second, the no two adjacent males condition implies a male shared X genealogical ancestor constrains the X genealogy such that the present-day X descendents are related through his two daughters. Given that the ratio of female to male X ancestors is skewed, our later distributions require

an expression for the probability that a shared X ancestor in the k^{th} generation is female, which we work through in this section.

As in equation (1.11), an ancestor shared in the k^{th} generation of two present-day individuals' genealogies must have the same sex in each genealogy. Assuming both present-day cousins are females, in each genealogy there are $\mathcal{F}_k$ possible male ancestors and $\mathcal{F}_{k+1}$ female ancestors that could be shared. Across each present-day females' genealogies there are $(\mathcal{F}_k)^2$ possible male ancestor combinations and $(\mathcal{F}_{k+1})^2$ possible female ancestor combinations. Thus, if we let ♀_X and ♂_X denote that the sex of the shared is female and male respectively, the probability of a female shared ancestor is:

$$P(\text{♀}_X) = \frac{(\mathcal{F}_{k+1})^2}{(\mathcal{F}_k)^2 + (\mathcal{F}_{k+1})^2} \tag{1.13}$$

The probability that the shared ancestor is male is simply $1 - P(\text{♀}_X)$. One curiosity is that as $k \to \infty$, $P(\text{♀}_X) \to \frac{\varphi}{\sqrt{5}} = \frac{5+\sqrt{5}}{10} \approx 0.7236$, where φ is the Golden Ratio.

1.3.3 Partnered Shared Ancestors

Thus far, we have only looked at two present-day individuals sharing a single X ancestor k generations back. In monogamous populations, most shared ancestry is likely to descend from *two* ancestors; we call such relationships *partnered* shared ancestors. In this section, we look at full-cousins descending from two shared genealogical ancestors that may also be X ancestors. Two full-cousins could either (1) both descend from two X ancestors such that they are X full-cousins, (2) share only one X ancestor, such that they are X half-cousins, or (3) share no X ancestry. We calculate the probabilities associated with each of these events here.

Two individuals are full-cousins if the great^{k-2} grandfather and the great^{k-2} grandmother in one individual's genealogy are in the other individual's genealogy. For these two full-cousins to be X full-cousins, this couple must also be a couple in both individuals' X genealogies. In every X genealogy, the number of couples in generation k is the number of females in generation $k-1$, as every female has two X ancestors in the prior generation (while males only have one). Thus, the probability two female $k-1$ degree full-cousins are also X full-cousins is:

$$P(\text{X full-cousins} \mid \text{full-cousins}) = \left(\frac{\mathcal{F}_k}{2^{k-1}}\right)^2 \tag{1.14}$$

Now, we consider the event that two genealogical full-cousins are X half-cousins. Being X half-cousins implies that the partnered couple these full-cousins descend from includes a single ancestor that is in the X genealogies of both full-cousins. This single X ancestor must be a female, as a male X ancestor's female partner must also be an X ancestor (since mothers must pass an X). For a female to be an X ancestor but not her partner, one or both of her offspring must be male. Either of these events occurs with probability:

$$P(\text{X half-cousins} \mid \text{full-cousins}) = \frac{\mathcal{F}_{k-1}^2 + 2\mathcal{F}_{k-1}\mathcal{F}_k}{2^{2(k-1)}} \tag{1.15}$$

1.3.4 The Distribution of Recombinational Meioses between Two X Half-Cousins

To find distributions for the number and lengths of IBD segments shared between two half-cousins on the X chromosome, we first need to find the distribution for the number of females between two half-cousins with a shared ancestor in the k^{th} generation. We refer to the individuals connecting the two cousins as a *genealogical chain*. As we'll see in the next section, the number of IBD X segments shared between half-cousins depends on the sex of the shared ancestor; thus, we also derive distributions in this section for the number of recombinational meioses along a genealogical chain, conditioning on the sex of the shared ancestor. As earlier, our models assume two present-day female cousins but are easily extended to male cousins.

First, there are $2k-1$ ancestral individuals separating two present-day female $(k-1)^{\text{th}}$ degree cousins. These X ancestors in the genealogical chain connecting the two present-day female cousins follow the no two adjacent male condition; thus the distribution of females follows the approach used in equation (1.6) with k replaced with $2k-1$:

$$P_H(R = r|k) = \frac{\binom{r+1}{2k-r-1}}{\mathcal{F}_{2k+1}} \tag{1.16}$$

where the H (for half-cousin) subscript differentiates this equation from equation (1.6),

k is the generation of the shared ancestor. Similarly to equation (1.6), r is bounded such that $r_{H,M} \leq r \leq 2k-1$, where $r_{H,M} = \lfloor (2k-1)/2 \rfloor$.

Now, we derive the probability of $R = r$ females conditional on the shared ancestor being female, ♀_X. This conditional distribution differs from equation (1.16) since it eliminates all genealogical chains with a male shared ancestor. We find the distribution of recombinational meioses conditional on a female shared ancestor by placing the other $R' = r'$ females (the prime denotes we do not count the shared female ancestor here) along the two lineages of $k-1$ individuals from the shared female ancestor down to the present-day female cousins. These $R' = r'$ females can be placed in both lineages by positioning s females in the first lineage and $r'-s$ females in the second lineage, where s follows the constraint $\lfloor (k-1)/2 \rfloor \leq s \leq k-1$. Our equation (1.6) models the probability of an X genealogical chain having r females in k generations; here, we use this distribution to find the probabilities of s females in $k-1$ generations in one lineage and $r'-s$ females in $k-1$ generations in the other lineage. As the number of females in each lineage is independent, we take the product of these probabilities and sum over all possible s; this is the discrete convolution of the number of females in two lineages $k-1$ generations long. Finally, we account for the shared female ancestor, by the transform $R = R' + 1 = r$:

$$P_H(R = r | \text{♀}_X, k) = \sum_{s=\lfloor (k-1)/2 \rfloor}^{k-1} \frac{\binom{s+1}{k-s-1}\binom{r-s}{k+s-r}}{(\mathcal{F}_{k+1})^2} \tag{1.17}$$

In general, this convolution approach allows us to find the distribution of females in a genealogical chain under various constraints, and can easily be extended to the case of a shared male X ancestor (with necessarily two daughters).

Finally, note that we have modeled the number of *females* in a genealogical chain of $2k-1$ individuals. Thus far in our models, the number of females has equaled the number of recombinational meioses. However, when considering the number of recombinational meioses between half-cousins, *two* recombinational meioses occur if the shared ancestor is a female (as she produced two independent gametes she transmits to her two offspring).

Thus, for a single shared X ancestor, the number of recombinational meioses ρ is

$$\rho = \begin{cases} r+1 & \text{if } ♀_X \\ r & \text{if } ♂_X \end{cases} \tag{1.18}$$

which we use when parameterizing the rate of recombination in our IBD segment number distributions. Furthermore, since a shared female ancestor has two X haplotypes that present-day cousins could share segments IBD through, the binomial probability $1/2^{\rho}$ is doubled. Further constraints are needed to handle full-cousins; we will discuss these below.

1.3.5 Half-Cousins

In this section we calculate the distribution of IBD X segments shared between two present-day female X half-cousins with a shared ancestor in the k^{th} generation. We imagine we do not know any details about the lineages to this shared ancestor nor the sex of the shared ancestor, so we marginalize over both. Thus, the probability of two $(k-1)^{\text{th}}$ degree X half-cousins sharing $N = n$ segments is:

$$\begin{aligned} P(N=n|k) = \sum_{r=r_{H,M}}^{2k-1} & P_H(R=r|k) \\ & \times [P(N=n|♀_X, R=r)P(♀_X|R=r) + \\ & \times\ P(N=n|♂_X, R=r)P(♂_X|R=r)] \end{aligned} \tag{1.19}$$

As discussed in the previous section, the total number of recombinational meioses along the genealogical chain between half-cousins depends on the unobserved sex of the shared ancestor (i.e. equation (1.18)). Likewise, the binomial probability also depends on the shared ancestor's sex. Accounting for these adjustments, the probabilities $P(N =$

$n|\text{♀}_X, R = r)$ and $P(N = n|\text{♂}_X, R = r)$ are:

$$P(N = n|\text{♀}_X, R = r) = \sum_{b=0}^{\infty} \text{Pois}(B = b|\lambda = (r+1)\nu) \times \text{Bin}(N = n|l = b+1, p = 1/2^r) \tag{1.20a}$$

$$P(N = n|\text{♂}_X, R = r) = \sum_{b=0}^{\infty} \text{Pois}(B = b|\lambda = r\nu) \times \text{Bin}(N = n|l = b+1, p = 1/2^r) \tag{1.20b}$$

Since the sex of the shared ancestor depends on the number of females in the genealogical chain between the two cousins (e.g. if $r = 2k-1$, the shared ancestor is a female with certainty), we require an expression for the probability of the shared ancestor being male or female given $R = r$. Using Bayes' theorem, we can invert the conditional probability $P(R = r|\text{♀}_X)$ to find that the probability that a shared X ancestor is female conditioned on R females in the genealogical chain is

$$P_H(\text{♀}_X|R = r, k) = \frac{\mathcal{F}_{2k-1}}{\binom{r+1}{2k-r-1}\left((\mathcal{F}_{k+1})^2 + (\mathcal{F}_k)^2\right)} \times \sum_{s=\lfloor (k-1)/2 \rfloor}^{k-1} \binom{s+1}{k-s+1}\binom{r-s}{k+s-r} \tag{1.21}$$

and $P(\text{♂}_X|R = r)$ can be found as the complement of this probability.

Inserting equations (1.20a), (1.20b), and (1.21) into (1.19) gives us an expression for the distribution of IBD segment numbers between two half-cousins with a shared ancestor k generations ago. Figure 1.7 compares the analytic model in equation (1.19) with the IBD segments shared between half-cousins over 5,000 simulated pairs of X genealogies.

The density function for IBD segment lengths between X cousins (either half- or full-cousins; length distributions are only affected by the number of recombinations in the genealogical chain) is equation (1.10) but marginalized over the number of recombinational meioses between two cousins (equation (1.16)) rather than the number of recombinational meioses between a present-day individual and a shared ancestor. Simulations show the length density closely matches simulation results (see Figure 1.11 in the appendix).

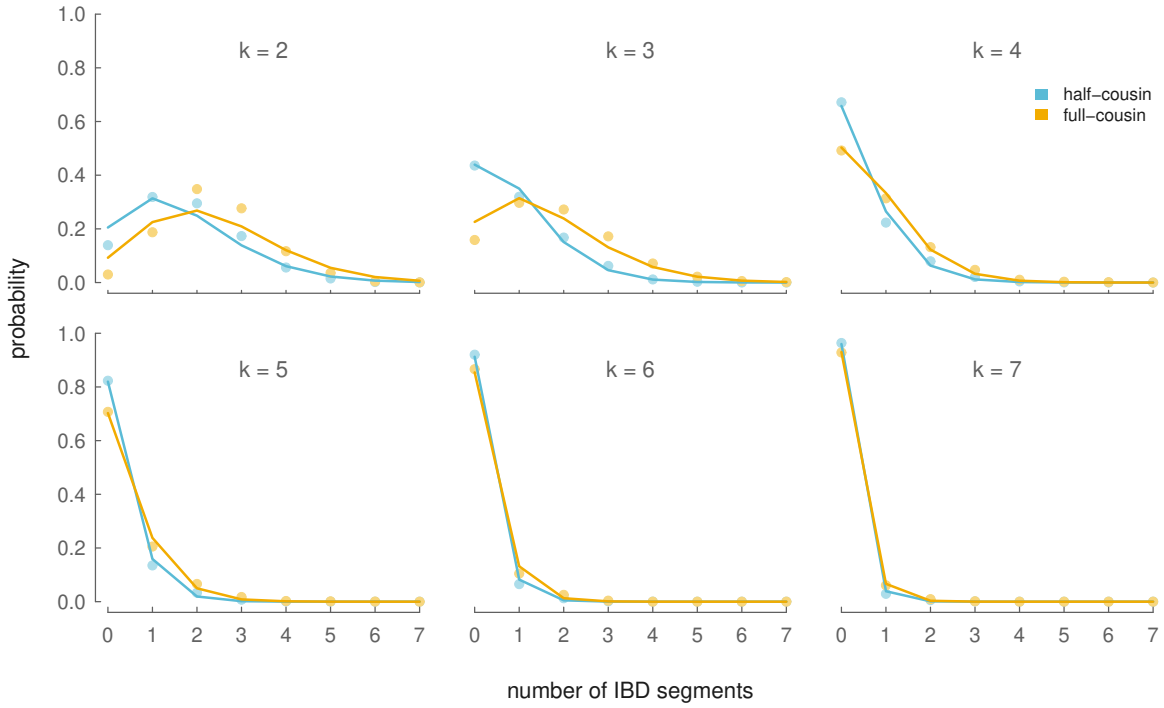

Figure 1.7: Distributions of X IBD segment number for X half- (blue) and X full-cousins (yellow). Lines show the analytic approximations (equations (1.19) and (1.23)) and blue and yellow points show the probabilities for X half- and X full-cousins averaged over 5,000 simulations.

1.3.6 Full-Cousins

Full-cousin relationships allow descendents to share IBD autosomal segments from either their shared maternal ancestor, shared paternal ancestral, or both. In contrast, since males only pass an X chromosome to daughters, only full-sibling relationships in which both offspring are female (due to the no to adjacent males condition) are capable of leaving X genealogical descendents. We derive a distribution for the number of IBD segments shared between $(k-1)^{\text{th}}$ degree full X cousins by conditioning on this familial relationship and marginalizing over the unobserved number of females from the two full-sibling daughters to the present-day female full-cousins.

First, we find the number of females (including the two full-sibling daughters in the $(k-1)^{\text{th}}$ generation) in the genealogical chain between the two X full-cousins (omitting the shared male and female ancestors, which we account for separately). Like equation (1.17), this is a discrete convolution:

$$P_F(R=r,k) = \sum_{s=\lfloor (k-2)/2 \rfloor}^{k-2} \frac{\binom{s+1}{k-s-2}\binom{r-s-1}{k-r+s}}{(\mathcal{F}_k)^2} \tag{1.22}$$

where the F subscript indicates this equation is for full-cousins. This probability is valid for $r_{F,M} + 2 \leq r \leq 2k-2$ and is 0 elsewhere, where $r_{F,M} = 2\lfloor (k-2)/2 \rfloor + 2$. For $N = n$ segments to be shared between two X full-cousins, z segments can be shared via the maternal shared X ancestor (where $0 \leq z \leq n$) and $n - z$ segments can be shared through the paternal shared X ancestor. We marginalize over all possible values of z, giving us another discrete convolution:

$$\begin{aligned} P(N=n|R=r) = \sum_{r=r_{F,M}}^{2k-2} \sum_{z=0}^{n} & P(N=z|\text{♀}_X) \\ & \times P(N=n-z|\text{♂}_X) P_F(R=r) \end{aligned} \tag{1.23}$$

where

$$\begin{aligned} P(N=n|\text{♀}_X, R=r) = \sum_{b=0}^{\infty} & \text{Bin}(N=n|l=b+1, p=1/2^{r+1}) \\ & \times \text{Pois}(B=b|\lambda=\nu(r+2)) \end{aligned} \tag{1.24}$$

$$\begin{aligned} P(N=n|\text{♂}_X, R=r) = \sum_{b=0}^{\infty} & \text{Bin}(N=n|l=b+1, p=1/2^{r}) \\ & \times \text{Pois}(B=b|\lambda=\nu r) \end{aligned} \tag{1.25}$$

are the probabilities of sharing n segments through the shared female and male X ancestors respectively. For the female shared ancestor, we account for two additional recombinational meioses (one for each of the two gametes she passes to her two daughters), and the fact she can share segments through either of her X chromosomes (hence, why the binomial probability is $1/2^{r+1}$). We compare our analytic X full-cousin IBD segment number results to 5,000 genealogical simulations in Figure 1.7.

1.4 Inference

With our IBD X segment distributions, we now turn to how these can be used to infer details about recent X ancestry. In practice, inferring the number of generations back to a

common ancestor (k) is best accomplished through the signature of recent ancestry from the 22 autosomes, rather than through the short X chromosome. A number of methods are available for the task of estimating k through autosomal IBD segments (Durand et al. 2014; Henn et al. 2012; Huff et al. 2011). Therefore, we concentrate on questions about the extra information that the X provides conditional on k being known with certainty.

Here, we focus on two separate questions: (1) what is the probability of being an X genealogical ancestor given that no IBD segments are observed, and (2) can we infer details about the X genealogical chain between two half-cousins? These questions address how informative the number of segments shared between cousins is about the precise relationship of cousins. We assume that segments of X chromosome IBD come only from the k^{th} generation, and not from deeper relationships or from false positives. In practice, inference from the X IBD segments would have to incorporate both of these complications, and as such our results represent best case scenarios.

It's possible that k generations back, an individual is a genealogical X ancestor but shares no X genetic material with a present-day descendent. To what extent is the lack of sharing on the X chromosome with an ancestor informative about our relationship to them? Similarly, how does the lack of sharing of the X chromosome between $(k-1)$th cousins change our views as to their relationship? To get at these issues, we can use our analytic approximations to calculate the probability that one is an X ancestor given that no segments are observed, $P(\text{X ancestor} \mid N = 0)$:

$$P(\text{X ancestor} \mid N = 0) = \frac{P(\text{X ancestor} P(N = 0 \mid \text{X ancestor})}{P(N = 0 \mid \text{X ancestor}) P(\text{X ancestor}) + P(\text{not X ancestor})} \quad (1.26)$$

Here, $P(N = 0 \mid \text{X ancestor})$ is given by equation (1.8) and $P(\text{X ancestor})$ is given by equation (1.4). This function is shown in Figure 1.8 (yellow lines). We can derive an analogous expression for the probability of two female half-cousins sharing an X ancestor but not having any X segments IBD by replacing $P(\text{X ancestor} \mid N = 0)$ with equation (1.19), and replacing $P(\text{X ancestor})$ with $P(\text{shared X ancestor})$ which is given by equation

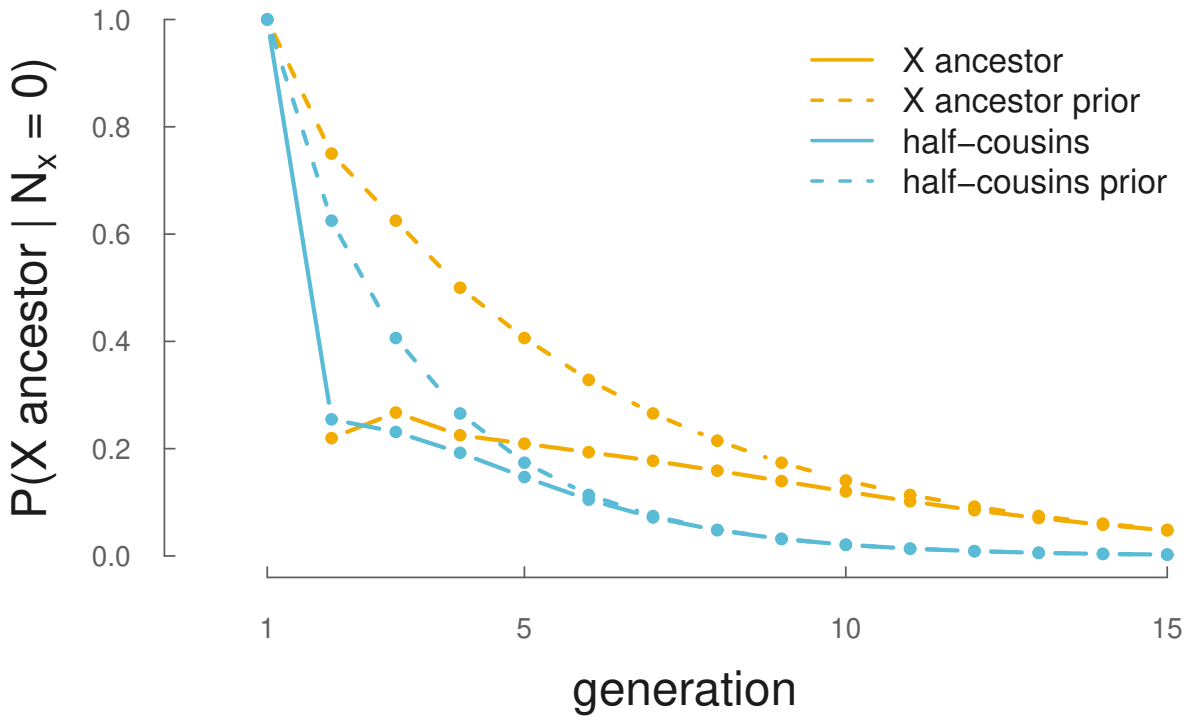

Figure 1.8: The probability of X ancestry given no shared X genetic material. Yellow solid line: the probability an individual in the k^{th} generation (x-axis) is an X ancestor to a present-day female, given they share no X genetic material with her. Blue solid line: the probability that two half-cousins share an X ancestor in the k^{th} generation, given they share no X genetic material between them. Dashed lines indicate the prior probabilities.

(1.11), and plotted in Figure 1.8 (blue lines). We also plot the prior distributions to show the answer if no information about the X chromosome was observed. In both cases, observing zero shared segments on the X chromosome makes it more likely that a shared ancestor was not a shared X ancestor. This additional information is strongest—as compared to the prior—for close relationships ($k < 5$), where segments on the X are likely to be shared if the ancestor was an X genealogical ancestor.

Additionally, X IBD segments carry information about genealogical details that are not possible considering autosome IBD segments alone. While IBD autosome segments leave a signature of recent ancestry between two individuals, the uniformity of recombinational meioses across every lineage to the shared ancestor leaves no signal of *which* genealogical chain connects two present-day cousins. In contrast, since the number of females varies along X lineages and effects the number of recombination events, the number and length

of X segments carries information about which genealogical chain connects two cousins. Information about the genealogical chain between cousins is summarized by the number of female ancestors between two cousins, R, and constrains the possible X genealogical chains between these two cousins by varying amounts dependent on R and k.

Our approach to inference is through the posterior distribution of R given an observed number of IBD segments N and conditioning on k. We calculate this posterior conditional on the cousins sharing an X ancestor; we do this to separate it from the question of whether a pair share an X ancestor (as derived in equation (1.26)). Our posterior probability is given by Bayes' theorem

$$P(R|N=n,k) = \frac{P(N=n|R)P(R)}{P(N=n)} \tag{1.27}$$

where the prior $P(R)$ is readily calculable through equation (1.16) and $P(N=n)$ given by equation (1.19). The data likelihood $P(N=n|R)$ is given by equation (1.7).

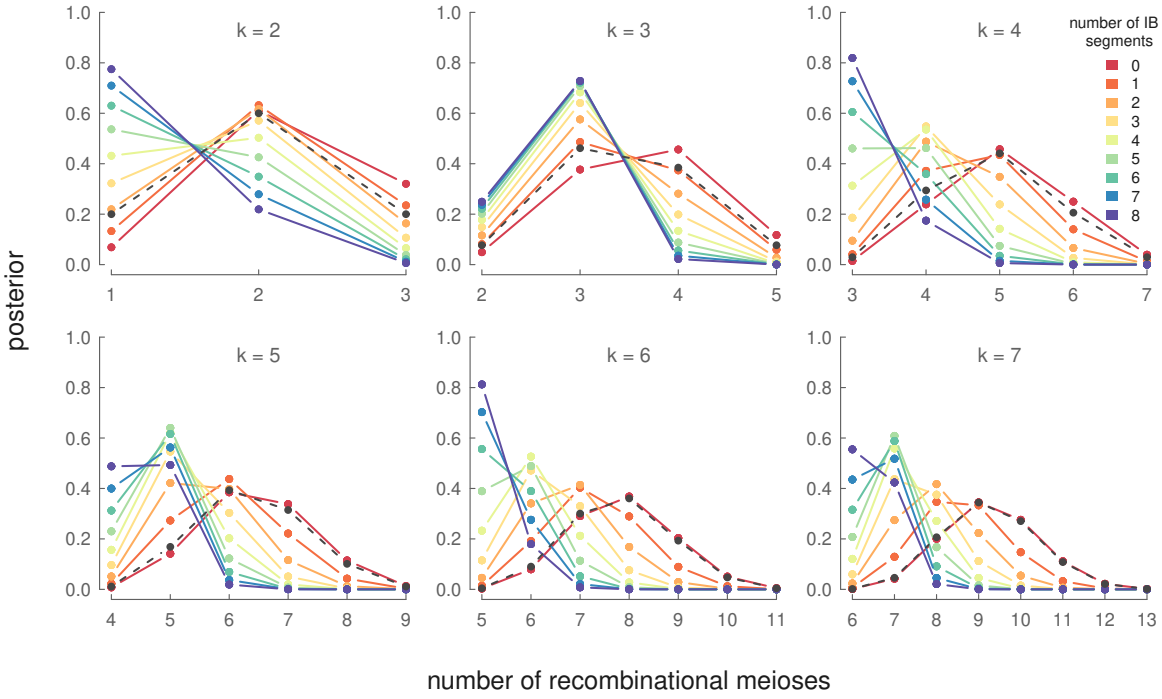

Figure 1.9: Posterior probability distribution $P(R=r|N=n,k)$ for different generations (each panel), and the observed number of IBD segments (each colored line). The prior distribution of recombinational meioses given k is indicated by a black dashed line.

In Figure 1.9, we show the posterior distributions over the number of recombinational

meioses, given an observed number of IBD segments between two females known to be X half-cousins. Again, these posterior distributions condition on knowing how many generations have occurred since the shared ancestor, k. With an increasing number of generations to the shared ancestor, fewer segments survive to be IBD between the present-day cousins. Consequently, observing IBD segments increases the likelihood of fewer females (and thus fewer recombinational meioses) between the cousins. For example, for $k = 6$, observing (the admittedly unlikely) six or more IBD segments leads to a posterior mode over the fewest possible number of females in the genealogical chain ($\lfloor (2k-1)/2 \rfloor = 5$; Figure 1.9). Similarly, observing between three and five segments places the posterior mode over six females in the genealogical chain. For $k > 4$, seeing zero segments provides little information over the prior about the relationship between the cousins, as sharing zero segments is the norm. In each case, a posterior distribution over the number of females in a genealogical chain can greatly reduce the number of likely genealogical configurations. For example, observing $n = 3$ shared X segments between half-cousins $k = 4$ generations back first restricts their shared ancestor to be one of the 34 possible shared X ancestors (out of the total 128 possible shared ancestors). Furthermore, these three shared X segments combined with our posterior distribution over recombinational meioses, leads to a *maximum a posteriori* estimate of $\hat{R} = 4$ females along the genealogical chain connecting the half-cousins. Only 10 genealogical chains connecting these cousins contain four females, thus the likely relationship of these cousins is considerably narrowed from the original 128 possible relationships. Therefore, sharing genetic segments on the X can provide considerable information about genealogical relationships.

1.5 Discussion

Detecting and inferring the nature of recent ancestry is important to a range of applications and the nature of such relationships are often of inherent interest. As the sample sizes of population genomic data sets increase, so will the probability of sampling individuals that share recent ancestry. In particular, the very large data sets being developed in human genetics will necessitate taking a genealogical view of recent relatedness. Our

methods extend existing methods for the autosomes by accounting for the special inheritance pattern of the X. Specifically, recent ancestry on the X differs from the autosomes since males only inherit an X from their mothers, and fathers pass an unrecombined (ignoring the PAR) X to their daughters. Consequently, the number of recombinational meioses, which determine the length and number of IBD segments, varies across the X genealogy. Since in most cases the number of females between two individuals in a genealogical chain is often unknown, we derive a distribution for recombinational meioses (equation (1.6)).

We also derive distributions for the length and number of IBD X segments by marginalizing over the unknown number of recombinational meioses that can occur between two individuals connected through a genealogical chain. In both cases, we condition on knowing k (the generations back to a shared ancestor) which can be inferred from the autosomes (Huff et al. 2011). Our models for IBD segment number and length use a Poisson-Binomial approximation to the recombination process, which match simulation results closely.

The genomic information about the genealogical relationship between pairs of individuals is inherently limited (due to the small number of segments shared and the stochasticity of the process); thus making full use of all shared segments on all chromosomes will be key to better inference. Our results here not only allow X IBD segments to be used to model recent ancestry, but in fact provide qualitatively different informative about genealogical ancestry than autosomal data alone. This additional information occurs through two avenues. First, sharing IBD segments on the X immediately reduces the potential genealogical ancestors two individuals share, since one's X ancestors are only a fraction of their possible genealogical ancestors (i.e. $\mathcal{F}_{k+2}/2^k$ in the case of a present-day female). Second, the varying number of females in an X genealogy across lineages combined with the fact that recombinational meioses only occur in females to some extent leave a lineage-specific signature of ancestry.

Unfortunately, the X chromosome is short, such that the chance of any signal of recent ancestry on the X decays rather quickly. However, growing sample sizes will increase both the detection of the pairwise relatedness and cases of relatedness between multiple

individuals. In these large data sets, overlapping pairwise relationships (e.g. a present-day individual that shares X segments with two distinct other individuals) could be quite informative about the particular ancestors that individuals share.

Our results should also be of use in understanding patterns of admixture on the X chromosome. In particular our results about the posterior information from the number and length of X segments shared with a genealogical ancestor can help us understand what can be learned from the presence (or absence) of segments of particular ancestry on the X chromosome. For example, if you observed long segments of a particular ancestry on your X chromosome our results could be used to aid the identification of which parts of your family tree this ancestry has been inherited from. These genetic genealogical inferences can provide informative details in genealogy reconstruction where historical genealogical information is missing or uncertain. While this information for an individual decays somewhat quickly after a small number of generations, models of X chromosome segment ancestry will be useful at a population-level for understanding sex-biased admixture (Bryc et al. 2010; Goldberg and Rosenberg 2015; Shringarpure et al. 2016).

1.6 Convergence of the Thinned Poisson Process to Poisson-Binomial Model

We compared the Poisson thinning approximation and the Poisson-Binomial models. One can show using the law of total expectation that the Poisson-Binomial and Poisson model have the same expected value:

$$\mathbb{E}[N] = \sum_{b=0}^{\infty} \mathbb{E}[N|B=b]P(B=b)$$
$$\mathbb{E}[N] = \frac{1}{2^d}\left(\sum_{b=0}^{\infty} b\text{Pois}(B=b) + c\sum_{b=0}^{\infty}\text{Pois}(B=b)\right)$$
$$\mathbb{E}[N] = \frac{1}{2^d}(\nu d + c)$$

This is the same expected value as the thinned Poisson process with rate $(\nu d + c)/2^d$. However, the Poisson thinning and Poisson-Binomial models differ in their variance. Using Eve's law, we can show the Poisson-Binomial model has variance

$$\text{V}[N] = \mathbb{E}_B[\text{V}[N|B]] + \text{V}_B[\mathbb{E}[N|B]]$$
$$\text{V}[N] = \frac{dv+1}{2^d} - \frac{1}{2^{2d}}$$

This differs from the thinned Poisson process variance by the term $1/2^{2d}$, which grows smaller with increasing d. Finally, we numerically show these two distributions (here, we label the two distributions for k generations $\mu_k(x)$ and $\nu_k(x)$, where x is the number of segments) converge quickly in total variational distance ($d_{TV}(\mu_k, \nu_k) = 1/2\sum_{n=0}^{\infty}|\mu_k(n) - \nu_k(n)|$) as k increases, in Figure 1.10.

1.7 Additional Autosomal Segment Distributions

1.7.1 The distribution of IBD segments between cousins

Similar to the distribution of autosomal segments between a present-day individual and an ancestor (Section 1.1.1), we can derive the distribution for the number of IBD segments shared between two half-cousins with an ancestor in the k^{th} generation. Two half-cousins are separated by $2k$ meioses, thus the distribution for number of segments is:

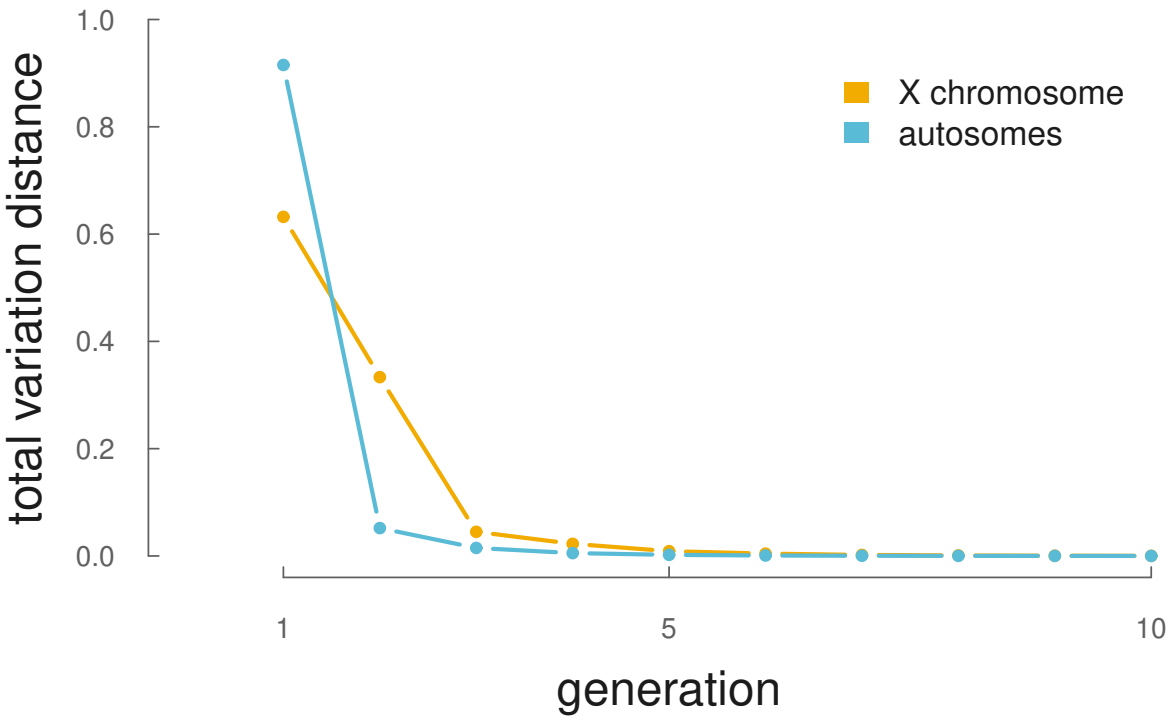

Figure 1.10: The total variation distance between the Poisson thinning and the Poisson-Binomial model for IBD segment number for X segments (yellow) and the autosomal segments (blue).

$$P(N = n \mid k, \nu, c) = \text{Pois}\left(N = n \mid \lambda = (c + 2k\nu)/2^{2k-1}\right) \tag{1.28}$$

Since either of the shared ancestor's haplotypes can be shared IBD between the two cousins, the Poisson process rate is doubled. Full-cousins can share segments via either of their two shared ancestors, leading the distribution to be:

$$P(N = n \mid k, \nu, c) = \text{Pois}\left(N = n \mid \lambda = (c + 2k\nu)/2^{2k-2}\right)$$

1.7.2 The distribution of autosome segment lengths

In addition to the number of IBD segments, the length of segments is also informative about ancestry (e.g. Palamara et al. 2012). As we model crossing over as a Poisson process, a one Morgan region will experience on average d recombination events over d meioses. Therefore, the probability density of segment lengths shared IBD between two individuals d meioses apart is exponential with rate d:

$$p(U = u|d) = de^{-du} \tag{1.29}$$

Equations (1.29) and (1.28) specify a model of the number and lengths of segments shared between various degree relatives. Various authors have used these types of results to derive likelihood-based models for classifying the genealogical relationship between pairs of individuals using autosome IBD data (Durand et al. 2014; Henn et al. 2012; Huff et al. 2011).

1.8 Generating Function for Recombinational Meioses

We also develop a generating function $g(x, k)$ that encodes the number of recombinational meioses in the k^{th} generation as the coefficient for the term x^k. This generating function can also be used in approximations and finding moments of the distribution $p_k(r)$.

An expansion of the generating function below encodes the number of lineages with r females in a genealogical chain k generations long ($n_{k,r}$) as the coefficient of the term x^k

$$\begin{aligned} g(x,k) = \frac{1}{2^{k+1}\sqrt{x}\sqrt{x+4}} \Big[& x\left(\left(R^+\right)^k - \left(R^-\right)^k\right) \\ & + \sqrt{x}\sqrt{x+4}\left(\left(R^-\right)^k + \left(R^+\right)^k\right) \\ & + -2\left(R^-\right)^k + 2\left(R^+\right)^k \Big] \end{aligned}$$

where

$$\begin{aligned} R^- &= x - \sqrt{x}\sqrt{x+4} \\ R^+ &= x + \sqrt{x}\sqrt{x+4} \end{aligned}$$

Proof. We begin by stating some recurrences that occur from the inheritance pattern of X ancestry:

$$n_{k,r} = m_{k,r} + f_{k,r} \tag{1.30a}$$

$$m_{k,r} = f_{k-1,r} \tag{1.30b}$$

$$f_{k,r} = f_{k-1,r-1} + m_{k-1,r-1} \tag{1.30c}$$

$$\tag{1.30d}$$

Starting from equation (1.30a):

$$\begin{aligned}
n_{k,r} &= m_{k,r} + f_{k,r} \\
n_{k,r} &= f_{k-1,r} + f_{k,r} \\
n_{k,r} &= f_{k-1,r} + f_{k-1,r-1} + m_{k-1,r-1} \\
n_{k,r} &= f_{k-1,r} + n_{k-1,r-1} \\
n_{k,r} &= f_{k-2,r-1} + m_{k-2,r-1} + n_{k-1,r-1}
\end{aligned}$$

finally, substituting equation (1.30a) again gives us the desired recurrence relation for $n_{k,r}$:

$$n_{k,r} = n_{k-2,r-1} + n_{k-1,r-1} \tag{1.31}$$

We can now use generating functions (Wilf 2013) to tackle this recurrence. Define:

$$A_k(x) = \sum_{r \geq 0} n_{k,r} x^r$$

then, multiply both sides of (1.31) by x^r and sum over r. On the right hand side:

$$= \sum_{r \geq 0} n_{k-2,r-1} x^r + \sum_{r \geq 0} n_{k-1,r-1} x^r$$

Note that $n_{k,r} = 0$ if $r < 0$. Multiplying and dividing the second term by x yields:

$$x(n_{k-1,0}x + n_{k-1,1}x^2 + n_{k-1,2}x^3 + \ldots)/x = xA_{k-1}(x)$$

An identical derivation works for the first term. We find:

$$A_k(x) = xA_{k-1}(x) + xA_{k-2}(x)$$

This generating function is in the form of another recurrence. We can solve this recurrence (i.e. with Mathematica) with the initial conditions below (which can be derived from (1.30a) and its initial conditions)

1. $A_0(x) = 1$
2. $A_1(x) = 1 + x$

to find a solution with these initial conditions, giving us our desired generating function $g(x, k)$.

□

We can see that our generating function works via an expansion and verify the coefficients match known numbers of recombinational meioses for some k. For example, let's expand $g(x, k)$ at $k = 5$:

$$x^2 + 6x^3 + 5x^4 + x^5$$

which matches the $n_{k,r}$ values found via computational calculation.

1.9 Half-Cousins IBD Length Distribution Simulation Results

Figure 1.11 show the concordance between our cousin IBD segment length analytic distributions and the binned average (1.98cM bin intervals) of 5,000 simulations.

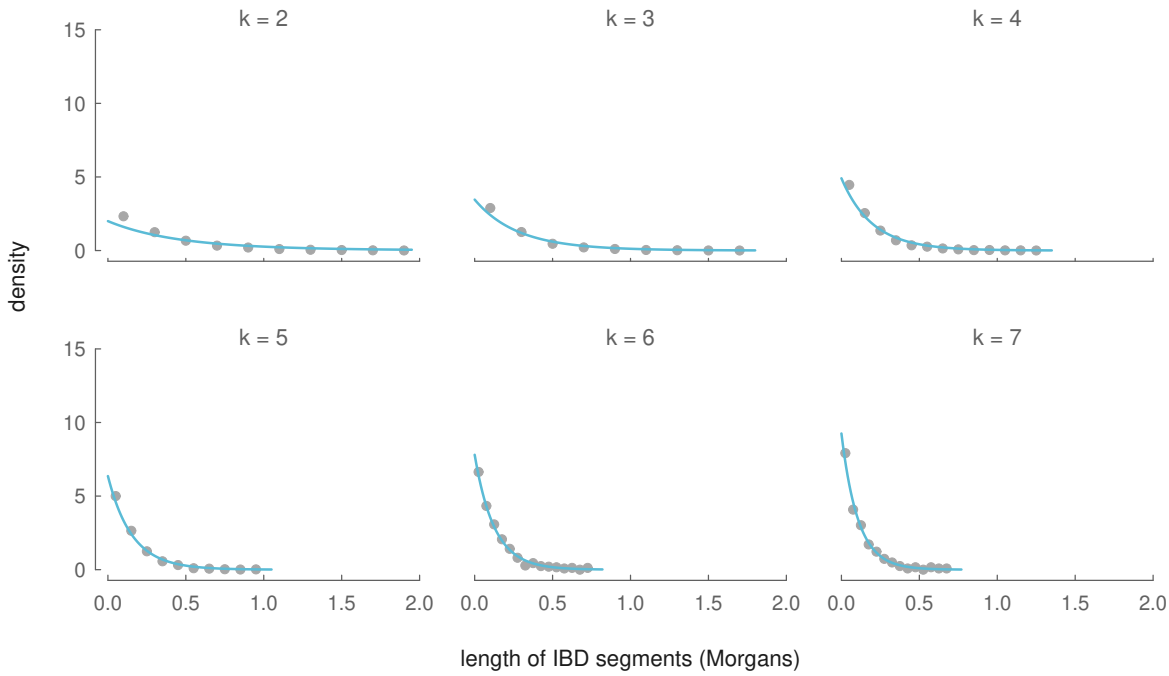

Figure 1.11: The analytic distributions of IBD segment length (blue lines) between two-present-day female half-cousins with a shared ancestor in the k^{th} generation (each panel), and the binned average 5,000 simulations (gray points).

1.10 An Approximation of X Pedigree Collapse

Since our models of recent X ancestry omit the possibility of pedigree collapse, it is worthwhile to see when this assumption breaks down. To see how pedigree collapse becomes an increasing problem further generations back, we look at the probability that all of a single individual's $\mathcal{F}_{k+2}$ X ancestors, when sampled from a population of N individuals with replacement, are distinct. We treat generations as discrete and non-overlapping, and look at the probability that all $\mathcal{F}_{k+2}$ are distinct individuals as a function of how many generations we go back. This problem is similar to the celebrated birthday problem, but with two rooms of participants: one room of females and another of males. Assuming random mating, each generation, one's X ancestors must be randomly selected with replacement from a population of N individuals. For all ancestors to be distinct, all $\mathcal{F}_k$ male ancestors selected from a pool of $N/2$ and $\mathcal{F}_{k+1}$ female ancestors selected from a pool of $N/2$ must be unique:

$$
\begin{aligned}
P(\text{X ancestors all distinct}) &= P(\text{male X ancestors unique}) \\
&\quad \times P(\text{female X ancestors unique}) \\
&= \prod_{i=1}^{\mathcal{F}_k} \left(1 - \frac{2i}{N}\right) \prod_{j=1}^{\mathcal{F}_{k+1}} \left(1 - \frac{2j}{N}\right)
\end{aligned}
$$

This probability as a function of k is plotted in Figure 1.12. For X ancestors, the probability that at least two individuals are non-distinct only becomes a significant problem after around 12 generations. Note that this is a very conservative account of how pedigree collapse could affect our calculations; even if two ancestors were to be non-distinct, this is unlikely to affect our calculations greatly. For pedigree collapse to affect our IBD segment models, an individual has to both be a genealogical ancestor *and* a genetic ancestor of the present-day individual; pedigree collapse has no genetic affect if non-distinct individuals are not genetic ancestors.

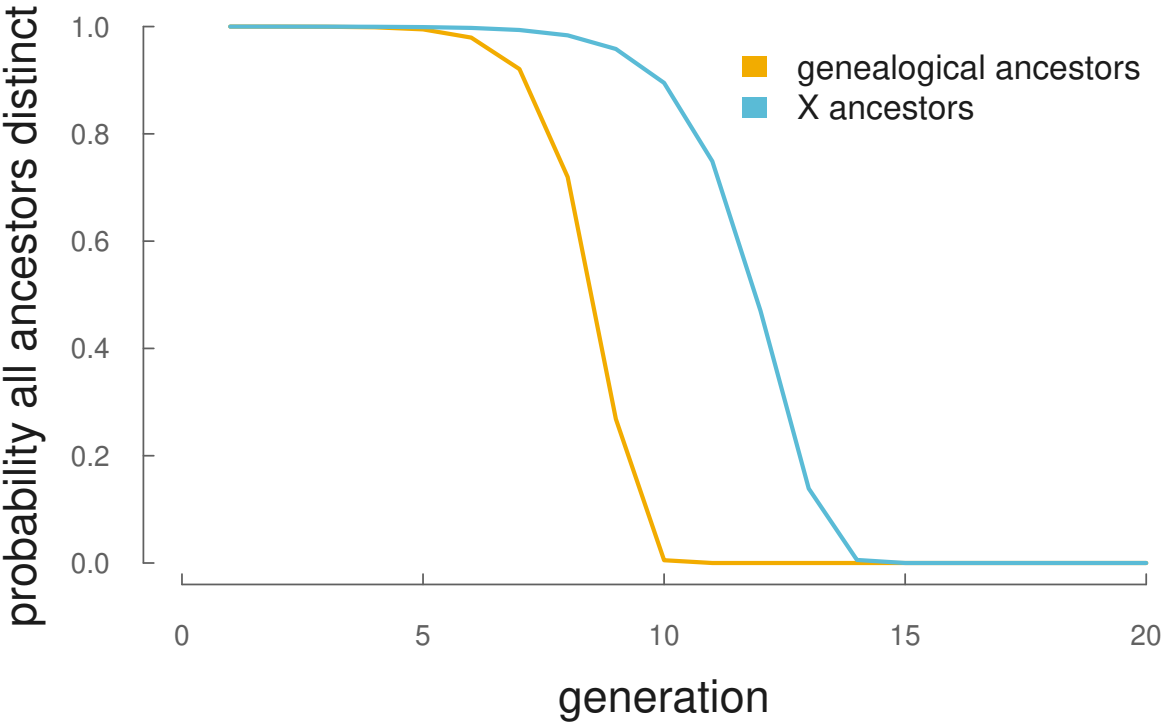

Figure 1.12: The probability that all genealogical and X ancestors are distinct in a population of $N = 100,000$.

For other pedigree collapse related quantities (e.g., what's the average number of distinct ancestors k generations back), see Wachter et al. (1979) approximations which use Feller's (1950) occupancy models.

Chapter 2

The Linked Selection Signature of Rapid Adaptation in Temporal Genomic Data

Adaptation can occur over remarkably short ecological timescales, with dramatic changes in phenotype occurring over just a few generations in natural populations. This rapid pace of adaptive change has been known to be mirrored at the genetic level since the early work of Fisher and Ford (1947) testing whether the rapid decline in a coloration polymorphism was consistent with natural selection or genetic drift. Since then, researchers have continued to use temporal data to detect selection on polymorphisms over short timescales in natural populations (Dobzhansky 1943, 1971; Fisher and Ford 1947; Kettlewell 1958, 1961; Mueller et al. 1985b), as well as quantify the rate of genetic drift (Mueller et al. 1985a; Nei and Tajima 1981; Pollak 1983; Prout 1954; Wallace 1956; Wang and Whitlock 2003; Waples 1989). However, this line of work in sexual populations has been partially eclipsed by a vast body of work examining large-scale population-genetic and -genomic data sets from a single contemporary timepoint. More recently, studies have applied similar temporal approaches to whole-genome data to discover selected loci in contemporaneous natural populations (Bergland et al. 2014; Rajpurohit et al. 2018), evolve and re-sequence studies (Barghi et al. 2019; Burke et al. 2010; Franssen et al. 2017; Johansson et al. 2010; Orozco-terWengel et al. 2012; Teotónio et al. 2009; Turner and Miller

2012; Turner et al. 2011), and ancient DNA (Fu et al. 2016; Mathieson et al. 2015). Furthermore, numerous methods have been developed to estimate effective population size (Nei and Tajima 1981; Pollak 1983; Waples 1989) and detect selected loci (Feder et al. 2014; Malaspinas et al. 2012; Mathieson and McVean 2013; Terhorst et al. 2015) from time-series data.

Overall, these approaches have identified compelling examples where selection has driven extreme allele frequency change at particular loci that is inconsistent with drift alone. However, most adaptation on ecological timescales likely involves selection on phenotypes with polygenic architecture and abundant standing variation (Endler 1986; Hendry and Kinnison 1999; Kinnison and Hendry 2001; Kopp and Hermisson 2009b). We know from theory that adaptation on such traits can result from very subtle allele frequency changes across the many loci that underlie the trait (Bulmer 1980), at least for the short-term evolutionary response (Chevin and Hospital 2008; Hermisson and Pennings 2005; Höllinger et al. 2019; Jain and Stephan 2015, 2017; Thornton 2018). These changes may be individually indistinguishable from genetic drift in temporal data. This poses a challenge for population genetic approaches to quantify selection: rapid phenotypic adaptations occurring on ecological timescales may leave a signal on genome-wide patterns of diversity that is undetectable by methods focused on individual loci.

Here, we explore an alternative: rather than aiming to find selected loci, we can use temporal data to quantify the genome-wide effects of linked selection during polygenic adaptation. Linked selection introduces a new source of stochasticity into evolution, as a neutral allele's frequency change depends on the fitness of the set of random genetic backgrounds it finds itself on (Gillespie 2000). The impact linked selection has on neutral loci is mediated by associations (linkage disequilibria, or LD) with selected loci and hence their recombination environment; neutral loci tightly linked to selected sites experience greater average reductions in diversity than more loosely coupled sites. Studies using a single timepoint have long exploited this idea, with some of the first evidence of pervasive natural selection being the correlation between diversity and recombination in *Drosophila* (Aguade et al. 1989; Begun and Aquadro 1992). Various forms of linked selec-

tion give rise to such patterns with much attention focusing on the hitchhiking (positive selection; Maynard Smith and Haigh 1974), or background selection models (negative, or purifying selection; Charlesworth et al. 1993; Hudson and Kaplan 1995). Recent genomic studies have modeled patterns of genome-wide diversity considering substitutions, functional constraint, and recombination environments to estimate parameters of hitchhiking and background selection models, and have begun to differentiate between these models (Elyashiv et al. 2016; Hernandez et al. 2011; McVicker et al. 2009). Across-taxa comparisons have shown that signals of linked selection are present in many sexual organisms, and that in some species a proportion of the stochastic change in allele frequencies is due to the randomness of linked selection instead of genetic drift (Coop 2016; Corbett-Detig et al. 2015; Cutter and Payseur 2013). Likewise, in asexual and facultatively sexual organisms both theory and empirical work show that linked selection and interference are a primary determinant of the levels of genetic diversity (Good et al. 2017, 2014; Neher and Shraiman 2011; Neher 2013).

In this paper, we extend this well-established approach of quantifying genome-wide selection through its indirect impact on linked neutral sites to temporal genomic data. We show that during rapid polygenic selection, linked selection leaves a signal in temporal genomic data that can readily be differentiated from neutral processes. Specifically, selected alleles perturb the allele frequency trajectories of neighboring neutral loci, increasing the variance of neutral allele frequency change and creating covariance between the neutral allele frequency changes across generations. Earlier work has modeled this effect on neutral alleles as a long-term reduction in the effective population size (J A Woolliams, N R Wray, R Thompson 2008; Robertson 1961; Santiago and Caballero 1995, 1998; Wray and Thompson 1990), but the increasing availability of genome-wide frequency data across multiple timepoints allows us to directly quantify the extent of linked selection over short ecological timescales (tens of generations). We develop theory for the variances and covariances of neutral allele frequency change under selection, and show that analogous to diversity in a single timepoint study, their magnitude depends on the local fitness variation, recombination, and linkage disequilibria. Furthermore, we show that our theory can

(1) directly partition the variation in genome-wide frequency change into the components caused by drift and selection, (2) estimate the additive genetic variance for fitness and how it changes over time, and (3) detect patterns of fluctuating selection from temporal data. Overall, we believe our approach to modeling temporal genomic data will provide a more complete picture of how selection shapes allele frequency changes over ecological timescales in natural populations, potentially allowing us to understand short-term effects of linked selection that would otherwise not be perceptible from studies using a single timepoint.

2.1 Outline of Temporal Autocovariance Theory

Our goal is to understand how linked selection affects the frequency trajectories of neutral sites by modeling the variances and covariances of neutral allele frequency changes ($\Delta p_t = p_{t+1} - p_t$, where p_t is the population frequency at time t). We assume a closed population with discrete, non-overlapping generations. When there are no heritable fitness differences between individuals, genetic drift is the only source of stochasticity of allele frequency change due to two sources of variation: random non-heritable, or environmental differences in offspring number, and Mendelian segregation of heterozygotes. Both are directionless such that when averaged over evolutionary replicates, the expected change in allele frequency due to drift alone is $\mathbb{E}(\Delta p_t) = 0$ and quantified by the variance in allele frequency change $\mathrm{Var}(\Delta p_t)$ (as quantified by the variance effective population size; Charlesworth 2009; Crow and Kimura 1970; Wright 1938).

When there are heritable fitness differences between individuals in the population, a third source of stochasticity affects a neutral allele's frequency change: neutral alleles can become randomly associated with the genetic backgrounds that determine the fitness differences between individuals (Robertson 1961; Santiago and Caballero 1995, 1998). Even though the neutral alleles do not impact fitness, their frequency trajectories are perturbed by their fitness background, as those on advantage backgrounds leave more descendants, while those on disadvantageous backgrounds leave fewer. We can partition a neutral allele frequency's change into these three uncorrelated stochastic components

(following Santiago and Caballero, 1995, see our Appendix Section 2.6.1 for proof),

$$\Delta p_t = \underbrace{\Delta_{N} p_t + \Delta_{M} p_t}_{\text{drift}} + \underbrace{\Delta_{H} p_t}_{\text{selection}} \tag{2.1}$$

where, $\Delta_{N} p_t$, $\Delta_{M} p_t$, and $\Delta_{H} p_t$ are the neutral allele's frequency changes due to non-heritable variation in fitness between diploid individuals, Mendelian segregation of heterozygotes into offspring, and heritable variation in fitness (we refer to this as the *heritable change* in neutral allele frequency), respectively. Note that while throughout the paper we consider the allele frequency change between adjacent generations, the same approach can be extended to situations where the study system cannot be observed every generation. Like the stochastic components of drift, the allele frequency change due to heritable fitness differences is directionless ($\mathbb{E}(\Delta_{H} p_t) = 0$). Additionally, since each component is uncorrelated with the others, the variance in allele frequency change is

$$\mathrm{Var}(\Delta p_t) = \mathrm{Var}(\Delta_{N} p_t) + \mathrm{Var}(\Delta_{M} p_t) + \mathrm{Var}(\Delta_{H} p_t). \tag{2.2}$$

The terms $\mathrm{Var}(\Delta_{N} p_t)$ and $\mathrm{Var}(\Delta_{M} p_t)$ capture the variance due to the random reproduction process, and the former can accommodate extra non-heritable variance in offspring number (as long as individuals are exchangeable with respect to their genotype; Cannings 1974), while the term $\mathrm{Var}(\Delta_{H} p_t)$ captures heritable fitness variation due to systematic differences in the fitness of individuals caused by their genotypes.

In addition to inflating the within-generation variance in allele frequency change, heritable fitness variation has another profound affect on neutral alleles: while the stochastic components of drift have independent effects on frequency change each generation, heritable variation in fitness creates *temporal autocovariance* in neutral allele frequency changes across generations. The contribution of temporal autocovariance is evident by writing the total cumulative allele frequency change as the sum of allele frequency changes each generation,

$$
\begin{aligned}
\mathrm{Var}(p_t - p_0) &= \mathrm{Var}(\Delta p_{t-1} + \Delta p_{t-2} + \ldots + \Delta p_0) \\
&= \sum_{i=0}^{t-1} \mathrm{Var}(\Delta p_i) + \sum_{i \neq j} \mathrm{Cov}(\Delta p_i, \Delta p_j) \\
\mathrm{Var}(p_t - p_0) &= \underbrace{\sum_{i=0}^{t-1} \left(\mathrm{Var}(\Delta_{N} p_i) + \mathrm{Var}(\Delta_{M} p_i)\right)}_{\text{drift}} + \\
&\qquad \underbrace{\sum_{i=0}^{t-1} \mathrm{Var}(\Delta_{H} p_i)}_{\text{genetic variance in offspring number}} + \underbrace{\sum_{i \neq j} \mathrm{Cov}(\Delta_{H} p_i, \Delta_{H} p_j)}_{\text{temporal autocovariance}} . \qquad (2.3)
\end{aligned}
$$

These covariance terms are expected to be non-zero only when there is heritable variation in fitness (assuming there is neither non-Mendelian segregation nor covariance between parental and offspring environment, e.g. as in Heyer et al. 2005).

Temporal autocovariance is caused by the persistence over generations of the statistical associations (linkage disequilibria) between a neutral allele and the fitnesses of the random genetic backgrounds it finds itself on; as long as some fraction of associations persist, the heritable variation for fitness in one generation predicts the change in later generations, as illustrated by the fact that $\mathrm{Cov}(\Delta p_2, \Delta p_0) > 0$ (see Figure 2.1A). Ultimately segregation and recombination break down haplotypes and shuffle alleles among chromosomes, leading to the decay of autocovariance with time.

The effect heritable variation has on neutral alleles has traditionally been modeled in a quantitative genetics framework where a large number of loosely linked polymorphisms contribute to heritable fitness differences between individuals, and the impact of heritable fitness variation on a neutral allele is quantified as a reduction in its long-run effective population size (Robertson 1961; Santiago and Caballero 1995, 1998). This form of linked selection can be contrasted with classic population genetic hitchhiking theory (Maynard Smith and Haigh 1974), which considers how neutral alleles closely linked to a new beneficial mutation are affected as it sweeps to fixation. While classic population genetic linked selection models consider how neutral variation is affected by strong associations caused by tight linkage to an advantageous site, quantitative genetic models of linked selection

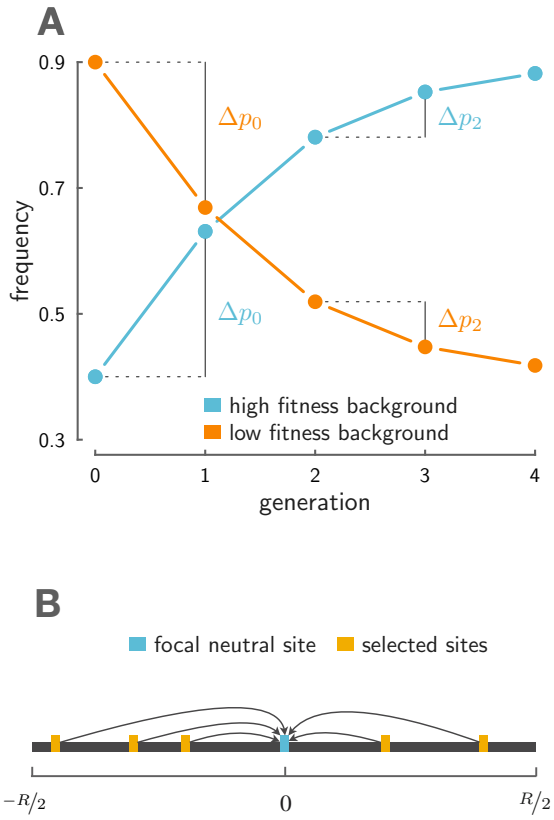

Figure 2.1: A: On an advantageous background (light blue), a neutral allele increases in frequency leading to a positive change in allele frequency early on, $\Delta p_0 = p_1 - p_0$. As long as some fraction of neutral alleles remain associated with this advantageous background, the neutral allele is expected to increase in frequency in later generations, here, $\Delta p_2 = p_3 - p_2$. This creates temporal autocovariance, $\mathrm{Cov}(\Delta p_2, \Delta p_0) > 0$. Similarly, had the neutral allele found itself on a low-fitness background (orange), this would also create temporal autocovariance. B: This depicts the setup for our multilocus model. Multiple alleles (yellow) determine the fitness in a region R Morgans in length, and these perturb the allele frequency trajectory of a focal neutral site (light blue).

considered the weakest forms of associations: those between unlinked loci within an individual (Morley 1954; Robertson 1961; Santiago and Caballero 1995; see Barton 2000 for more on the two models of linked selection). These distant associations are quickly established but are rapidly broken down by segregation and independent assortment, yet still can have a marked effect on diversity (Robertson 1961; Santiago and Caballero 1995). However, since the impact of heritable fitness variation has traditionally been modeled as causing a reduction in the effective population size, there has been no direct way to sepa-

rately estimate its effects from those of drift. We show that with temporal genomic data, one can directly measure the levels of temporal variances and autocovariances of allele frequency change in the population. Additionally, we that show temporal autocovariance is created under both tight and loosely linked selection, and below, develop expressions for its magnitude that are applicable to both, bridging the two regimes of linked selection.

2.2 A model for multilocus temporal autocovariance

Here, we develop theory for the temporal autocovariance in a neutral allele's frequency changes through time, generated by the presence of heritable fitness in the population. We measure the temporal autocovariance $\mathrm{Cov}(\Delta p_t, \Delta p_s)$ at a single diallelic neutral locus. Since only allele frequency changes due to heritable variation in *fitness* contribute to temporal autocovariance, we can focus exclusively on the behavior of $\Delta_H p_t$ in deriving our expressions for the autocovariance across timepoints. We imagine that an individual i has fitness f_i, i.e. that their expected number of children is f_i. We assume a constant population size, and so the population average fitness $\mathbb{E}_i(f_i) = 1$. Additionally, we assume that all fitness variation has an additive, polygenic architecture. Then, with L loci contributing to fitness, we can write individual i's fitness as $f_i = 1 + \sum_{l=1}^{L} \alpha_{t,l} g_{i,l}$, where $\alpha_{t,l}$ is the effect size in generation t and $g_{i,l} \in \{0, 1, 2\}$ is individual i's gene content at locus l. Here, each $\alpha_{t,l}$ is analogous to a selection coefficient acting at locus l, since the fitnesses for genotypes A_1A_1, A_1A_2, and A_2A_2 are 1, $1 + \alpha_{t,l}$, and $1 + 2\alpha_{t,l}$ respectively. This formulation is approximately equivalent to exponential directional selection on some additively determined trait, implying that selection does not create linkage disequilibria between unlinked loci; see Appendix 2.6.2 for more detail.

When fitness variation exists in the population (that is, $\mathrm{Var}_i(f_i) > 0$), the frequency of the neutral allele changes stochastically, as more fit individuals leave more descendents that inherit the neutral allele they carry and less fit individuals leave fewer. Across the population, stochastic associations can form between the genetic components of an individual's fitness and the neutral allele they carry, leading the neutral allele frequency to change due to fitness differences across individuals. The total heritable change in neutral

allele frequency $\Delta_H p_t$ can then be partitioned into each individual's contribution to this change based on their fitness f_i and the number of the tracked neutral alleles they carry, $x_i \in \{0, 1, 2\}$, giving us

$$\Delta_H p = \frac{1}{2N} \sum_{i=1}^{N} x_i (f_i - 1) \tag{2.4}$$

(Santiago and Caballero 1995). Substituting each fitness f_i with its genetic basis and simplifying (see Appendix Section 2.6.2 for derivation and eqn. 10 of Kirkpatrick et al. 2002) gives,

$$\Delta_H p_t = \sum_{l=1}^{L} \alpha_{t,l} D'_{t,l} + \sum_{l=1}^{L} \alpha_{t,l} D''_{t,l} \tag{2.5}$$

where $D'_{t,l}$ is the *gametic* linkage disequilibrium between the neutral allele and the allele at the selected site l on the same gamete, whereas $D''_{t,l}$ is the *non-gametic* linkage disequilibria, or the covariance *across* the neutral and selected allele on the two different gametes forming an individual (see Weir 1996, p. 121 for details and Appendix Figure 2.6.2A for an illustration). Intuitively, this expression tells us that the heritable change in neutral allele frequency is determined by the gametic and non-gametic linkage disequilibrium between the neutral site and all sites that affect an individual's fitness, scaled by the magnitude of each selected locus's effect. Alternatively, we can see this as the multivariate breeder's equation, where the neutral allele is a correlated trait responding to selection on other traits/loci (Lande 1979). This expression is the multilocus analog of the change in a neutral site's frequency due to hitchhiking at a single linked site (see e.g. equations (2) and (3) in Stephan et al. 2006).

Because the effects of the non-gametic LD are relatively weak compared to the gametic LD for tightly linked loci (see Appendix Section 2.6.6 for an expression of their strength), we ignore these, and hereafter omit the primes in our notation so that $D_{t,l}$ refers to $D'_{t,l}$. Since $\mathbb{E}(\Delta_H p_t) = 0$, we can write the covariance $\mathrm{Cov}(\Delta_H p_t, \Delta_H p_s)$ as $\mathbb{E}(\Delta_H p_t \Delta_H p_s)$. Hereafter, we also omit the subscript H since $\mathrm{Cov}(\Delta p_t, \Delta p_s) = \mathrm{Cov}(\Delta_H p_t, \Delta_H p_s)$. Expanding

these terms, the covariance between the allele frequency changes at generations t and s can be written as

$$\begin{aligned}\mathrm{Cov}(\Delta p_t, \Delta p_s) &= \mathbb{E}\left[\left(\sum_{l=1}^{L} \alpha_{t,l} D_{t,l}\right)\left(\sum_{l=1}^{L} \alpha_{t,l} D_{s,l}\right)\right] \\ &= \underbrace{\sum_{l=1}^{L} \alpha_{t,l}\alpha_{s,l}\mathbb{E}(D_{t,l}D_{s,l})}_{\text{persistence of associations with selected site } l} + \underbrace{\sum_{l\neq k} \alpha_{t,k}\alpha_{s,l}\mathbb{E}(D_{t,k}D_{s,l})}_{\text{cross-associations between two selected sites}} .\end{aligned} \tag{2.6}$$

This statement for temporal autocovariance is fairly general, as it can handle fluctuating selection (e.g. when $\alpha_{t,l}$ varies with time t) and any additive multilocus evolution (as long the linkage disequilibria dynamics can be specified). Looking at the first term in this sum, we see the temporal autocovariance is determined in part by the terms $\mathbb{E}(D_{t,l}D_{s,l})$. These expected LD products reflect the degree to which the association between the neutral locus and a selected site persists from generation t to s (here, $t < s$). Intuitively, the higher the initial association between the neutral and selected loci, and the slower rate of decay of LD between sites, the greater temporal autocovariance will be.

2.2.1 The multilocus temporal autocovariance model with directional selection

Thus far, in reaching Equation (2.6) we assume only that fitness is additive across loci. In this section, we develop a model of how temporal autocovariance behaves specifically under directional selection beginning at a specific time. We make three assumptions to simplify our expressions. First, we assume that the effect size remains constant through time, such that $\alpha_l := \alpha_{t,l}$ for all t (we relax this assumption in Section 2.3.2). Second, we ignore the contribution of the second term of Equation (2.6), $\mathbb{E}(D_{t,k}D_{s,l})$ (for $k \neq l$), to temporal autocovariance. Under the case where the population is initially at mutation-drift-recombination equilibrium, we expect this product to be zero as there is no directional association between the two selected sites and the neutral site. However, we note that interaction between selected sites (Hill-Robertson interference) will

cause this term to become negative (Barton and Otto 2005), a point we return to later. Third, we assume that the selected sites increase in frequency independently, such that the dynamics of the linkage disequilibria between the neutral and selected sites pairs can be modeled using two-locus dynamics. Using a deterministic continuous-time model for the dynamics of the linkage disequilibrium between the selected and neutral site (Barton 2000; Maynard Smith and Haigh 1974), we rewrite the $\mathbb{E}(D_{t,l}D_{s,l})$ terms in the expression for temporal autocovariance as

$$\begin{aligned}\mathrm{Cov}(\Delta p_t, \Delta p_s) &= \sum_{l=1}^{L} \alpha_l^2 \mathbb{E}(D_{t,l}D_{s,l}) \\ &= \sum_{l=1}^{L} \alpha_l^2 \mathbb{E}(\mathcal{R}_{t,l}^2) p_t(1-p_t) p_{s,l}(1-p_{s,l})(1-r_l)^{s-t} \qquad (2.7a)\end{aligned}$$

$$\frac{\mathrm{Cov}(\Delta p_t, \Delta p_s)}{p_t(1-p_t)} = \sum_{l=1}^{L} \alpha_l^2 p_{s,l}(1-p_{s,l}) \mathbb{E}(\mathcal{R}_{t,l}^2)(1-r_l)^{s-t}, \qquad (2.7b)$$

where $\mathbb{E}(\mathcal{R}_{t,l}^2)$ is the square of the correlation between the neutral site and selected site l at time t (a common measure of LD; Hill and Robertson 1968), and r_l is the recombination fraction between the neutral site and selected site l.

We can further simplify this expression by assuming that there is no covariation between the additive genic variation at a selected site and the linkage disequilibrium between that selected site and the neutral site (see Appendix Section 2.6.2 for more detail). This allows us to factor out the average additive genic variation for fitness at time s and write the covariance as

$$\frac{\mathrm{Cov}(\Delta p_t, \Delta p_s)}{p_t(1-p_t)} = \frac{V_a(s)}{2L} \sum_{l=1}^{L} \mathbb{E}(\mathcal{R}_{t,l}^2)(1-r_l)^{s-t} \qquad (2.8)$$

where $V_a(s)$ is the additive genic variance for fitness, which is the additive genetic variance for fitness (V_A) without the contribution of linkage disequilibria between selected sites, $V_a(s) = 2\sum_l \alpha_l^2 p_l(s)(1-p_l(s))$. In part, our expression not relying on the linkage disequilibria between selected sites is a result of ignoring the second term in Equation (2.6); we revisit the consequences of this assumption further on in Section 2.2.5.

This expression allows us to calculate the temporal autocovariance in cases where we know the vector of recombination fractions between the neutral and each of the selected sites, $r_1, r_2, \ldots, r_L$. Often we do not know the exact positions of these sites, but we can treat these positions as randomly placed on a chromosome and further simplify our model to understand the factors that determine temporal autocovariance.

2.2.2 Temporal autocovariance for an average neutral polymorphism

In the second part of our derivation, we develop a simple intuitive model of how temporal autocovariance is determined by a few key parameters when we make two additional assumptions. First, we assume selected sites are randomly and uniformly distributed along the chromosome, such that a site's position on the genetic map is a random variable $g \sim U(-R/2, R/2)$ (where R is the region's length in Morgans), and the focal neutral site with which we calculate temporal autocovariance lies in the middle of this idealized chromosome at the origin (as depicted in Figure 2.1B). Then, the recombination fraction between the focal neutral site and a selected site at random position g is given by the mapping function $r(g)$, which maps the position g to a recombination fraction. A simple choice for $r(g)$ is Haldane's mapping function, $r(g) = \frac{1}{2}(1 - e^{-2|g|})$, (Haldane 1919; note we take the absolute value of g to translate the position g to a distance to the focal neutral site) and we use that here. Second, we assume the linkage disequilibrium between each selected site and the focal neutral site depends only the recombination fraction $r(g)$ between the two loci, and not their absolute positions or effect sizes; then, we rewrite $\mathbb{E}(\mathcal{R}^2_{t,l})$ as the function $\mathbb{E}(\mathcal{R}^2_t(r(g)))$. For example, if the population was initially at drift-recombination balance, this would be $\mathbb{E}(\mathcal{R}^2) = (10 + \rho)/(22 + 13\rho + \rho^2)$ where $\rho = 4Nr(g)$ (Hill and Robertson 1968; Ohta and Kimura 1969). These assumptions allow us to conceptually understand the factors that determine temporal autocovariance; in practice, in temporal studies with linkage disequilibria data and recombination maps, one can directly calculate the sum in Equation (2.8) (see Appendix Section 2.6.5). We then write the temporal autocovariance experienced by a neutral allele in a region R Morgans long containing $V_a(s)$ fitness variation at time s as

$$\frac{\mathrm{Cov}(\Delta p_t, \Delta p_s)}{p_t(1-p_t)} \approx \frac{V_a(s)}{2R} \int_{-R/2}^{R/2} \mathbb{E}(\mathcal{R}_t^2(r(g)))(1-r(g))^{(s-t)}\, dg \tag{2.9}$$

(see Appendix Section 2.6.2 for details).

This integral is the sum of the initial LD between a typical neutral locus and selected site, weighted by the decay of LD due to recombination over $s-t$ generations. Selection enters here through the total additive genic variance for fitness for the region divided by the genetic map length of the region ($V_a(s)/R$). Thus a key compound parameter in describing the temporal covariance is the additive genic variance per Morgan, a quantity somewhat similar to the ratio of new adaptive mutations per basepair to recombination per basepair, $\nu_{\mathrm{BP}}/r_{\mathrm{BP}}$, that occurs in models of recurrent sweeps (Stephan et al. 1992) and models of the limits of selection with linked loci (Robertson 1970; Robertson 1976). Note that this does not include the effects of genome-wide fitness variation, e.g. the impact unlinked selected sites have on the neutral site due to the associations created when the sites sort within the same individuals. We quantify the magnitude of these in Appendix 2.6.3.

To validate our theory, we simulate a fixed region of R Morgans and calculate the covariance in allele frequency changes by averaging over many uniformly distributed neutral sites within this region. Then, the random distance between a neutral site's position n and a selected site's position g is $c = |n-g|$, where $n, g \sim U(0,R)$; this random variable c has a triangle distribution, $f(c) = 2(R-c)/R^2$. Averaging over the positions of both randomly placed neutral and selected sites, the temporal autocovariance is

$$\Sigma_{t,s} := \frac{\mathbb{E}_n(\mathrm{Cov}(\Delta p_t, \Delta p_s))}{\mathbb{E}_n(p_t(1-p_t))} = \frac{V_a(s)}{2} \underbrace{\int_0^R \mathbb{E}(\mathcal{R}_t^2(r(c)))\,(1-r(c))^{(s-t)} \frac{2(R-c)}{R^2}\, dc}_{\mathcal{A}(R,t,s)} \tag{2.10}$$

where $\mathbb{E}_n(\cdot)$ indicates an expectation taken over the position of the randomly placed neutral sites, and we define $\mathcal{A}(R,t,s)$ as the average linkage disequilibrium between selected and neutral sites that persists from generations t to s ($t \leq s$). As is common with estimating the expected values of other ratios like F_{ST} (Bhatia et al. 2013), we use a ratio of

expectations rather than the expectation of the ratio.

We can also use this expression to calculate the variance of allele frequency change. The standardized variance $\mathrm{Var}(\Delta p_t)/p_t(1-p_t)$ has two components: the drift term and the heritable variance in offspring number. Adding these independent contributions, the standardized variance is

$$\frac{\mathbb{E}_n(\mathrm{Var}(\Delta p_t))}{\mathbb{E}_n(p_t(1-p_t))} = \frac{V_N + 2}{8N} + \frac{V_a}{2}\mathcal{A}(R, t, s) \tag{2.11}$$

where V_N is the non-heritable variance in offspring number. Under a Wright–Fisher model of reproduction, $V_N \approx 2$, this simplifies to

$$\Sigma_{t,t} := \frac{\mathbb{E}_n(\mathrm{Var}(\Delta p_t))}{\mathbb{E}_n(p_t(1-p_t))} = \frac{1}{2N} + \frac{V_a}{2}\mathcal{A}(R, t, s). \tag{2.12}$$

When combined, this expression for the variance in allele frequency change and our expression for temporal autocovariance are in agreement with Robertson (1961) and Santiago and Caballero (1995; 1998) when predicting the total variance in allele frequency change; see Appendix 2.6.7. With the above expressions for the variances and covariances, we have a complete set of theoretical expressions for the variance-covariance matrix of allele frequency change, which we call $\mathbf{\Sigma}$, with the diagonal variance elements $\Sigma_{t,t}$ given by Equation (2.12), and the upper- and lower-triangle covariance elements $\Sigma_{t,s}$ $(t \neq s)$ given by Equation (2.10).

2.2.3 Modeling the dynamics of additive genic and genetic variation

Our expressions for temporal autocovariance (Equation 2.10) requires an expression for $V_a(t)$, the additive genic variation through time. However, we lack general expressions for the dynamics of the additive genic variation during selection, as these dynamics are quite complex for a few reasons. First, since our theory considers polygenic selection at a finite number loci in a region, additive genic variation is not constant as it would be under an infinitesimal model (Bulmer 1980). Second, we allow for arbitrary levels of recombination

from very tight linkage to loose linkage. Previous work has shown that predicting the dynamics of additive genic variation in a system with an arbitrary level of recombination is difficult, as both the additive genic and genetic variances depend on the higher-order moments of linkage disequilibrium (see Barton and Turelli 1987, and p. 607 of Turelli and Barton 1990).

A primary determinant of the additive genic variation is the heterozygosity of the selected sites. Assuming effect sizes are constant through time and across loci, we can rewrite the additive genic variation, $V_a(t) = 2\alpha^2 \sum_l p_l(t)(1 - p_l(t))$, as

$$V_a(t) = \alpha^2 SSH(t) \tag{2.13}$$

$$V_a(t) = V_a(1)\frac{SSH(t)}{SSH(1)} \tag{2.14}$$

where $SSH(t) = 2\sum_l p_l(t)(1 - p_l(t))$ is the sum of site heterozygosity at time t. Ideally, we would directly use $SSH(t)$ in a region; however, this would require knowing *a priori* which sites are being selected. Instead, we assume that the trait is sufficiently polygenic that frequency changes due to selection are weak, and that the change in heterozygosity at neighboring neutral polymorphic sites approximately mirrors that at selected polymorphisms (this is the case under the infinitesimal model; (**Barton2017-ac**; **Turelli2017-sw**)). Then, using the sum of site heterozygosity at neutral sites, $SSH_n(t)$, as a proxy for the sum of site heterozygosity at selected sites,

$$V_{a,ssh_n}(t) := V_a(1) ssh_n(s) \tag{2.15}$$

where we define $ssh_n(s) = {}^{SSH_n(s)}/_{SSH_n(1)}$ as the factor by which $V_a(1)$ decreases at time s, approximated by neutral sites' allele frequency changes. Under this approximation, the dynamics of genic variation are determined by one free parameter, $V_a(1)$, and the directly measurable sum of site heterozygosity at neutral sites through time.

Our focus here is on the short-term response of a population, and so we look at the decay of genetic backgrounds present at the onset of directional selection. In reality, new

mutations consistently create additive genetic variation for fitness; thus, an equilibrium level of additive genetic variance in the population can be maintained. The long-run effect of linked selection under this equilibrium model is handled by Santiago and Caballero (1995, 1998); see Appendix 2.6.7.

2.2.4 Multilocus Simulation Details

To test our theoretical expressions, we have conducted extensive forward simulations of directional selection on a polygenic trait. We vary four critical parameters in these simulations: (1) the level of additive genetic variance at the onset of selection (V_A), (2) the level of recombination (R in Morgans), (3) the number of selected sites in the region (L), and (4) the population size (N). We choose our grid of the selection and recombination parameters based on the levels we would expect across a wide variety of organisms; see Appendix Section 2.6.8 for details. We used three different population sizes ($N \in \{100, 500, 1000\}$), but note that we use $N = 1000$ and a subset of the other parameters in our figures.

Before the onset of selection, we create the initial diploid population from a pool of gametes created by `msprime` (Kelleher et al. 2016), such that the initial allele frequency distribution and linkage disequilibria between sites is at mutation-drift-recombination balance. Details of how `msprime` was called are available this paper's code repository (`https://github.com/vsbuffalo/tempautocov`), in `R/simpop.r`. Then, we pass this pool of gametes into a forward Wright–Fisher-with-recombination simulation routine and let it evolve for four generations neutrally before initiating selection on the fifth generation. These first four generations of neutral evolution (without mutation) serve as a control to validate that the variance in neutral allele frequency change is as expected under a Wright–Fisher model and that temporal autocovariance between a generation before selection and during selection is zero.

We generate genetic variation for fitness by choosing L random loci from the neutrally evolved sites, and randomly assign an effect size of $-\alpha$ or $+\alpha$, such that the expected total amount of additive genic variation is V_A (note that the initial additive genic and genetic variance are equal, $V_A = V_a$, as the LD contribution is zero for randomly chosen

sites). The details of this are given in Appendix Section 2.6.8. This approach creates some additional variance around the target level of additive genic variation, as the sum of site heterozygosities will vary stochastically across simulation replicates. At the onset of selection, an individual i's trait value is calculated as $z_i = \sum_{i=1}^{L} \alpha g_{i,l}$ where $g_{i,l}$ is their number of alleles with effect size α at locus l. Then, their absolute fitness is calculated using an exponential fitness function $w(z_i) = e^{z_i}$ (Turelli and Barton 1990, p. 17). Under our Wright–Fisher model, we sample the parents of the next generation according to a multinomial distribution, where the probability of individual i being a parent is $w(z_i)/\bar{w}$.

We record 50 generations of simulated evolution, after which we compute the standardized sample temporal variance-covariance matrix $\mathbf{Q}$ (this is the sample analog of our theoretical variance-covariance matrix $\mathbf{\Sigma}$), for each replicate as follows. First, we mark frequencies reaching fixation or loss as missing values. This allows the frequency changes before fixation/loss to contribute to the measured covariance, rather than removing the entire locus's trajectory, which would act to condition the covariance on more intermediate frequencies. Note that one cannot ignore fixations or losses, as these have $\Delta p_t = 0$ and thus an autocovariance of zero, which would act to underestimate the true level of autocovariance at segregating sites. Having marked fixations/losses as missing, we take the frequency matrix and calculate a vector of allele frequency changes $\Delta\vec{p}_n = [\Delta p_{n,1}, \Delta p_{n,2}, \ldots, \Delta p_{n,\tau}]$ using each neutral locus n's $\tau + 1$ observed generations. Finally, we calculate the $\tau \times \tau$ sample standardized variance-covariance matrix $\mathbf{Q}$, averaging over M neutral loci such that element $Q_{t,s}$ is calculated as

$$Q_{t,s} = \frac{\frac{1}{M-1}\sum_{n=1}^{M}\left(\Delta p_{n,t}\Delta p_{n,s} - \left(\frac{1}{M}\sum_{n=1}^{M}\Delta p_{n,t}\right)\left(\frac{1}{M}\sum_{n=1}^{M}\Delta p_{n,s}\right)\right)}{\frac{1}{M}\sum_{n=1}^{M} p_{\min(t,s)}\left(1 - p_{\min(t,s)}\right)}, \tag{2.16}$$

though see Appendix Section 2.6.9 for a bias-corrected version when sample, rather than population allele frequencies are used. Sums over missing values only use pairwise-complete observations, implemented by R's `cov()` function's `use='pairwise.complete'` argument.

We have extensively validated our simulation procedure in a neutrally evolving popu-

lation, ensuring that the decay of linkage disequilibrium and the allele frequency change match expectations (see Supplementary Figures 2.6.5, 2.6.6, and 2.6.7).

2.2.5 Comparing theory to simulation results

To validate our expressions for temporal autocovariance, we compare the levels of autocovariance and variance predicted by Equation (2.10) and (2.12) to the average levels observed across simulation replicates. To calculate the theoretical values of temporal autocovariance and variance, our expression requires the additive genic variation at s, $V_a(s)$; however, as described in Section 2.2.3, we lack an analytic expression for the dynamics of genic variation to plug into $V_a(s)$. Following the approach of others in evolutionary quantitative genetics (Turelli and Barton 1994, p. 930), we substitute the numerical values calculated directly from the simulation data for $V_a(s)$. Additionally we consider two other numerical values related to the additive genic variance: the observed additive genetic variance from our simulations ($V_A(s) = \mathrm{Var}_i(z_i)$ at time s, which includes the contribution of LD between selected sites), and the additive genic variation at time s as approximated by the observed decay in the sum of site heterozygosity at neutral sites ($V_{a,ssh_n}(1)$, as described in Section 2.2.3).

Figure 2.2 compares the fit of our theory with differing additive genetic variances with the empirical covariances from our multilocus simulations. In each panel, we plot the level of temporal autocovariance between the allele frequency change across the first two generations of selection (Δp_5) and some later allele frequency change Δp_s where s varies along the x-axis. Each point represents the temporal autocovariance (calculated across all sites in a region according to Equation 2.16) averaged across 100 replicate simulations, with the color of the point indicating the number of selected sites in the region. Within each panel, the temporal autocovariance predicted by Equation (2.10) is plotted as a set of three lines, one for each of the three different types of variance we have substituted in for $V_a(s)$. Overall, the fit is close but varies depending on the type of variance used for $V_a(s)$; we discuss each in turn below.

Using empirical additive genic variation (solid lines), our theory provides a good fit to the simulation results for a short period after selection is initiated ($\sim$5 generations)

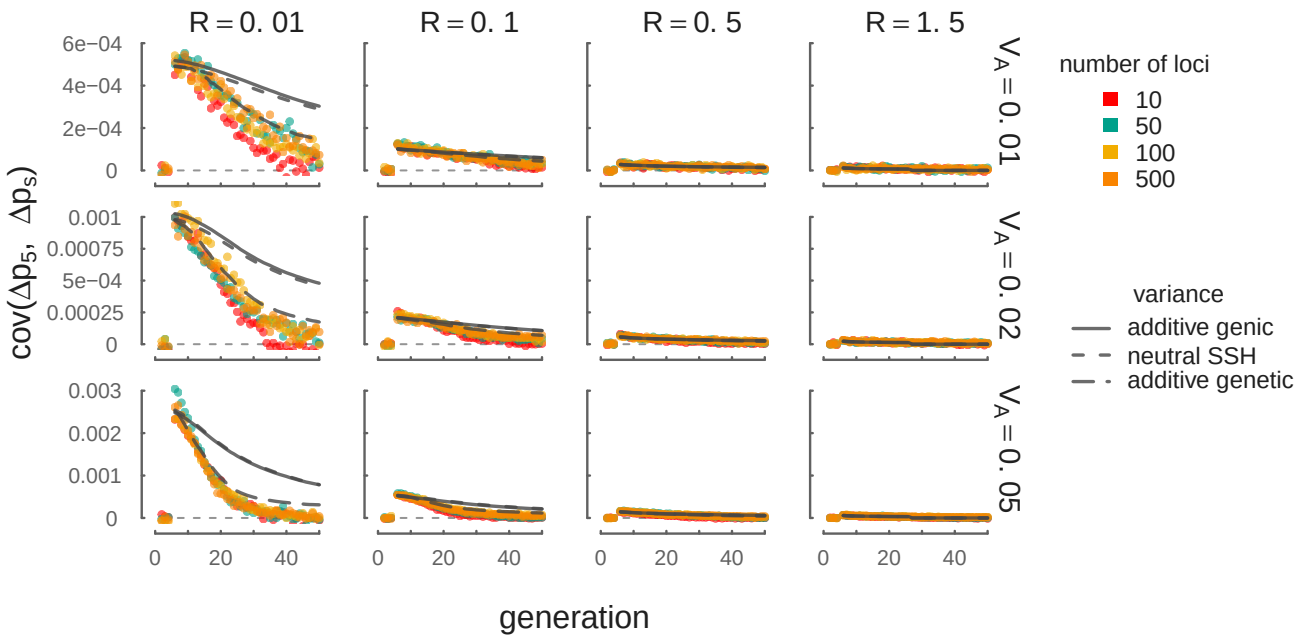

Figure 2.2: In each panel the temporal autocovariance $\mathrm{Cov}(\Delta p_5, \Delta p_s)$ is shown on the y-axis while generation s varies along the x-axis. Selection is initiated on the 5^{th} generation, so Δp_5 is the neutral allele's frequency change across the first generation of selection. Each point is the temporal autocovariance between Δp_5 and the Δp_s in a region, averaged over 100 simulation replicates, with the colors indicating the number of selected loci. The gray curves indicate the theoretical predictions (for $L = 500$ loci only) using Equation (2.10), with the equation's variance provided by the empirically observed additive genic (solid), the additive genetic (long dashes), and the neutral sum of site heterozygosity approximation (short dashes). A thin horizontal dashed line indicates $y = 0$. Across the columns, the level of recombination (in Morgans) is varied; across rows, the initial level of additive genetic variation is varied. Note that while our results here are between the frequency change at the onset of selection Δp_5 and some later change Δp_s, our covariance theory matches simulation results between any two arbitrary frequency changes Δp_t, and Δp_s; see Supplementary Figure 2.6.9.

in regions with tighter linkage ($R = 0.01$ Morgans) across a range of additive genetic variation parameters ($0.01 \leq V_A \leq 0.05$; see Supplementary Figure 2.6.10 for V_A varying over orders of magnitude). With looser linkage ($R \geq 0.1$ Morgans), our theory using the empirical additive genic variation fits much more closely over a longer duration (∼10-15 generations). Note that some variability is caused by the noise of each simulation replicate around the target initial additive genetic variation V_a (see Section 2.2.4), as each replicate samples sites from a neutral coalescent. Our theory also accurately predicts the temporal autocovariance for different choices of reference generation, i.e. varying t, see

Supplementary Figure 2.6.9.

When we use the sum of site heterozygosity at neutral sites (V_{a,ssh_n}, shown as a short-dashed lines) as a proxy for additive genic variation, the theory fits simulations over the same timespan as using the empirical additive genic variation. This is because (1) the SSH at neutral sites closely matches the SSH at selected sites, and (2) both closely follow the dynamics of additive genic variation through time (see Supplementary Figure 2.6.8). Using V_{a,ssh_n} has the advantage that we can directly measure neutral SSH, which proves useful later in Section 2.3, as we use this approach to help infer the initial additive genic variation at the onset of selection.

Finally, we find using the additive genetic variance $V_A(s) = \text{Var}_i(z_i)$ accurately predicts the dynamics of temporal autocovariance over tens of generations (see the long-dashed lines in Figure 2.2). Furthermore, calculating the temporal autocovariance using the empirical additive genetic variation better fits simulation data in regimes with tight recombination, where using genic variation performs poorly after the first few generations (e.g. the column of panels where $R = 0.01$). Thus using the additive genetic variance in our framework provides a good fit to the temporal dynamics over relatively long time spans.

What differentiates $V_A(s)$ from $V_a(s)$ that could explain this better fit? The additive genic variation $V_a(s)$ ignores the contribution of linkage disequilibria between selected sites. We can write the additive genetic variance as

$$V_A(s) = \text{Var}_i(z_i, s) = \underbrace{2\alpha^2 \sum_{l=1}^{L} p_l(s)(1 - p_l(s))}_{\text{genic variation, } V_a(s)} + \underbrace{\alpha^2 \sum_{i \neq j} D_{i,j}(s)}_{\text{LD contribution}} \tag{2.17}$$

where $D_{i,j}(s)$ is the LD between selected sites i and j at time s. At the onset of selection, there is no expected linkage disequilibria between selected sites since the sites and effect sizes were randomly sampled — in other words, $\mathbb{E}(D_{i,j}(s)) = 0$. We see this in Figure 2.2, as the temporal autocovariance predicted with $V_a(s)$ match those of $V_A(s)$ when $s = 6$ (see also Supplementary Figure 2.6.8, which plots the empirical additive genic and genetic variances over time). Over time, these two quantities diverge as negative linkage

disequilibria build up. While negative linkage disequilibria between selected sites build up due to epistasis under some forms of selection (known as the Bulmer effect, Bulmer 1971; Bulmer 1980), this is known not to happen under multiplicative selection (Bürger 2000, p. 50, 177) that is equivalent to the exponential directional selection fitness surface we have used in our simulations. Instead, the build up of negative linkage disequilibria between selected sites is likely due to Hill-Robertson interference (HRi) between selected sites (Hill and Robertson 1966), which affects the total additive genetic variation that selection is acting on. HRi refers to the creation of negative LD among beneficial alleles in finite population resulting from the fact that beneficial alleles that are on the same haplotype move more quickly through the population than beneficial alleles on deleterious backgrounds, resulting in negative LD. This negative LD among beneficial alleles lowers V_A compared to the genic V_a (Barton and Otto 2005; Crouch 2017; Good et al. 2014; Hill and Robertson 1966). In the derivation of our expression for temporal autocovariance, we greatly simplified the multilocus dynamics by ignoring the second term in Equation (2.6). This term includes the expected product of two LD terms; each is the LD between the neutral site and a selected site. Using full multilocus theory, one may find that by including these LD products, that V_A rather than V_a factors out the expression in Equation (2.7), but we leave this for future work. Importantly, our simulation results suggest that the negative linkage disequilibria created by selective interference only affects the temporal autocovariances through the variance term $V_a(s)$, and that the actual variance determining temporal autocovariance is the additive genetic variance, $V_A(s)$.

In addition to modeling autocovariance through time, our theory can predict the total temporal variance in allele frequency, $\mathrm{Var}(p_t - p_0)$, when there is heritable variation for fitness. Furthermore, from Equation (2.3) recall that we can decompose $\mathrm{Var}(p_t - p_0)$ into variance and covariance components. The variance components are determined by both the magnitude of drift ($1/2N$) and selection according to Equation (2.11), and the covariance components are determined solely by selection according to Equation (2.10) (assuming no inheritance of environmental factors). Using our theory, we have predictions for each of these components given the amount of additive genic/genetic variation for

fitness, the population size (N), and the amount of recombination (R). In Figure 2.3, we compare the magnitudes of these components (averaged over the replicates of our simulations) to our theoretical predictions. We depict the predictions for the variance and covariance components using both the empirical additive genetic variance (V_A) and the neutral sum of site heterozygosity proxy (V_{a,ssh_n}) as adjacent bars, each around a point range with the point representing the average value over simulation replicates, and the bars indicating the lower and upper quartiles over simulations.

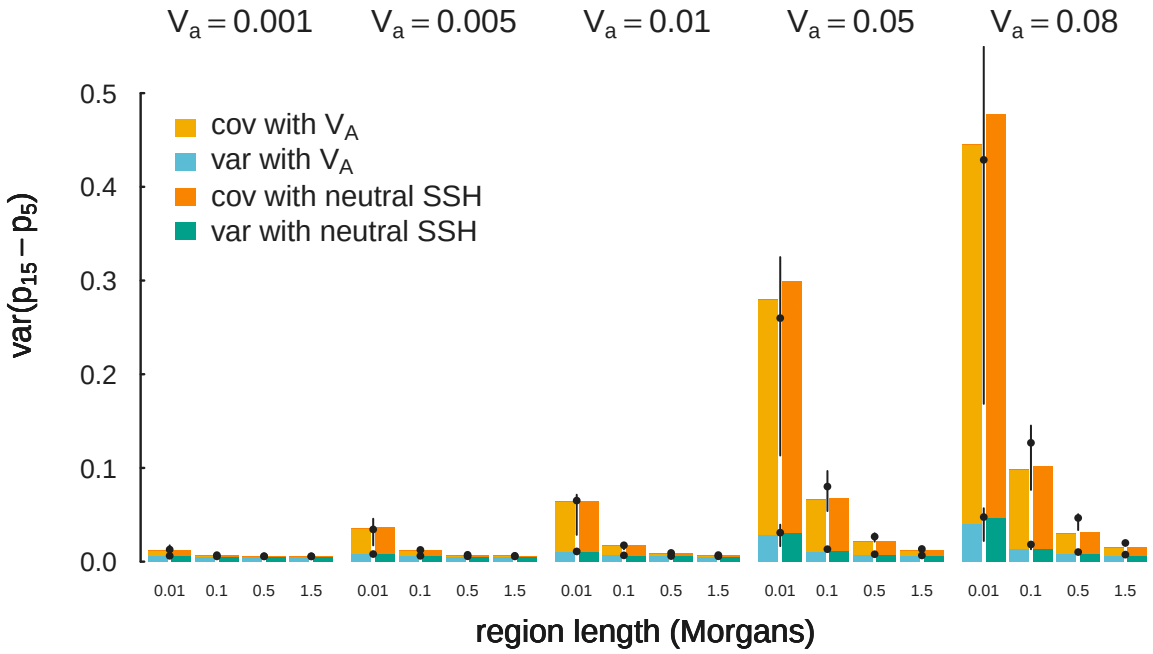

Figure 2.3: Summing over generations, Equations (2.6) and (2.12) accurately predicts the total variation in allele frequency change due to variance and covariance components. The predicted cumulative variance in allele frequency change across the ten generations after selection ($\mathrm{Var}(p_{15} - p_5)$) is shown as bars, using both the empirical additive genetic variation V_A (bars to the left of the pointrange), and the empirical neutral sum of site heterozygosity (bars to the right of the pointrange). The variance and covariance components are represented by blue/green and orange/yellow tones respectively. Finally, we show the averaged results of our simulations as pointranges, with the point depicting the average and the bars representing the lower and upper quartiles.

Finally, we have found that across a wide range of recombination and additive genetic variation parameters, the temporal autocovariance $\mathrm{Cov}(\Delta p_t, \Delta p_s)$ is largely determined by the compound parameter V_A/R and the number of generations between t and s, which

is a factor in Equation (2.9). We show in Figure 2.4 that the temporal autocovariance $\mathrm{Cov}(\Delta p_5, \Delta p_s)$ from simulations across a wide range of V_A and R parameters fall roughly on the same curve for each number of elapsed $s - t$ generations.

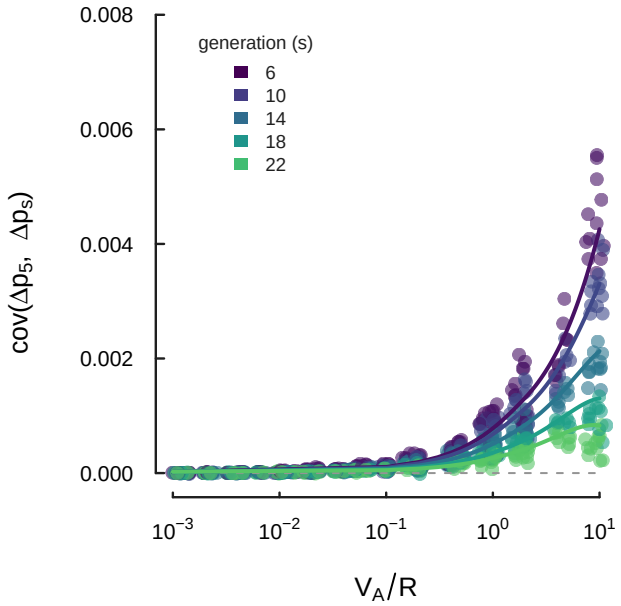

Figure 2.4: The compound parameter V_A/R and the number of generations between the temporal autocovariance $s - t$ largely determines the magnitude of the temporal autocovariance across a wide spectrum of V_A and R parameters. Each point is a simulation replicate with its x-axis position given by V_A/R, the y-axis position equal to the temporal autocovariance, and the number of elapsed generations $(s - t)$. Each line is a loess curve fit through each set of points for a particular generation (with smoothing parameter $\alpha = 0.9$).

2.3 Estimating linked-selection parameters from temporal autocovariance

Our multilocus theory provides analytic expressions for the expected variances and covariances of a neutral allele's frequency; thus a natural approach to parameter estimation is to equate these expectations to averages from the data and apply the method-of-moments. We describe a method-of-moments procedure below to estimate the initial additive genetic variance at the onset of selection $(V_A(1))$ in the first generation, and the drift-effective population size (N) from temporal data within a single region R Morgans long, and then show a simple extension that allows this to be applied to genome-wide data. Our ba-

sic approach is to calculate first the sample variances and covariances of the τ observed generation-to-generation allele frequency changes, averaging over all of the putatively neutral sites in a region. We then equate these sample variances and covariances to our analytic expressions for the variance and covariances, leaving us with an overdetermined system of equations, which we solve using least squares. We demonstrate that this simple estimation procedure provides accurate estimates of initial additive genetic variance and the drift-effective population size. We focus on this procedure, as it is simple and handles incomplete trajectories due to missing data or fixation/loss well. Calculating pairwise-complete covariances can leave sample covariances matrices non-positive definite, which makes maximum likelihood estimation perhaps much more difficult. Throughout, we use population allele frequencies (i.e. there is no sampling noise) which simplifies the description of the method; in Appendix Section 2.6.9 we describe how the method is changed by finite sampling of chromosomes from a population.

From our multilocus theory, we have analytic expressions for each element of the $\tau \times \tau$ covariance matrix of allele frequency changes in a region. To model the additive genic variance through time, we use the empirical neutral sum of site heterozygosity approximation as described in Section 2.2.3. This approximates the rate that the additive genic variation decreases through time from some initial level, $V_A(1)$, which we wish to estimate. In total, we have $\tau + {}^{\tau(\tau-1)}/_2$ unique moment equations, which for the variance and covariance are defined as

$$\frac{\mathrm{Var}(\Delta p_t)}{\mathbb{E}(p_t(1-p_t))} = \frac{\widehat{V_A(1)}}{2}\frac{SSH_n(t)}{SSH_n(1)}\mathcal{A}(R,t,t) + \widehat{F} := \Sigma_{t,t} \tag{2.18}$$

$$\frac{\mathrm{Cov}(\Delta p_t, \Delta p_s)}{\mathbb{E}(p_t(1-p_t))} = \frac{\widehat{V_A(1)}}{2}\frac{SSH_n(s)}{SSH_n(1)}\mathcal{A}(R,t,s) := \Sigma_{t,s} \text{ (for } s > t). \tag{2.19}$$

Here the first line gives the form of τ equations for the variance of allele frequency changes between subsequent generations, which includes the effect of genetic drift, $\widehat{F} = {}^1/_{2N}$. The second line gives the form of the covariances of allele frequency changes among different generations. The term $\mathcal{A}(R,t,s)$ is the average level of linkage disequilibrium after the $s-t$ generations that have elapsed, given there are R Morgans of recombination. In

our multilocus theory section and simulations, this is equal to the integral in Equation (2.10). However, we can also directly calculate a sample $\overline{\mathcal{A}(R,t,s)}$ from observed linkage disequilibrium in a region (for details, see Appendix Equation (2.55)).

Following the method-of-moments, we equate each of these independent $\tau + {}^{\tau(\tau-1)}/_{2}$ equations for $\Sigma_{t,s}$ to the observed sampling moments, the elements $Q_{t,s}$ of the upper triangle of the observed heterozygosity-normalized covariance matrix $\widehat{\mathbf{Q}}$ described in Equation (2.16). This yields $\tau + {}^{\tau(\tau-1)}/_{2}$ equations with 2 unknown parameters: $\widehat{V_A(1)}$ and $\widehat{N}$. We solve this overdetermined system of equations using least squares, an approach similar to the generalized method-of-moments in econometrics (Hansen 1982). This approach finds parameter estimates that minimize the squared error between the moment-based parameter estimate and the true parameter value, with respect to the true parameter value. We write the elements $Q_{t,s}$ of the upper triangle of the observed covariance matrix in the vector $\vec{q}$, and write the method-of-moments equations as,

$$\vec{q} = \widehat{V_A(1)}\vec{a} + \widehat{F}\vec{b} + \vec{\varepsilon} \tag{2.20}$$

where the elements of $\vec{a}$ and $\vec{b}$, in the same order as $\vec{q}$, are given by

$$a_{t,s} = \frac{1}{2}\frac{SSH_n(s)}{SSH_n(t)}\mathcal{A}(R,t,s),\ b_{t,s} = \delta_{t,s} \tag{2.21}$$

where $\delta_{t,s}$ is an indicator variable that is 1 when $s = t$ and zero otherwise.

Then, we can readily estimate the parameters $\widehat{V_A(1)}$ and $\widehat{F}$ using least squares. We then obtain an estimate of $\widehat{N}$ by taking ${}^{1}/_{2\widehat{F}}$. Since these equations are not statistically independent, we cannot assume $\mathrm{Cov}(\vec{\varepsilon}) = \sigma^2\mathbf{I}$. However, this does not affect our estimates $\widehat{V_A(1)}$ and $\widehat{F}$, as the least squares procedure is unbiased regardless of the covariance structure between the error terms (Christensen 2011, p. 26).

Using this method-of-moments approach, we sought to infer the parameters of 20 of the replicates across the 254 parameter combinations (the same as used in Figure 2.2). We use the first five generations after the onset of selection to infer $\widehat{V_A(1)}$ and $\widehat{N}$, as for this short timespan the additive genetic variance is well approximated using sum of neutral site

heterozygosity approach (see Section 2.2.5). Each simulation replicate includes around 500 neutral sites (the exact number is random, see Appendix 2.6.8 for details).

Applying our approach to these simulations, we find we can infer both the initial level of additive genetic variation $V_A(1)$, and the effective population size N from multilocus temporal data. In Figure 2.5A, we show that our method-of-moments gives reasonable estimates for the initial level of additive genetic variance over orders of magnitude of additive genetic variation, and different recombination regimes. As additive genetic variation for fitness becomes weaker (the left side of the figure), our estimates become more noisy. In Figure 2.5B we show the simultaneously estimated population size N against the true population size value. We also plot the estimated N_e (not accounting for selection) from a simple temporal estimator, $N_e = -t/(2\log(1-F))$ (Krimbas and Tsakas 1971; Waples 1989) where F is Wright's standardized variance (Wright 1931). While with high V_A and low R, the method-of-moments approach still underestimates N, it performs far better than a standard temporal N_e estimator that does not account for selection. In Appendix Figure 2.6.3, we include a version of this figure calculated using the method of moments on sample allele frequencies for a sample of size $n = 100$ chromosomes.

We can extend this approach to whole-genome data by imagining partitioning the genome into B non-overlapping windows of length w_{BP} in basepairs (e.g. megabase windows). We first assume that windows contribute uniformly to the genome-wide level of additive genetic variance for fitness, and show how our method-of-moments approach can be used to estimate a global $V_A(1)$. Assuming a uniform distribution of genetic variance across basepairs, the total additive variance is $V_A(1) = v_A(1)Bw_{\mathrm{BP}}$, across our B windows, where $v_A(1)$ is the additive genetic variance per basepair. As each window i contributes to $v_A(1)w_{\mathrm{BP}}$, our least squares approach given by Equation (2.20) becomes

$$\Sigma_{t,s,i} = \frac{\widehat{V_A(1)}}{2}\frac{1}{B}\frac{SSH_n(s)}{SSH_n(1)}\mathcal{A}(R_i,t,s) + \widehat{F}\delta_{t,s} + \varepsilon, \quad \text{for } s \geq t. \tag{2.22}$$

However, we expect *a priori* that windows containing more coding bases might disproportionately contribute to the total additive genetic variance. This suggests an alternative model to fit where partitions of the additive genetic variance across windows are propor-

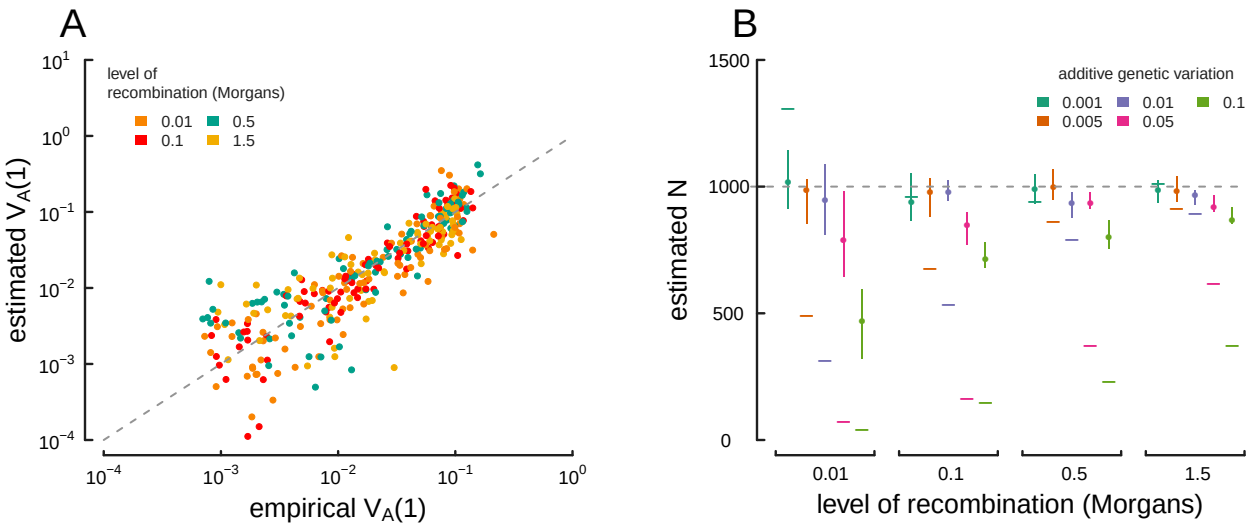

Figure 2.5: True parameter values and estimates using the method-of-moments approach on multilocus simulation data. (A) The true $V_A(1)$ (x-axis) and $\widehat{V_A(1)}$ estimated from the variance/covariance matrix (y-axis) for each simulation replicate across different levels of recombination (indicated by each point's color). The dashed gray line shows the $y = x$ line where an estimate is exactly true to its real value. Note that the plot is on a log-log scale, as V_A varies across orders of magnitude in our simulations. (B) Estimated drift-effective population size ($\widehat{N}$) across a range of simulations with different levels of additive genetic variance and recombination. Each point denotes the median, with lines denoting the interquartile range. A simple temporal estimate of the effective population size, estimated accounting for the effects of selection, is averaged for each replicate and plotted as a dash. The true value ($N = 1,000$) is shown with the dashed gray line. Population frequencies (without sampling noise) are used in this figure; see Appendix Figure 2.6.3 for an analogous figure calculated with sample frequencies.

tional to the number of coding bases, similar to background selection and other linked selection models (Corbett-Detig et al. 2015; McVicker et al. 2009; Rockman et al. 2010). Thus, we could write total $V_A(1) = v_A(1) \sum_{i=1}^{B} w_{\text{CBP},i}$ where $w_{\text{CBP},i}$ is the number of coding or exonic basepairs in window i (this could be any quantifiable annotation feature in the window), and $W_{\text{CBP}} = \sum_{i=1}^{B} w_{\text{BP}}, i$ is the total number of coding bases in the genome. With window i contributing $v_A(1) w_{\text{CBP},i}$ to the additive genetic variance and having map length R_i, we now define $\vec{q}$, $\vec{a}$, and $\vec{b}$ as having elements given by the equations

$$\Sigma_{t,s,i} = \frac{\widehat{V_A(1)}}{2} \frac{w_{\text{CBP},i}\ SSH_n(s)}{W_{\text{CBP}}\ SSH_n(1)} \mathcal{A}(R_i, t, s) + \widehat{F}\delta_{t,s} + \varepsilon, \quad \text{for } s \geq t. \tag{2.23}$$

Again, the parameters of this model, $\widehat{V_A(1)}$ and $\widehat{N}$, can be estimated with least squares. When analyzing genome-wide data, these various models could potentially be compared to an out-of-sample procedure, using inferred parameters to estimate the mean-squared predictive error between the two models for the remaining windows (Elyashiv et al. 2016). The confidence intervals for our method-of-moments estimates could be obtained through bootstrapping genomic windows since the errors are not identically and independently distributed.

2.3.1 Estimating the proportion of variance in frequency change due to linked selection

We can also estimate what fraction of allele frequency change over t generations ($\mathrm{Var}(p_t - p_0)/t$) is due to linked selection acting to perturb the frequency trajectories of neutral alleles. We have developed two approaches: first, a more conservative approach that considers only the contribution of selection to the temporal autocovariance, and second, a more exact approach that uses the estimated effective population size to include the contribution of selection to both variances and covariances of allele frequency change.

First, a simple estimate of the total fraction of the variance in allele frequency change (G) caused by linked selection is

$$G = \frac{\sum_{t \neq s} \mathrm{Cov}(\Delta p_t, \Delta p_s)}{\mathrm{Var}(p_t - p_0)}. \tag{2.24}$$

However, this estimator is conservative because it ignores the contribution that linked selection has on the variance in allele frequency change across a single generation (the $\mathrm{Var}(\Delta_H p_t)$ term in Equation 2.2). If we include these variance terms, we have a less-conservative estimator we call G',

$$\begin{aligned} G' &= \frac{\sum_{t \neq s} \mathrm{Cov}(\Delta p_t, \Delta p_s) + \sum_{i=1}^{t} \mathrm{Var}(\Delta_H p_i)}{\mathrm{Var}(p_t - p_0)} \\ &= 1 - \frac{\sum_{i=1}^{t} \mathrm{Var}(\Delta_M p_i) + \sum_{i=1}^{t} \mathrm{Var}(\Delta_N p_i)}{\mathrm{Var}(p_t - p_0)}. \end{aligned} \tag{2.25}$$

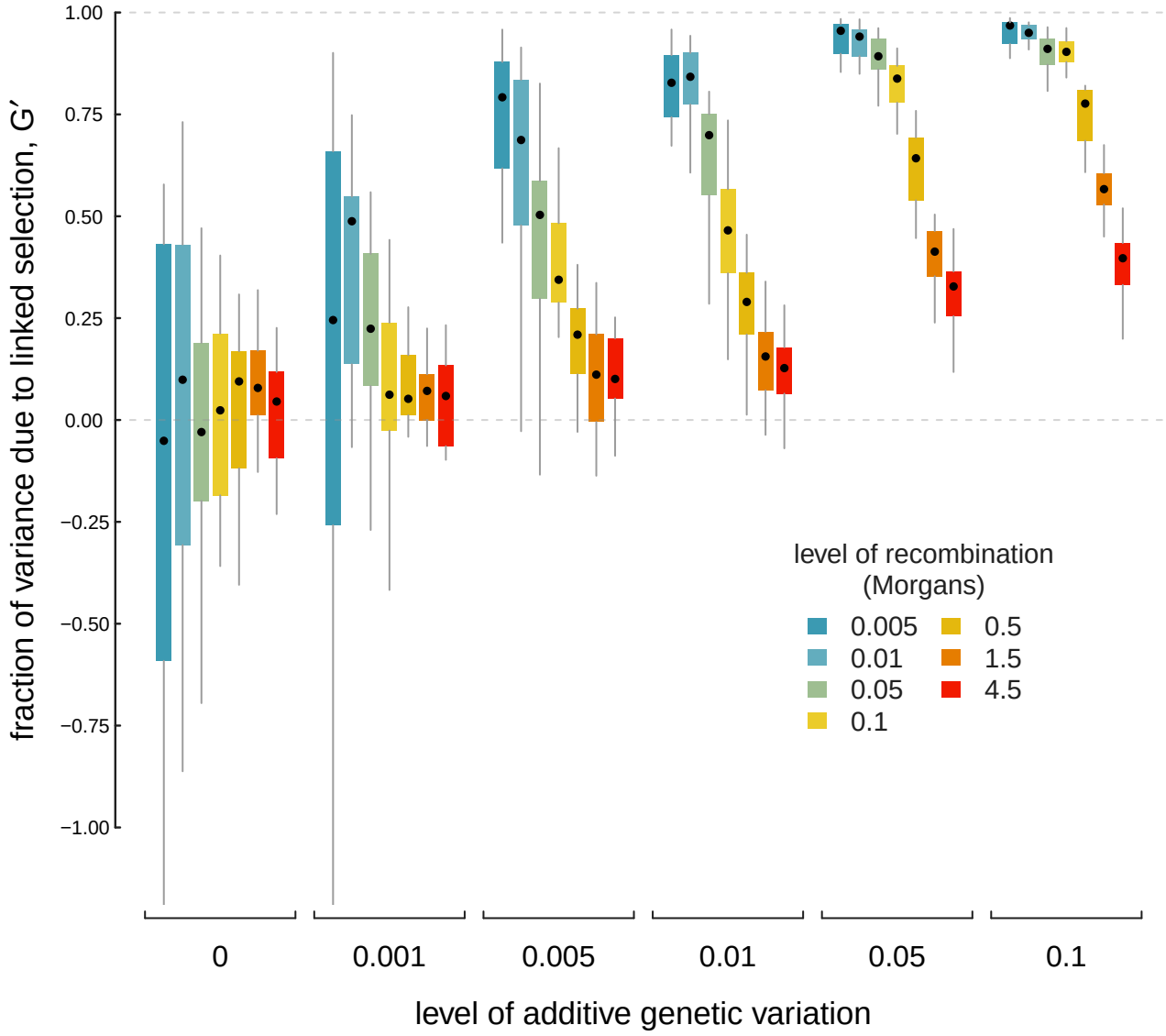

Figure 2.6: The proportion of total variance in allele frequency changes caused by linked selection, G', across a variety of different levels of additive genetic variance (each group of boxplots), and different levels of recombination (each colored boxplot within a group). Each boxplot shows the spread of values across 20 replicates, with $\widehat{N}$ being calculated across each replicate.

We can think of the numerator of the second term in Equation (2.25) as the variance in allele frequency change in a Wright–Fisher population without selection. Recall that under a Wright–Fisher model, the standardized variance across t generations is approximately $(1 - \exp(-t/2N)) \approx p_0(1 - p_0) \times t/2N$, where this second approximation works for short time spans ($t/2N \ll 1$). This suggests that we can use our method-of-moments estimate of the effective population size without the effects of selection, $\widehat{N}$, and compare the fraction of standardized variance we expect under this rate of drift to the empirical standardized variance,

$$G' = 1 - \frac{t\mathbb{E}(p_0(1-p_0))}{2\widehat{N}\,\mathrm{Var}(p_t - p_0)}. \tag{2.26}$$

Figure 2.6 shows the estimated G' from the method-of-moment $\widehat{N}$ estimates using 20 replicates of simulated data. We learn three important points about our G' estimator. First, for low V_A, or $V_A = 0$, the estimator is quite noisy. Second, although the signal can be noisy for low V_A, the relationship between G' and level of recombination is consistent with selection affecting the total variance in allele frequency changes across the genome. Finally, this suggests that a negative relationship between G' and recombination rate, calculated in windows across the genome, is a robust signal of linked selection impacting the total variance in allele frequency change. Furthermore, we would expect a positive relationship between the number of coding basepairs per window (when such information is available) and G', which could serve as another robust signal of linked selection impacting the total variance in allele frequency change.

2.3.2 Fluctuating Selection

Thus far we have assumed that fitness effect sizes are constant through time, that is $\alpha_{t,l} = \alpha_{s,l}$, for all t, s. In natural populations, changes in the environment or composition of the population may cause these effect sizes to change through time, due to changing selection pressures and changes in the epistatic environment experienced by alleles. If these changes occur within the timeframe of recorded allele frequency changes, the levels of temporal autocovariance will differ from the levels predicted from our directional selection theory.

However, from Equation (2.6) we can see that the magnitude of temporal autocovariance is determined in large part by $\mathbb{E}(\alpha_t \alpha_s)$.

Here, we discuss how temporal autocovariance behaves under an example of strong fluctuating selection: when selection on a trait changes direction at some point. Specifically, we change the fitness function $w(z_i) = e^{z_i}$ to $w(z_i) = e^{-z_i}$ after some timepoint t^*; this is equivalent to changing $\alpha_{s,l} = -\alpha_{t,l}$ iff $s \geq t^*$, and $\alpha_{s,l} = \alpha_{t,l}$ otherwise for all other $s < t^*$.

When such a strong change in the direction of selection occurs, the temporal autocovariance between timepoints before and after the change becomes negative, since temporal autocovariance is determined by the product $\alpha_t \alpha_s$ for $t \neq s$ (here we are holding effects constant across loci). We have validated this using the same simulation procedure as described in Section 2.2.4, except on generation 15 we reverse the direction of selection on the trait by changing the fitness function $w(z) = e^z$ to $w(z) = e^{-z}$. In Figure 2.7A, we show the temporal autocovariance $\mathrm{Cov}(\Delta p_5, \Delta p_s)$ for varying s along the x-axis (in this case, $V_a = 0.05$, $R = 0.1$, and $L = 500$). During the first five generations, the temporal autocovariance behaves as it does under directional selection, decaying due to the decrease in additive genetic variance and the breakdown of linkage disequilibrium. Then, on the 15^{th} generation, the direction of selection on the trait with breeding value z_i reverses and temporal autocovariance becomes negative since $\alpha_{s,l}\alpha_{t,l} < 0$ for all $s \geq t^*$ and $t < t^*$. Under this simple flip in the direction of selection pressure, the genic variance, $V_a(s) = 2\alpha^2 \sum_l p_{s,l}(1 - p_{s,l})$, in the expressions for the temporal autocovariance can be replaced with $V_a(s) = 2\alpha_s \alpha_t \sum_l p_{s,l}(1 - p_{s,l})$, akin to a genetic/genic covariance. In Figure 2.7A, the gray line is our predicted level of temporal autocovariance proportional to $V_A \mathcal{A}(R, t, s)$ given by Equation (2.8) before generation 15, and after generation it is proportional to $-V_A \mathcal{A}(R, t, s)$ (using the empirical additive genetic variance). Note, however, that the dynamics of additive genetic variance under fluctuating selection are more complex than under directional selection. Whereas under directional selection the genetic variance decays as selection proceeds, under fluctuating selection there can be a transient increase in the additive genetic variance (seen in Figure 2.7A between gener-

ations 15-24). This transient inflation of the additive genetic variance is caused by the increase in the heterozygosity of haplotypes that had experienced reduced heterozygosity due to directional selection. With the direction of selection reversed, previously selected haplotypes move to more intermediate frequencies, which increases the additive genetic variance until selection proceeds and this variance decays (generations 25 and onwards). Overall, the dynamics of additive genetic variance under fluctuating selection are more complicated than under directional selection which makes inference using our sum of site heterozygosity approximation infeasible.

Since fluctuating selection can create *negative* temporal autocovariance, the total amount of autocovariance over time (e.g. $\sum_{t \neq s} \mathrm{Cov}(\Delta p_t, \Delta p_s)$) can misrepresent the actual amount that linked selection is affecting allele frequencies on shorter timescales. This, in turn, leads our estimator G, for the fraction of variance in allele frequency due to linked selection, to underestimate the total contribution of linked selection to variation in allele frequencies over the time period. We show an example of this in Figure 2.7B, which depicts the total variance in allele frequency change $\mathrm{Var}(p_t - p_0)/t$ through time, partitioned into variance and covariance components and colored according to whether the generation was before and after the reverse in directional selection. The covariances $\sum_{t \neq s} \mathrm{Cov}(\Delta p_t, \Delta p_s)$ increase as they would under directional selection, but after generation 15, the contribution of covariance begins to decrease as negative autocovariances accumulate. By generation 20, the total covariance terms have a net negative effect, and actually act to decrease the total variance $\mathrm{Var}(p_t - p_0)/t$ for a few generations below the constant level expected under drift and heritable variation.

To more fully capture the contribution of selection allele frequency change, we modify G, using the absolute value of the covariances,

$$G_{abs} = \frac{\sum_{t \neq s} |\mathrm{Cov}(\Delta p_t, \Delta p_s)|}{\mathrm{Var}(p_t - p_0)} \tag{2.27}$$

which prevents negative temporal autocovariances from canceling out the effects of positive temporal autocovariances, since both are a reflection of linked selection acting on neutral allele frequency changes. We show G_{abs} in Figure 2.7C, where even after the

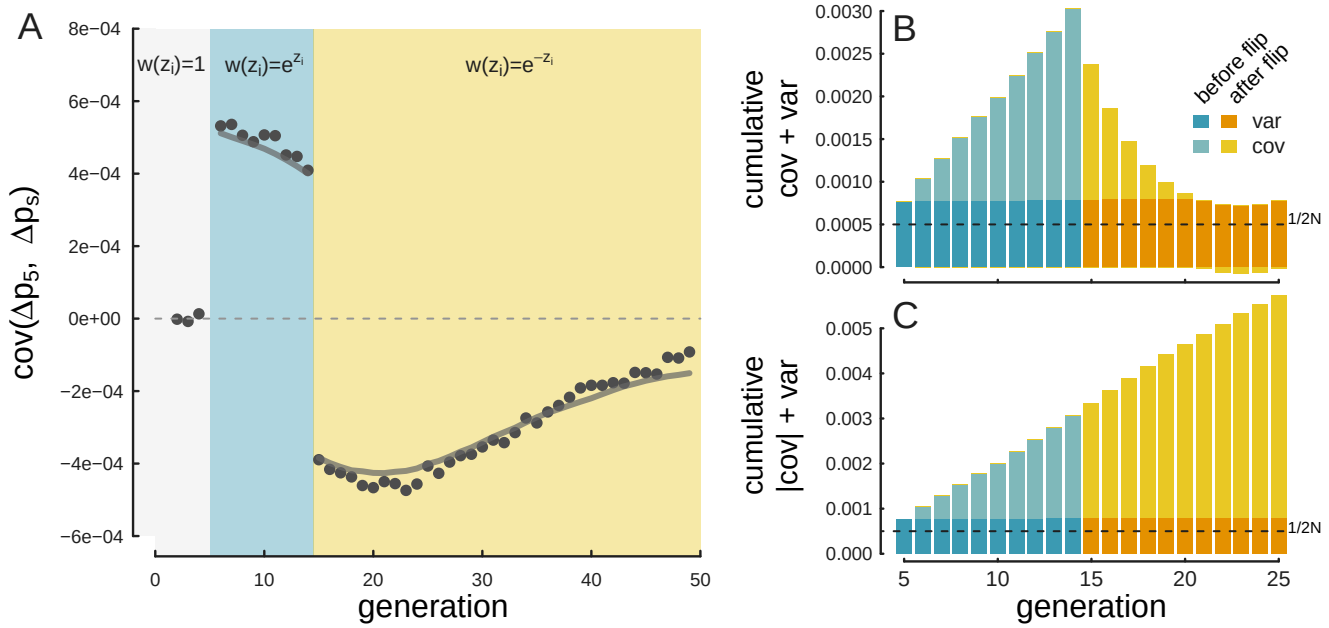

Figure 2.7: A: The covariance $\mathrm{Cov}(\Delta p_5, \Delta p_s)$, where s is varied on the x-axis, for $V_a = 0.05$, $R = 0.1$, and $L = 500$ averaged over 100 replicates. Selection begins in generation 5 (with the fitness function $w(z_i) = e^{z_i}$) and on generation 15 the direction of selection flips (and the fitness function becomes $w(z_i) = e^{-z_i}$). The gray line shows our directional selection temporal autocovariance prediction modified so that after the flip in the direction the trait is selected, we plot the *negative* theoretical level of temporal autocovariance. B: The average cumulative variance and covariances through the generations for the same simulation parameters, with the height of the bar representing the total cumulative variation $\mathrm{Var}(p_t - p_0)/t$. Since the direction of selection flips, the covariances terms after generation 15 become negative, leading the total variance to decrease (the negative covariances are plotted below the x-axis line). After generation 21, the total covariance is negative, leading the total variance to dip below the level of variance alone (determined by drift and heritable fitness variation). The dark gray dashed line shows the level of variance expected by drift alone ($^{\mathrm{Var}(p_t - p_0)}/_t = {}^1/_{2N}$). C: The effect of using the absolute value of covariance, which prevents the negative autocovariances from canceling out the effects of other covariances before the direction of selection changed.

change in the directional selection we see a steady accumulation of covariance contributing to total variance $\mathrm{Var}(p_t - p_0)/t$. This also suggests one plausible way to check for genomically wide-spread fluctuating selection would be to test if $G_{abs} > G$. However, we note that in contrast to our simulations, it is likely that in natural populations only a subset of alleles change their relationship to fitness. This may act to dampen the magnitude of, but not completely reverse the direction of genome-wide temporal autocovariance, and so different approaches may be needed to identify fluctuations.

2.4 Discussion

Currently, the prevailing empirical approach to studying linked selection relies on using samples from a single timepoint and modeling the patterns of diversity subject to different functional constraints and in different recombination environments. The early theoretical work underpinning empirical analyses of linked selection's effects on diversity were primarily full sweep, recurrent hitchhiking models, where beneficial mutations arise in the population and then sweep to fixation (Kaplan et al. 1989; Maynard Smith and Haigh 1974; Stephan et al. 1992). Furthermore, by looking at the patterns of diversity around amino acid substitutions or the site frequency spectrum in low recombination regions, researchers have teased apart the effects of background selection and hitchhiking in *Drosophila* (Begun et al. 2007; Elyashiv et al. 2016), humans (Hernandez et al. 2011; McVicker et al. 2009), and some plants species (Beissinger et al. 2016; Nordborg et al. 2005b; Schmid et al. 2005; Williamson et al. 2014). Yet, as other theoretical models of hitchhiking incorporating changes in the environment (Kopp and Hermisson 2007, 2009a,b), sweeps originating from standing variation (Hermisson and Pennings 2005), and multiple competing beneficial haplotypes (Pennings and Hermisson 2006) have been developed, it has become rather more difficult to detect the signal of these hitchhiking phenomenon in empirical data. We have proposed here that temporal autocovariance offers a unique and measurable signal of linked selection over shorter timescales that provides a fuller picture of the ways in which genome-wide diversity has affected by these other hitchhiking phenomena.

2.4.1 Empirical Applications and Future Directions

Here, we've developed expressions for temporal variances and autocovariances, and applied these to model temporal variances and covariances during directional selection on a trait. We have demonstrated how one can (1) estimate the additive genetic variance for fitness and the drift-effective population size, (2) estimate the fraction of variance in allele frequency change due to linked selection, and (3) evaluate whether fluctuating selection is operating from these temporal variances and autocovariances. However we recognize a series of limitations and difficulties when applying these methods to empirical data and natural populations.

First, one difficulty with temporal sampling of natural populations is the risk that the genetic composition may change drastically due to migration or biased sampling across timepoints. Since our theory assumes a constant-sized and isolated population, migration into the sampled population presents a serious potential confounder. For example, seasonal migration could create an influx of new alleles that could at best dampen signals of directional selection across seasons, or at worst create a signal of artificial covariance between like seasons. Similar biases could occur if a sampling method incidentally preferred certain subgroups in a stratified population. This could occur, for example, if individuals differ in some behavior affecting their likelihood of being sampled across different temporal environments, which could cause spurious covariances. While such sampling issues and migration might be able to be detected *post hoc* from exploratory data analysis approaches like PCA, studying isolated natural populations and carefully designing sampling schemes would lead to the best inference. Importantly, the effects of gene flow and other temporal inhomogeneities could differ across recombination environments, as among population differentiation will be more pronounced in regions of low recombination and high functional density (Burri 2017; Keinan and Reich 2010; Nachman and Payseur 2012). In situations where migration is a factor, one way forward might be to study the contribution of linked selection after partitioning out the effects of gene flow across recombinational and functional environments by extending admixture inference approaches that estimate the genome-wide effect of drift and admixture.

Second, our method-of-moments approach relies on assuming we can approximate the dynamics of the decay of the additive genetic variance that was present at a reference timepoint by using the observed changes in sum of site heterozygosity in a region as a proxy for its decay. While we have shown this model works under directional selection in a relatively idealized setting, inference in natural populations may be complicated by changes in the environment that induce the effect sizes across loci to vary across timepoints. While our fluctuating selection results show that our directional selection theory extends to changes in the direction of selection with minor adjustments (e.g. Figure 2.7), having the effect sizes vary across each generation would complicate the dynamics of additive genetic variance through time and make inference of V_A difficult. Similarly, we assume that effect sizes are constant across sites. Variance in effect sizes across a region will not bias our results unless there is covariance between effect size and local recombination rate. Further work is required to develop statistical methods to test for violations of our assumptions about effect sizes remaining constant across time, and to potentially incorporate these complications into inference.

Along similar lines, we have focused on directional selection under a multiplicative model. However, selection experiments, a natural place to apply our method, often use truncation selection, which generates systematic epistasis for fitness and thus linkage disequilibria among loci (Bürger 2000; Walsh and Lynch 2018). Similarly, in natural populations stabilizing selection will act on many traits, which can also generate LD among loci. These selective processes will act to rapidly reduce the additive genetic variance for fitness across time, especially in low recombination regions, and to reduce the initial additive genetic variance in low recombination regions. Simulating the effect of truncation selection and stabilizing selection on temporal covariances in allele frequencies seems a useful direction. Our model may prove to be a useful null model of selection that the complications of epistasis and different dynamics of the additive genetic variance could be tested against.

Finally, while we demonstrate that our method-of-moments estimation approach is simple and leads to unbiased estimators, we see opportunities for simple extensions and

other inference procedures. Differences in recombination rates and coding density are relatively easily accommodated (Equation 2.23). In fitting our model we assumed a parametric form to the initial LD between neutral and selected loci; however, in practice the initial linkage disequilibria between neutral polymorphisms and putatively functional sites could be estimated empirically. Using the empirical LDs in Equation (2.23) could make the inference somewhat analogous to LD Score regression (Bulik-Sullivan et al. 2015). The LD Score of a SNP is simply the sum of the R^2's of the focal SNP to all SNPs within some large physical genomic window, which could be used in place of the integral in Equation (2.10). Using this equation, V_A could be estimated by regressing the temporal covariance of a SNP on its LD Score. An alternate approach would be to use likelihood methods to model each neutral site's frequency changes using the set of pairwise linkage disequilibria and recombination distances between the neutral site and all neighboring polymorphic sites. Then, genome-wide or region-wide estimates could be found via composite likelihood methods, in a similar manner to McVicker et al. (2009) and Elyashiv et al. (2016). Furthermore, one could include different V_A parameters for neighboring polymorphic sites with specific functional annotations, such as those in genic regions, introns, exons, etc. to see how different classes of sites contribute to the additive genetic variance for fitness. Our hope is that statistical methods to quantify the effects of linked selection over short timescales will improve and be combined with measures of phenotypic change, leading to a more synthetic view of how selection on ecological timescales occurs at the genetic and phenotypic levels.

As the number of empirical temporal genomic studies continue to increase, it is worth mentioning how our study of temporal autocovariance suggests a few ways to optimize experimental design to increase the power to differentiate the effects of selection from drift. First, one should ideally sample frequencies from consecutive generations for at least some timepoints during the duration of the experiment. This is because the variance in allele frequency change $\mathrm{Var}(\Delta p_t)$ between adjacent generations is only impacted by the heritable variance in offspring number, $\mathrm{Var}(\Delta_H p_t)$ (see Equation 2.2), and not by the accumulation of temporal autocovariance terms (e.g. Equation 2.3); this allows for more

accurate estimates of G. In cases where a long study duration is needed but sequencing is limited to only a subset of generations, a mixed duration sampling design, such as sampling generations 1 through 4, and then 10 through 14, and so forth could serve as a compromise. Second, as described in Appendix Section 2.6.9, the shared sampling noise between adjacent timepoints creates a negative bias in autocovariance that must be corrected for. As described in Equations (2.98) and (2.99), we can estimate this bias from data, but this introduces additional uncertainty into our parameter estimates. In cases where the experimenter suspects *a priori* that fluctuating selection is occurring, e.g. between two seasons, we recommend at least two temporal samples per season. This allows one to differentiate negative covariance occurring from the bias correction procedure underestimating bias from negative covariance caused by fluctuating selection through comparing non-adjacent timepoints that differ in season. Finally, once can directly remove the effects of the technical sampling noise created by variation in sequencing by dividing up temporal samples and barcoding them into two groups (e.g. A and B). Then, the sample covariance estimate $\mathrm{Cov}(\Delta p_{t,A}, p_{s,B})$ does not share the technical sampling noise, reducing the bias (but note some bias remains due to the sampling process where individuals are sampled from the population.)

2.4.2 Connecting Temporal Linked Selection with Single Timepoint Studies

Our goal in this paper is to suggest that quantifying variance and autocovariance using temporal data sets can help us understand the impact linked selection has across the genome on short timescales, which supplements our current view informed mainly by single timepoint studies. A range of approaches to estimate the parameters and impact of models of linked selection from a single contemporary timepoint have been developed (Begun and Aquadro 1992; Elyashiv et al. 2016; Hudson 1994; McVicker et al. 2009; Sella et al. 2009; Wiehe and Stephan 1993). These estimates necessarily reflect linked selection over tens to hundreds of thousands of generations. One question is whether these estimates of the proportion of allele frequency change due to linked selection should line up with those over shorter time periods? Some forms of linked selection may be fairly uniform

over time, whereas rare, strong sweeps will have a huge impact on long-term patterns of variation but may be hard to catch in temporal data. Conversely, as we discuss below, fluctuating selection may lead to stronger signals of linked selection on short timescales than seen in long-term snapshots.

Studies of contemporary data have revealed multiple lines of evidence for the effect of linked selection in a variety of taxa. If linked selection is pervasive across the genome, diversity could be severely dampened as most sites would be in the vicinity of selected sites, thus reducing the genome-wide level of diversity without leaving strong local signals differentiated from the background. This is one proposed resolution of Lewontin's paradox, the observation that diversity levels occupy a narrow range across taxa with population sizes that vary by orders of magnitude (Gillespie 2001; Leffler et al. 2012; Lewontin 1974; Maynard Smith and Haigh 1974). Elyashiv et al. (2016) estimated a 77 - 89% reduction in neutral diversity due to selection on linked sites in *Drosophila melanogaster*, and concluded that no genomic window was entirely free of the effect of selection. Similarly, Corbett-Detig et al. (2015) has found evidence of a stronger relative reduction in polymorphism due to linked selection in taxa with larger population sizes. However, these reductions fall short of the many orders of magnitude required for linked selection to explain Lewontin's paradox (Coop 2016).

One limitation of these approaches is that they require estimating π_0, the level of diversity in the absence of linked selection, usually from the diversity in high-recombination regions with low gene content. The average genome-wide reduction of diversity can then be judged relative to π_0. Ideally, π_0 would be a measure of the average diversity due entirely to drift and demographic history, i.e. unaffected by heritable fitness variation. However, there are two complications with this. First, as Robertson (1961) first showed, even a site completely unlinked from sites creating heritable fitness variation experiences a reduced effective population size due to the total additive genetic variance for fitness at these unlinked sites, and thus lower diversity (see also Santiago and Caballero 1995). The second complication is that if linked selection is sufficiently strong, the bases used to measure π_0 may not be sufficiently unlinked from fitness-determining sites to plateau to

the Robertson (1961) level of diversity, a known potential limitation (Coop 2016; Elyashiv et al. 2016). Overall, the empirical studies relying on present-day samples from a single timepoint could be underestimating the effects pervasive linked selection has on diversity. If linked selection can be observed over suitable timescales in temporal data, we might be able to disentangle some of these effects. For example, if high recombination regions still show temporal autocovariance in allele frequency change, we would have evidence that even these regions are not free of the effect of linked selection and we might be able to estimate its long term impact on levels of diversity.

Temporally or spatially fluctuating selection has long been discussed as an explanation for abundant, rapid phenotypic adaptation over short timescales, yet over longer timescales both phenotypic changes and molecular evolution between taxa are slow (Gingerich 1983; Hendry and Kinnison 1999; Messer et al. 2016). However, most of our approaches to population genomic data are built on simple models with constant selection pressures, as typically we have not had the data to move beyond these models (Messer et al. 2016). Currently, many approaches to quantify the impact of linked selection due to hitchhiking assume classic sweeps, where a consistent selection pressure ends in the fixation of a beneficial allele (Hernandez et al. 2011; Sella et al. 2009; Wiehe and Stephan 1993). However, fluctuating selection can have a larger effect on reducing diversity than classic sweeps (Barton 2000) depending on the timescales over which such fluctuations occur. In fact as Barton (2000) points out, the total effect of classic Maynard-Smith and Haigh-type sweeps on diversity is limited by the relatively slow rate of substitutions. We show that when the direction of selection on a trait abruptly reverses, this creates negative autocovariance between the allele frequency changes before and after the reverse in direction. We can observe the shift by plotting autocovariances over time and noting when they become negative, indicating a negative additive genetic covariance between fitness at two timepoints. Here we assume a simple form of fluctuating selection: where selection pressures on all of our sites flip at some timepoint. In reality, selection pressures will change on only some traits, and some of the genetic response will be constrained by pleiotropy, thus only some proportion of the additive genetic variance will change. Still, we expect

some level of negative covariance after a reversal in the direction of selection, and there is additional signal of fluctuating selection by comparing how the strength of temporal autocovariance varies with recombination and the initial level of linkage disequilibrium in the genome.

2.4.3 Connecting Estimates of V_A from Temporal Genomic Data and Quantitative Genetic Studies

The temporal covariance of allele frequencies potentially offers a way to estimate the additive genetic variance for fitness, as illustrated by our method-of-moments approach across genomic windows. The additive genetic variance for fitness can, like any other trait, be estimated through quantitative genetics methods, which exploit the phenotypic resemblance between relatives and their known kinship coefficients (Kruuk 2004; Shaw and Shaw 2013; see Hendry et al. 2018 for a review), and these methods have been applied to estimate the additive genetic variance for fitness from natural populations (Burt 1995; Mousseau and Roff 1987). Ideally, one could reconcile quantitative genetic measures of fitness variance with estimates from allele frequency covariance. For example, Charlesworth (2015) undertook a similar analysis in *Drosophila melanogaster*, comparing population genetic estimates of fitness variance to quantitative genetics estimates, highlighting a discordance potentially consistent with undetected large-effect alleles that are likely maintained by some form of balancing selection. By allowing us to directly measure fitness variation from population genetic data over very short timescales, temporal data could help untangle the causes of this discordance. A natural extension of this would be to see which regions contain the greatest inferred levels of additive genetic variance for fitness, and test for functional covariates such as the number of coding bases, etc. Whereas previous temporal studies have focused on finding loci under selection, inferring the level of additive genetic variance could provide a more complete view of how much selection operates over short timescales.

2.4.4 Concluding Thoughts

With temporal data we can directly partition the total variance in allele frequency change across generations, $\mathrm{Var}(p_t - p_0)$ into components according to the underlying process governing their dynamics: drift and linked selection. Since the trajectory of a neutrally drifting polymorphism does not autocovary, evidence of temporal autocovariance across neutral sites in a closed population is consistent with linked selection perturbing these sites' trajectories. If we consider drift to be the process by which non-heritable variation in reproductive success and Mendelian segregation cause allele frequencies to change, then this is estimable from and separable from the effects of linked selection using temporal data. This helps frame the long-running debate about the roles neutral drift and linked selection have in allele frequency dynamics into a problem that can potentially be directly quantified by the contribution of each distinct process with temporal data.

2.5 Code and Data Availability

All code and simulation data to reproduce these results are available on GitHub at `https://github.com/vsbuffalo/tempautocov`.

2.6 Appendix

2.6.1 Decomposition of Allele Frequency Change

This decomposition of *neutral* allele frequency change between two consecutive generations is based on that of Santiago and Caballero (1995). We imagine a closed Wright–Fisher population of N diploids, where each diploid i contributes $k_i \sim \text{Multinom}(f_i/N, 2N)$ gametes to the next generation. We assume that the population size is constant, such that one diploid begets one diploid and thus $\mathbb{E}_i(f_i) = 1$. The neutral allele frequency in the next generation can be thought of as each of the N parents passing their average genotype $x_i/2$ (where $x_i \in \{0, 1, 2\}$ is the number of tracked neutral alleles individual i carries) to their k_i gametes, plus a random Mendelian deviation $b_{ij} \in \{0, -1/2, 1/2\}$ to each offspring j. Then, the frequency in the next generation can be written as

$$p_1 = \frac{1}{N} \sum_{i=1}^{N} \left(k_i \frac{x_i}{2} + \sum_{j=1}^{k_i} b_{ij} \right) \tag{2.28}$$

where $b_{ij} = \delta_{x_i,1}(1/2 - B_j)$, $B_j \sim \text{Bernoulli}(1/2)$ and $\delta_{x_i,1}$ is an indicator function that is one when the individual i is a heterozygote (i.e. $x_i = 1$), and zero otherwise.

If we further decompose the number of offspring of individual i into the genetic and non-genetic contributions, $k_i = f_i + d_i$, then

$$\begin{aligned} p_1 &= \frac{1}{N} \sum_{i=1}^{N} \left((f_i + d_i) \frac{x_i}{2} + \sum_{j=1}^{k_i} b_{ij} \right) \\ &= \frac{1}{2N} \sum_{i=1}^{N} f_i x_i + \frac{1}{2N} \sum_{i=1}^{N} d_i x_i + \frac{1}{N} \sum_{i=1}^{N} \sum_{j=1}^{k_i} b_{ij} \end{aligned} \tag{2.29}$$

and the change of the neutral allele's frequency is the difference $\Delta p = p_1 - p_0$ where $p_0 = 1/2N \sum_{i=1}^{N} x_i$. Then,

Table 2.1: Notation

Symbol	Usage
p_t	Allele frequency in generation/timepoint t
Δp_t	Allele frequency change between generations $t+1$ and t, $\Delta p_t = p_{t+1} - p_t$
$\Delta_{N} p_t$	Frequency change due to non-heritable variation in fitness, (2.1), (2.2)
$\Delta_{M} p_t$	Frequency change due to Mendelian segregation, (2.1), (2.2)
$\Delta_{H} p_t$	Frequency change due to heritable differences, (2.1), (2.2)
N	Census population size of breeding individuals
N_e	Effect population size
f_i	Fitness (expected number of offspring) of individual i, (2.28)
$\alpha_{t,l}$	Effect size in generation t and locus l, (2.5), (2.36)
L	Total number of loci impacting fitness, (2.5)
$g_{i,l} \in \{0,1,2\}$	Individual i's gene count at locus l, (2.37)
$x_i \in \{0,1,2\}$	Individual i's neutral gene count at the tracked neutral site, (2.5), (2.37), (2.38)
$D_{t,l}$ or $D'_{t,l}$	Gametic linkage disequilibrium between the tracked neutral site and selected locus l at time t, Supplementary Figure 2.6.2, (2.5), (2.37), (2.38)
$D''_{t,l}$	Non-gametic disequilibrium between the tracked neutral site and selected locus l at time t, Supplementary Figure 2.6.2, (2.5), (2.37), (2.38)
$\mathbb{E}(\mathcal{R}^2_{t,l})$	The squared correlation coefficient of linkage disequilibrium between the tracked neutral site and selected site l at time t, (2.7), (2.44)
r_l	The recombination fraction between the tracked neutral site and selected site l
$V_a(s)$	The additive genic variance, (2.8)
$V_A(s)$	The additive genetic variance, (2.17)
R	The total level of recombination in the region, in Morgans, (2.9) and Figure 2.1
$r(g)$	A mapping function (i.e. Haldane's), which maps a position g to a recombination fraction.
ρ	The population recombination rate, $\rho = 4Nr$, Section 2.2.2
$\mathcal{A}(R,t,s)$	The average linkage disequilibrium in a region of R Morgans, that persisted from generation t to generation s, (2.10)
V_N	The non-heritable variance in offspring number, (2.11)
$SSH(t)$	The sum of site heterozygosity at selected sites time t, (2.13)
$SSH_n(t)$	The sum of site heterozygosity at neutral sites at time t, (2.13)
$ssh_n(t)$	The proportion of sum of site heterozygosity at neutral sites at time t relative to $SSH(1)$, $SSH_n(t)/SSH_n(1)$ (2.15)
z_i	The breeding value of the trait that determines fitness, $z_i = \sum_{i=1}^{L} \alpha g_{i,l}$, see appendix section 2.6.2
$w(z_i)$	The fitness of individual i with fitness function $w(\cdot)$, see appendix section 2.6.2

Table 2.1: Notation, continued

Symbol	Usage
$\mathbf{Q}$	The sample standardized variance-covariance matrix, (2.16)
$Q_{t,s}$	The elements of the observed sample matrix $\mathbf{Q}$, (2.16)
$\mathbf{\Sigma}$	The standardized variance-covariance matrix, based on our theoretical expressions
$\Sigma_{t,s}$	The elements of the standardized variance-covariance matrix, (2.10), (2.11)
$\Delta p_{n,t}$	The allele frequency change at site n between times time $t+1$ and t, (2.16)
τ	The number of allele frequency changes observed, e.g. after sampling for $\tau+1$ timepoints
$V_{a,ssh_n}(t)$	The additive genic variation at time s as approximated by the observed decay in the sum of site heterozygosity at neutral sites, (2.15)
$\mathrm{Var}_i(z_i)$	The variance in trait values taken over individuals, (2.17)
$\widehat{V_A(1)}$	The method-of-moments estimate of the additive genetic variance in the first generation, (2.19), (2.18)
$\widehat{F}$	The method-of-moments estimate of Wright's standardized variance, $F = 1/2N$, (2.19), (2.18)
$\widehat{N}$	The method-of-moments estimate of drift-effective population size, $N = 1/2F$
σ^2	The sampling noise around each element of the sample variance-covariance matrix.
B	The total number of windows after partitioning the genome, (2.22)
w_{textBP}	Width of windows (in basepairs), (2.22)
$v_A(1)$	The average additive genetic variance per basepair
w_{CBP}	Number of coding basepairs in a window, (2.22)
W_{CBP}	Total number of coding basepairs in the genome, (2.23)
G	A conservative measure of the total variance in allele frequency change due to linked selection, (2.24)
G'	An alterate, less conservative measure of the total variance in allele frequnecy change due to linked selection, (2.25)
G_{abs}	A variant of G using the absolute value of covariances, (2.27)

$$\Delta p = p_1 - p_0 = \frac{1}{2N}\sum_{i=1}^{N} f_i x_i + \frac{1}{2N}\sum_{i=1}^{N} d_i x_i + \frac{1}{N}\sum_{i=1}^{N}\sum_{j=1}^{k_i} b_{ij} - \frac{1}{2N}\sum_{i=1}^{N} x_i$$
$$= \underbrace{\frac{1}{2N}\sum_{i=1}^{N} x_i(f_i - 1)}_{\Delta_H p_1} + \underbrace{\frac{1}{2N}\sum_{i=1}^{N} d_i x_i}_{\Delta_N p_1} + \underbrace{\frac{1}{N}\sum_{i=1}^{N}\sum_{j=1}^{k_i} b_{ij}}_{\Delta_M p_1}. \tag{2.30}$$

These d's broadly capture non-heritable variation in an individual's offspring number, with $\mathbb{E}[d_i] = 0$. In a quantitative genetics framework $\mathrm{Var}_i(d_i)$ can include non-genetic variation in the lifetime reproductive success of individuals (V_E), in population genetic models $\mathrm{Var}_i(d_i)$ can accommodate the sampling of parents to form the next generation, e.g. multinomial sampling of individuals from fitnesses (Santiago and Caballero 1995). From now forwards, we assume that variation in these d's is non-heritable. We note that in non-panmictic populations, chance covariances could be created between a neutral polymorphism and environmental component of their phenotype, especially as a population expands its range into new environments that affect the phenotype, and variants "surf" to higher frequencies (Edmonds et al. 2004; Excoffier and Ray 2008; Hallatschek and Nelson 2008).

Note that by construction, the allele frequency change components $\Delta_N p_t$ $\Delta_M p_t$, and $\Delta_H p_t$ are orthogonal within each individual, given the neutral allele frequency x. Partitioning the allele frequency change for an individual i into its components,

$$\Delta p_{t,i} = \underbrace{\frac{1}{2}x_i(f_i - 1)}_{\Delta_H p_{t,i}} + \underbrace{\frac{1}{2}x_i d_i}_{\Delta_N p_{t,i}} + \underbrace{\delta_{x_i,1}(k_i/2 - M(k_i))}_{\Delta_M p_{t,i}} \tag{2.31}$$
$$= \frac{1}{2}x_i(f_i - 1) + \frac{1}{2}x_i d_i + \delta_{x_i,1}(f_i/2 - M(f_i)) + \delta_{x_i,1}(d_i/2 - M(d_i)) \tag{2.32}$$

where $M(n) = \sum_{j=1}^{n} B_j \sim \mathrm{Binom}(n, 1/2)$.

Two random variables X, Y are uncorrelated if $\mathrm{Cov}(X,Y) = \mathbb{E}(XY) - \mathbb{E}(X)\mathbb{E}(Y) = 0$, and are orthogonal if either has an expected value of zero such that $\mathbb{E}(XY) = 0$. We show briefly that taking expectations *over conceptual evolutionary replicates*, the terms are orthogonal. First, the terms $x(f-1)$ and xd are orthogonal (dropping i subscripts),

$$
\begin{aligned}
{}^1\!/_4 \operatorname{Cov}(x(f-1), xd) &= {}^1\!/_4(\mathbb{E}(x^2 d(f-1)) - \mathbb{E}(x(f-1))\mathbb{E}(xd)) \\
&= {}^1\!/_4(\mathbb{E}(x^2)\mathbb{E}(d)\mathbb{E}(f-1) - \mathbb{E}(x)\mathbb{E}(f-1)\mathbb{E}(xd)) \\
&= 0 \qquad (2.33)
\end{aligned}
$$

since $\mathbb{E}(f) = 1$ across evolutionary replicates due to the assumption that population size is constant, and $x \perp f$, as across all evolutionary replicates, there is no dependence between a particular neutral allele an individual carries and their fitness (though in particular replicates, such associations occur). Similarly, for the case $x = 1$ (other cases are all zero, and can be ignored), it can be shown using the law of total expectation that $\operatorname{Cov}(xd, {}^d\!/_2 - M(d)) = 0$ (and likewise with $x(f-1)$ and ${}^f\!/_2 - M(f)$). Note that across individuals within a population, there are weak covariances in their number of offspring as the total number of offspring must sum to N; under a Multinomial offspring distribution, these are of order ${}^1\!/_N$.

2.6.2 Temporal variance and autocovariance under multilocus selection

We assume the phenotype of an individual i has an additive polygenic basis, such that their breeding value is $z_i = \sum_{l=1}^{L} \alpha_{t,l} g_{i,l}$ which deviates around a mean of zero, and $\alpha_{t,l}$ is the additive effect size at locus l in generation t, and $g_{i,l} \in \{0, 1, 2\}$ is individual i's allele count at this locus (note that effect of non-heritable environmental noise affecting the trait is accounted for in the d_i terms above). We impose directional selection on this trait using an exponential fitness function, such that individual i's fitness is $f_i = {}^{w(z_i)}\!/_{\bar{w}} \approx e^{z_i}$ (assuming $\bar{w} \approx 1$). If we assume individuals' phenotypic values do not deviate too far from their mean value of zero, we can approximate f_i as: $f_i \approx 1 + \sum_{l=1}^{L} \alpha_{t,l} g_{i,l}$. Then, we can write the change in neutral allele frequency due to only heritable variation in fitness ($\Delta_H p_t$) as a covariance between fitness and the neutral allele frequency across individuals in generation t,

$$\Delta_{H} p_t = \frac{1}{2N} \sum_{i=1}^{N} x_i \left(f_i - 1\right) \tag{2.34}$$

$$= \frac{1}{2} \operatorname{Cov}_i(x_i, f_i) \tag{2.35}$$

$$= \frac{1}{2} \operatorname{Cov}_i(x_i, \sum_{l=1}^{L} \alpha_{t,l} g_{i,l}) \tag{2.36}$$

which is the is the Robertson-Price covariance (Lynch, Walsh, et al. 1998; Price 1970; Robertson 1966; Walsh and Lynch 2018).

Now, we break up the genotypic value x_i into the contributions of each of the two gametes that formed individual i, $x_i = x'_i + x''_i$, and likewise with the trait locus $g_{i,l} = g'_{i,l} + g''_{i,l}$, where x'_i, x''_i, g'_i, and g''_i are all indicator variables. Expanding out the covariances, we have

$$\begin{aligned}
\Delta_{H} p_t &= \frac{1}{2} \operatorname{Cov}(x'_i + x''_i, \sum_{l=1}^{L} \alpha_{t,l}(g'_{i,l} + g''_{i,l})) \\
&= \frac{1}{2} \left(\operatorname{Cov}(x'_i, \sum_{l=1}^{L} \alpha_{t,l}(g'_{i,l} + g''_{i,l})) + \operatorname{Cov}(x''_i, \sum_{l=1}^{L} \alpha_{t,l}(g'_{i,l} + g''_{i,l})) \right) \\
&= \frac{1}{2} \left(\operatorname{Cov}(x'_i, \sum_{l=1}^{L} \alpha_{t,l} g'_{i,l}) + \operatorname{Cov}(x'_i, \sum_{l=1}^{L} \alpha_{t,l} g''_{i,l}) + \operatorname{Cov}(x''_i, \sum_{l=1}^{L} \alpha_{t,l} g'_{i,l}) + \operatorname{Cov}(x''_i, \sum_{l=1}^{L} \alpha_{t,l} g''_{i,l}) \right).
\end{aligned} \tag{2.37}$$

Each of these covariances is between the neutral allele and a selected allele, either on the same gamete (either maternal or paternal) or across gametes. These covariances can be written as linkage disequilibrium terms,

$$
\begin{aligned}
\Delta_H p_t &= \frac{1}{2}\left(\mathrm{Cov}(x'_i, \sum_{l=1}^{L}\alpha_{t,l}g'_{i,l}) + \mathrm{Cov}(x'_i, \sum_{l=1}^{L}\alpha_{t,l}g''_{i,l}) + \mathrm{Cov}(x''_i, \sum_{l=1}^{L}\alpha_{t,l}g'_{i,l}) + \mathrm{Cov}(x''_i, \sum_{l=1}^{L}\alpha_{t,l}g''_{i,l})\right) \\
&= \frac{1}{2}\left(\sum_{l=1}^{L}\alpha_{t,l}\,\mathrm{Cov}(x'_i, g'_{i,l}) + \sum_{l=1}^{L}\alpha_{t,l}\,\mathrm{Cov}(x'_i, g''_{i,l}) + \sum_{l=1}^{L}\alpha_{t,l}\,\mathrm{Cov}(x''_i, g'_{i,l}) + \sum_{l=1}^{L}\alpha_{t,l}\,\mathrm{Cov}(x''_i, g''_{i,l})\right) \\
&= \frac{1}{2}\left(\sum_{l=1}^{L}\alpha_{t,l}D'_l + \sum_{l=1}^{L}\alpha_{t,l}D''_l + \sum_{l=1}^{L}\alpha_{t,l}D''_l + \sum_{l=1}^{L}\alpha_{t,l}D'_l\right) \\
&= \sum_{l=1}^{L}\alpha_{t,l}D'_l + \sum_{l=1}^{L}\alpha_{t,l}D''_l
\end{aligned} \tag{2.38}
$$

where D'_L is the linkage disequilibrium between alleles on the same gamete (the gametic LD), and the D''_l is the across-gamete LD (non-gametic LD); see Weir (1996), p. 121. This equation also appears in Kirkpatrick et al. (2002) (eqn. 10).

We ignore non-gametic linkage disequilibria D''_l as these are weak under random mating, and write the multilocus temporal covariance between the allele frequency changes Δp_t and Δp_s as

$$
\begin{aligned}
\mathrm{Cov}(\Delta p_t, \Delta p_s) &= \mathbb{E}(\Delta p_t \Delta p_s) - \mathbb{E}(\Delta p_t)\mathbb{E}(\Delta p_s) \\
&= \mathbb{E}\left(\sum_{l=1}^{L}\alpha_{t,l}D'_{t,l}\sum_{l=1}^{L}\alpha_{s,l}D'_{s,l}\right) \\
&= \underbrace{\sum_{l=1}^{L}\alpha_{t,l}\alpha_{s,l}\mathbb{E}(D'_{t,l}D'_{s,l})}_{\text{persistence of association to selected site } l} + \underbrace{\sum_{l\neq k}\alpha_{t,k}\alpha_{s,l}\mathbb{E}(D'_{t,k}D'_{s,l})}_{\text{cross-associations between two selected sites } k \text{ and } l}
\end{aligned} \tag{2.39}
$$

since $\mathbb{E}(\Delta p_t) = 0$.

Modeling the dynamics of LD between selected and neutral sites Here, we outline a model of the changes in linkage disequilibria between the focal neutral site and selected sites, which allows us to derive an expression for the first term in Equation (2.39). Typically, models of multilocus selection track the genetic changes in a population by transforming between a representation of haplotype frequencies to a representation

of allele frequencies, linkage disequilibria, and higher-order linkage disequilibria (Barton and Turelli 1987, 1991; Turelli 1988; Turelli and Barton 1990). We for the moment avoid the difficulty of a full multilocus treatment by assuming that the linkage between selected sites is loose enough that one selected site's frequency change is independent of the change at other selected sites, e.g. there is no selective interference; this was an assumption in past treatments (Santiago and Caballero 1995, 1998; see Barton 2000 for discussion of this). Specifically, we model the dynamics of the LD between the neutral site and each selected site as they would behave under a single sweep model.

We adapt Barton's (2000) model for LD dynamics during a sweep. We imagine a polymorphic neutral locus has alleles B_1 and B_2 with frequencies p and $1-p$. We partition the allele frequency of B_1 by conditioning on which allele at the selected site (either A_1 or A_2) is carried on the same background, e.g. $P(B_1|A_1)$, and $P(B_1|A_2)$, such that $P(B_1) = P(B_1|A_1)P(A_1) + P(B_1|A_2)P(A_2)$. Then, the linkage disequilibrium between neutral and selected sites can be expressed as $D = P(A_1)P(A_2)(P(B_1|A_1) - P(B_1|A_2)))$. To simplify notation, we denote the frequency of the neutral allele on the different fitness backgrounds at time t by $P(B_1|A_1) = p_t^{(1)}$ and $P(B_1|A_2) = p_t^{(2)}$ and the selected allele at locus l frequency as $p_{t,l}$, we have the LD between the focal neutral site and selected site l at time t is

$$D_{t,l} = p_{t,l}(1 - p_{t,l})(p_t^{(1)} - p_t^{(2)}). \tag{2.40}$$

Selection changes the frequency $p_{t,l}$ through time, and recombination acts to disassociate the neutral allele with its backgrounds. The expected difference $p_t^{(1)} - p_t^{(2)}$ is maintained with probability $(1 - r_l)$ each generation (Barton 2000). If the initial generation is t and the future generation is s ($s > t$), and r_l is the recombination rate between the focal neutral locus and selected site l, this leads to

$$(p_s^{(1)} - p_s^{(2)}) = (p_t^{(1)} - p_t^{(2)})(1 - r_l)^{s-t}. \tag{2.41}$$

Then, we can use this to describe the dynamics of $D_{s,l}$ to generation t,

$$\frac{p_{s,l}(1-p_{s,l})}{p_{s,l}(1-p_{s,l})}(p_s^{(1)}-p_s^{(2)}) = \frac{p_{t,l}(1-p_{t,l})}{p_{t,l}(1-p_{t,l})}(p_t^{(1)}-p_t^{(2)})(1-r)^{s-t}$$
$$\frac{D_{s,l}}{p_{s,l}(1-p_{s,l})} = \frac{D_{t,l}}{p_{t,l}(1-p_{t,l})}(1-r)^{s-t}$$
$$D_{s,l} = D_{t,l}\frac{p_{s,l}(1-p_{s,l})}{p_{t,l}(1-p_{t,l})}(1-r_l)^{s-t} \tag{2.42}$$

(c.f. Stephan et al. 2006, equations (30) and (31)). Now, we can find the expected product $\mathbb{E}(D_{t,l}D_{s,l})$ by multiplying both sides by $D_{t,l}$ and taking expectations. We treat the allele frequency trajectory as deterministic, giving us,

$$D_{t,l}D_{s,l} = D_{t,l}^2\frac{p_{s,l}(1-p_{s,l})}{p_{t,l}(1-p_{t,l})}(1-r_l)^{s-t}$$
$$\mathbb{E}(D_{t,l}D_{s,l}) = \mathbb{E}(D_{t,l}^2)\frac{p_{s,l}(1-p_{s,l})}{p_{t,l}(1-p_{t,l})}(1-r_l)^{s-t}. \tag{2.43}$$

Then, we simplify this by replacing $\mathbb{E}(D_{t,l}^2)$ with $\mathbb{E}(\mathcal{R}_{t,l}^2)p_{t,l}(1-p_{t,l})p_t(1-p_t)$ (where $\mathbb{E}(\mathcal{R}_{t,l})$ is the square of the correlation between the neutral site and selected site l at time t; Hill and Robertson 1968),

$$\begin{aligned}\mathbb{E}(D_{t,l}D_{s,l}) &= \mathbb{E}(D_{t,l}^2)\frac{p_{s,l}(1-p_{s,l})}{p_{t,l}(1-p_{t,l})}(1-r_l)^{s-t}\\ &= \mathbb{E}(\mathcal{R}_{t,l}^2)p_t(1-p_t)p_{t,l}(1-p_{t,l})\frac{p_{s,l}(1-p_{s,l})}{p_{t,l}(1-p_{t,l})}(1-r_l)^{s-t}\\ &= \mathbb{E}(\mathcal{R}_{t,l}^2)p_t(1-p_t)p_{s,l}(1-p_{s,l})(1-r_l)^{s-t}.\end{aligned} \tag{2.44}$$

Returning to Equation (2.39) and replacing the $\mathbb{E}(D_{t,l}D_{s,l})$ terms with our expression above,

$$\mathrm{Cov}(\Delta p_t, \Delta p_s) = \sum_{l=1}^{L}\alpha_{t,l}\alpha_{s,l}\mathbb{E}(\mathcal{R}_{t,l}^2)p_t(1-p_t)p_{s,l}(1-p_{s,l})(1-r_l)^{s-t} \tag{2.45}$$

again ignoring the cross-associations between selected sites. Dividing our temporal covariance by the neutral site's $p_t(1-p_t)$, we can write the multilocus temporal covariance in a standardized form (analogous to Wright's F),

$$\frac{\mathrm{Cov}(\Delta p_t, \Delta p_s)}{p_t(1-p_t)} = \sum_{l=1}^{L} \alpha_{t,l}\alpha_{s,l}p_{s,l}(1-p_{s,l})\mathbb{E}(\mathcal{R}_{t,l}^2)(1-r_l)^{s-t}. \tag{2.46}$$

Using average additive genetic variation We can approximate Equation (2.46) by noticing that the terms $\alpha_{t,l}\alpha_{s,l}p_{s,l}(1-p_{s,l})$ are similar to an additive genic variation if effect sizes remain constant through time. We make that assumption here, writing $\alpha_l := \alpha_{t,l} = \alpha_{s,l}$, leading to

$$\frac{\mathrm{Cov}(\Delta p_t, \Delta p_s)}{p_t(1-p_t)} = \sum_{l=1}^{L} \alpha_l^2 p_{s,l}(1-p_{s,l})\mathbb{E}(\mathcal{R}_{t,l}^2)(1-r_l)^{s-t}. \tag{2.47}$$

We can further simplify this by assuming that there is no covariance between the additive genic variation at a selected site, and the LD between that selected site and the neutral site. We write the additive genic variation at site l at time s as $v_{a,l}(s) = 2\alpha_l^2 p_{s,l}(1-p_{s,l})$, and the average additive genic variation across loci as $\overline{v_a(s)} := {}^{V_a(s)}/_{L} = \frac{1}{L}\sum_l 2\alpha_l^2 p_{s,l}(1-p_{s,l})$. Then, each locus's additive genic variation can be expressed as: $v_{a,l}(s) = \overline{v_a(s)} + \varepsilon_l$. Substituting this, the autocovariance is

$$\begin{aligned}
\frac{\mathrm{Cov}(\Delta p_t, \Delta p_s)}{p_t(1-p_t)} &= \frac{1}{2}\sum_{l=1}^{L} v_{a,l(s)}\mathbb{E}(\mathcal{R}_{t,l}^2)(1-r_l)^{s-t} \\
&= \frac{1}{2}\sum_{l=1}^{L} (\overline{v_a(s)} + \varepsilon_l)\mathbb{E}(\mathcal{R}_{t,l}^2)(1-r_l)^{s-t} \\
&= \frac{1}{2}\underbrace{\overline{v_{a(s)}}}_{\substack{\text{average genic} \\ \text{variation per locus}}} \times \underbrace{\left(\sum_{l=1}^{L}\mathbb{E}(\mathcal{R}_{t,l}^2)(1-r_l)^{s-t}\right)}_{\text{sum of persistence associations}} + \frac{1}{2}\underbrace{\left(\sum_{l=1}^{L}\varepsilon_l\mathbb{E}(\mathcal{R}_{t,l}^2)(1-r_l)^{s-t}\right)}_{\text{effect-association covariation}}.
\end{aligned} \tag{2.48}$$

We assume that this last term, which is non-zero in expectation only if there is covariance between the additive genic variation at a selected site and the expected LD between the selected and the neutral sites is zero. Rewriting the total genic variation as $V_a(s)$,

$$\frac{\mathrm{Cov}(\Delta p_t, \Delta p_s)}{p_t(1-p_t)} = \frac{V_a(s)}{2L}\sum_{l=1}^{L}\mathbb{E}(\mathcal{R}_{t,l}^2)(1-r_l)^{s-t}. \tag{2.49}$$

Continuous approximation to chromosomes Currently, we have treated the positions of the selected sites are fixed, conditioning on knowing that a selected site l has a recombination fraction r_l away from the focal neutral site site. Here, we make a few further assumptions. First, we assume the L selected loci are each independently and identically uniformly distributed along a *continuous* region of R Morgans in length ($g \sim U(-R/2, R/2)$), and we now calculate the covariance at a focal neutral site at the origin by taking expectations over the random positions of these sites. Second, we assume that the LD between the neutral and selected site l only depends on the recombination fraction between the sites. Since g is the genetic distance, the recombination fraction is now provided by a mapping function $r(g)$ that maps genetic distances to recombination fractions. Throughout the paper and in the simulations, we use Haldane's mapping function, $r(g) = \frac{1}{2}(1 - e^{-2|g|})$ (note the absolute value translates positions on $[-R/2, R/2]$ to distances to the focal neutral site). Next, we assume the LD between two sites can be completely determined by the distance between the focal neutral site and a random selected site, allowing us to rewrite $\mathbb{E}(\mathcal{R}^2_{t,l})$ as the function $\mathbb{E}(\mathcal{R}^2_t(r(g)))$. Now, letting $\mathbb{E}_{r_l}(\cdot)$ represent the expectation taken over the random positions of selected sites on the genetic map,

$$\frac{\mathrm{Cov}(\Delta p_t, \Delta p_s)}{p_t(1-p_t)} = \frac{V_a(s)}{2L} \sum_{l=1}^{L} \mathbb{E}_{r_l}\left(\mathbb{E}(\mathcal{R}^2_t(r_l))(1-r_l)^{s-t}\right) \tag{2.50a}$$

$$= \frac{V_a(s)}{2L} \sum_{l=1}^{L} \int_{-R/2}^{R/2} \mathbb{E}(\mathcal{R}^2_t(r(g)))(1-r(g))^{s-t} \frac{1}{R} dg \tag{2.50b}$$

$$= \frac{V_a(s)}{2R} \int_{-R/2}^{R/2} \mathbb{E}(\mathcal{R}^2_t(r(g)))(1-r(g))^{s-t} dg \tag{2.50c}$$

since the $1/L$ cancels with the L from the sum of expectations.

As our trait is neutrally evolving before directional selection starts we use the expected neutral LD, $\mathbb{E}(\mathcal{R}^2) = (10+\rho)/(22+13\rho+\rho^2)$ where $\rho = 4Nr(g)$ (Hill and Robertson 1968; Ohta and Kimura 1969) when t is the first generation selection begins.

2.6.3 The contribution of the rest of the genome to temporal autocovariance at a locus

Additionally, we can consider the impact that other unlinked selected sites have on the neutral allele's frequency trajectory. In equation (2.50c), we are modeling the temporal autocovariance at focal neutral site in a chromosome with total length R. Here, we assume the whole genome can be modeled in a similar fashion, as a single very large chromosome with genetic length C, the entire map length of the genome, and the focal neutral falls in the center of this. Then, we can take a piecewise integral over all linked sites with respect to the recombination fraction (those less than a recombination fraction of one-half away), and all unlinked sites with respect to the genetic distance (those at a recombination fraction of one-half away). Our piece-wise integral gives us

$$\frac{\mathrm{Cov}(\Delta p_t, \Delta p_s)}{p_t(1-p_t)} = \frac{V_a(s)}{2C}\int_{-C/2}^{C/2} \mathbb{E}(\mathcal{R}_t^2(r(g)))(1-r(g))^{s-t}dg \tag{2.51}$$

$$= \frac{V_a(s)}{2C}\left[2\int_0^{g^*} \mathbb{E}(\mathcal{R}_t^2(r(g)))(1-r(g))^{s-t}dg + 2\frac{\mathbb{E}(\mathcal{R}_t^2(1/2))}{2^{s-t}}(C-g(1/2))\right] \tag{2.52}$$

where g^* is the map distance at which a selected site becomes approximately unlinked to the neutral site, e.g. the recombination fraction is $1/2$. As we move away from the neutral site, the first term in the braces accounts for the accumulation of linked selected sites. Eventually, the genetic distance away from the neutral site becomes unlinked and the second term accounts for the contribution of these unlinked sites on both the same chromosome, as well as sites on other chromosomes. Note that here we assume the density of additive genetic variance per Morgan is constant.

As a simple thought experiment, we might ask for what value of M does the contribution from unlinked sites dominate the contribution from linked sites? For $N = 1000$ and assuming that the level of LD is that under mutation-drift-recombination balance (e.g. using the equation of Tomoko Ohta), we plot the relative contributions of linked selected sites (on the focal chromosome) and unlinked selected sites (on other chromosomes) for various spans of the covariance (e.g. $|s-t|$) and the size of the remaining portion of the

genome in Morgans (M) in Figure 2.6.1.

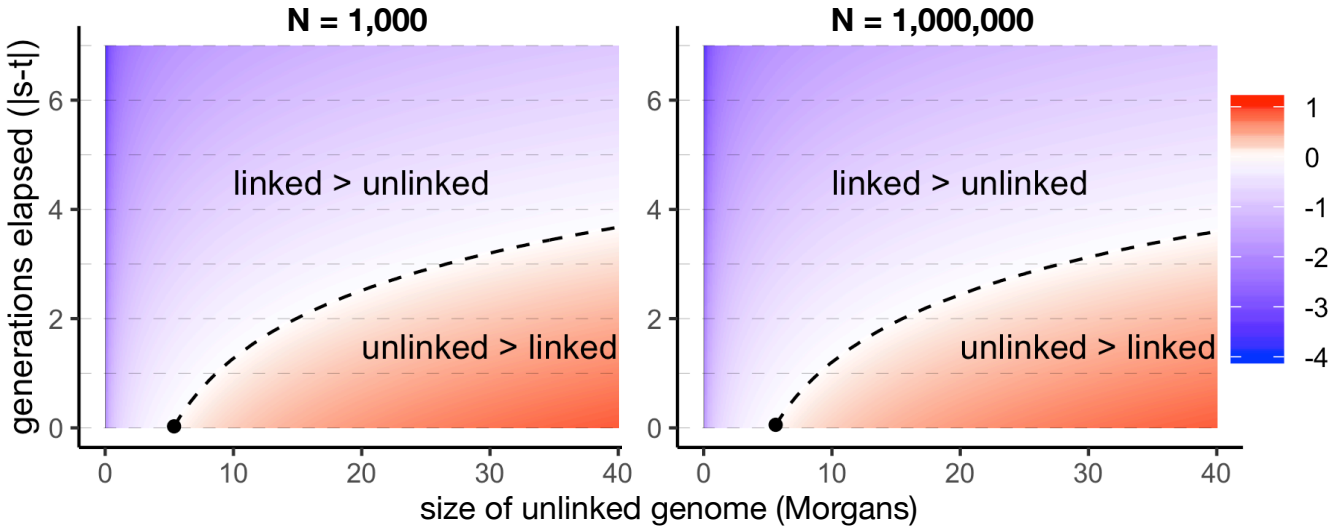

Figure 2.6.1: Here, we show the relative contributions of the linked and unlinked portions of the genome to the temporal autocovariance experienced by a neutral allele, for different generations elapsed (on the x-axis) and different map lengths of the unlinked genome (y-axis) for two different population sizes ($N = 10^3$ and $N = 10^6$). The color gradient is determined by the $\log_{10}$ value of the ratio of unlinked to linked contributions, the terms inside the braces in equation (2.52). The dashed line indicates where the log ratio is zero, e.g. the relative contributions are equal; this was determined numerically. These assume LD is determined by mutation-drift-recombination balance (Tomoko Ohta 1971).

2.6.4 Averaging covariance across multiple loci

Thus far, our covariance assumes that a single neutral site is positioned in the center of a region R Morgans long, with selected sites uniformly distributed along this region. In our simulations, however, we simulate a region that contains many neutral sites which we average over in calculating the temporal autocovariance. In this case, we average over the random distance between a neutral site's position n and a selected site's position g, which is $c = |n - g|$, where $n, g \sim U(0, R)$. This random variable c is distributed according to the triangle distribution, $f(c) = 2(R - c)/R^2$; we replace the uniform PDF in Equation (2.50b) with the triangle density PDF and average over the distance between sites,

$$\frac{\mathbb{E}_n(\mathrm{Cov}(\Delta p_t, \Delta p_s))}{\mathbb{E}_n(p_t(1-p_t))} = \frac{V_a(s)}{2}\int_0^R \mathbb{E}(\mathcal{R}_t^2(r(c)))\,(1-r(c))^{(s-t)}\frac{2(R-c)}{R^2}\,dc \tag{2.53}$$

$$= \frac{V_a(s)}{2}\mathcal{A}(R,t,s) \tag{2.54}$$

where $\mathbb{E}_n(\cdot)$ indicates we take the expectation also over neutral sites, and we use $\mathcal{A}(R,t,s)$ to denote the average linkage disequilibrium between selected and neutral sites that persists from generations t to s ($t \leq s$). Note that in calculating the standardized covariance above, we use a ratio of expectations rather than the expectation of the ratio (Bhatia et al. 2013).

2.6.5 Empirically Calculating the Average LD Persisting Across Generations

In the previous expressions for temporal autocovariance, we stepped through a conceptual model for the average levels of linkage disequilibria between neutral and selected sites that persists across $|s-t|$ generations ($\mathcal{A}(R,t,s)$), where the positions of selected and neutral sites are randomly distributed along a chromosomal region. In systems with a known recombination map and studies where linkage disequilibria can be calculated, we have the recombination fraction $r_{i,j}$ and the pairwise linkage disequilibria $\mathbf{R}^2_{i,j}$ between between two loci i and j (where $\mathbf{R}^2$ is the $M \times M$ matrix of pairwise LD calculated at time t). Since we do not *a priori* know whether a site is selected or not, we sum over all polymorphic M loci, thus characterizing the average linkage disequilibria in a region as

$$\overline{\mathcal{A}(t,s)} = \frac{2}{M(M-1)}\sum_{i=1}^{M}\sum_{j>i}\mathbf{R}^2_{i,j}(1-r_{i,j})^{|t-s|}. \tag{2.55}$$

This sum is the empirical analog to the integral in Equation (2.10).

2.6.6 The Strength of Unlinked and Non-gametic Associations

Here, we characterize the contribution of completely genetically unlinked loci segregating for fitness variation to the change in frequency of our neutral allele. Across evolutionary replicates, there is no expected covariance between the neutral allele an individual carries

and their fitness ($\mathbb{E}(\Delta_{H} p_t) = \mathbb{E}(\mathrm{Cov}(x_i, f_i)) = 0$); rather, for unlinked loci, chance associations are created from the variance around this sampling process of neutral alleles into individuals with varying fitness ($\mathrm{Var}(\Delta_{H} p_t) = \mathrm{Var}(\mathrm{Cov}(x_i, f_i))$). As the neutral allele and fitness variation independently assort themselves into individuals, the chance associations that form have a variance given by $\mathrm{Var}(\mathrm{Cov}_i(x_i, f_i))$. This has the form of the sampling variance of a covariance, which for random variables X and Y is given by Kendall et al. (1994, p. 472),

$$\mathrm{Var}(\mathrm{Cov}(X, Y)) = \frac{(n-1)^2}{n^3}(\mu_{22} - \mu_{11}^2) + \frac{n-1}{n^3}(\mu_{20}\mu_{02} - \mu_{11}^2) \tag{2.56}$$

$$\text{where } \mu_{rs} = \mathbb{E}(X - \mu_X)^r (Y - \mu_Y)^s) \tag{2.57}$$

where μ_X and μ_Y are the means of X and Y respectively, and the variance is taken over conceptual replicate populations and the covariance is calculated over the individuals in a population. Then, applying this to our covariance $\Delta_{H} p_1 = \mathrm{Cov}_i(x_i, f_i)$,

$$\begin{aligned}
\mathrm{Var}(\Delta_{H} p_1) &= {}^1\!/_4 \,\mathrm{Var}(\mathrm{Cov}_i(x_i, f_i)) \\
&= \frac{(N-1)^2}{4N^3}\left(\mathbb{E}[(x_i - p_0)^2 (f_i - 1)^2] - \mathbb{E}[(x_i - p_0)(f_i - 1)]^2\right) + \\
&\quad \frac{N-1}{4N^3}\left(\mathbb{E}[(x_i - p_0)^2]\mathbb{E}[(f_i - 1)^2] - \mathbb{E}[(x_i - p_0)(f_i - 1)]^2\right) \\
&= \frac{(N-1)}{4N^3}\,\mathrm{Var}(x_i)\,\mathrm{Var}(f_i) \\
&\approx \frac{p_0(1-p_0)}{2N}\,\mathrm{Var}(f_i).
\end{aligned} \tag{2.58}$$

Thus the chance covariances that form between the neutral alleles individuals carry and their fitness have a variance proportional to ${}^{\mathrm{Var}(f_i)}\!/_{2N}$.

Non-gametic linkage disequilibrium's contribution to temporal autocovariance Throughout the paper, we ignore the effects of non-gametic linkage disequilibria, $D''_{t,l}$, the disequilibria that occurs between the two gametes (maternal and paternal) at two loci (see Figure 2.6.2 (A) for an illustration of gametic LD D' and non-gametic LD D''). Following Weir's equation for the sampling variance of non-gametic LD $D_{A/B}$ (p. 124,

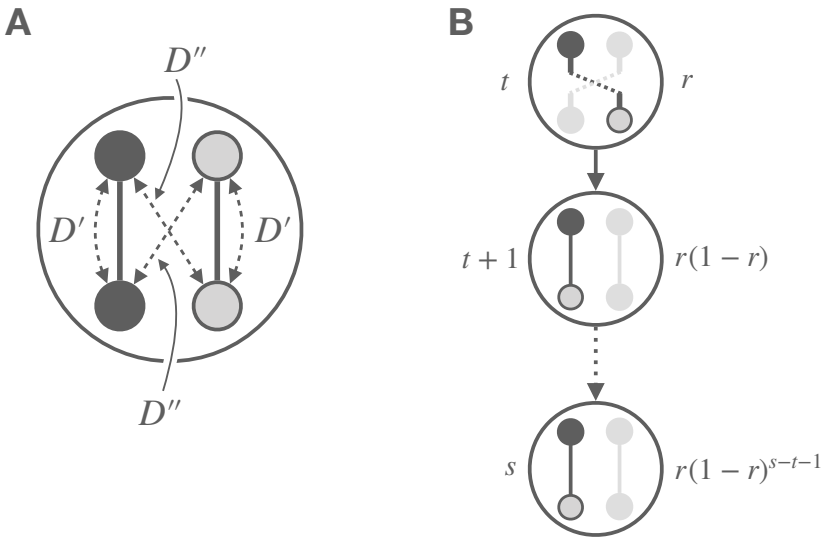

Figure 2.6.2: A: An illustration of gametic (D') and non-gametic (D'') linkage disequilibria between two loci in a diploid. B: An illustration of how non-gametic linkage disequilibria in generation t is converted to gametic linkage disequilibria through recombination (which happens with probability r, the recombination fraction between the two loci), and is then maintained until generation s with probability $(1-r)^{s-t-1}$. The gray loci on the gray gamete indicate the homologous, but not tracked focal association. Overall, the covariance created by the conversion of non-gametic LD to gametic LD is $\mathbb{E}(D'_s D''_t) = r(1-r)^{s-t-1}\mathbb{E}\left((D''_t)^2\right)$.

1996), the chance non-gametic disequilibrium that builds up sampling $2N$ gametes into N individuals is,

$$\mathbb{E}\left((D''_{t,l})^2\right) = \mathrm{Var}(D_{A/B}) = \frac{1}{2N} p_A(1-p_A)p_B(1-p_B). \tag{2.59}$$

Note the similar form to Equation (2.58) as both the unlinked and non-gametic LD arise from the random sampling of alleles at different loci into individuals.

There is no expected covariance between our gametic and non-gametic LD within a generation $\mathbb{E}(D''_{t,l}, D'_{t,l}) = 0$, assuming random mating. However, $\mathbb{E}(D''_{t,l}, D'_{s,l}) > 0$ for $s > t$, as a fraction of the non-gametic LD may be converted into gametic LD in the next generation. Specifically, following Santiago and Caballero (1995), we can write the product of the non-gametic LD in generation t with the gametic LD in generation s as

$$\mathbb{E}(D''_{t,l}, D'_{s,l}) = r(1-r)^{(s-t-1)}\mathbb{E}\left((D''_{t,l})^2\right) \tag{2.60}$$

where a proportion r the non-gametic LD in generation t is converted into gametic LD, and a proportion $(1-r)^{(s-t-1)}$ of this is carried forward unbroken by recombination over the remaining $s-t-1$ generations (see Figure 2.6.2B for an illustration of this process).

In our analysis in the main text, we ignore these terms as $D''_{t,l}$ is expected to be small due to its inverse dependence on N. However, these terms are necessary for the analysis of looser linkage (Santiago and Caballero 1995, 1998).

2.6.7 Connecting our model with the models of Robertson (1961) and Santiago and Caballero (1995, 1998)

Here, we describe the models of Santiago and Caballero (1995, 1998), relating their work on the long-run effective population size experienced by a neutral allele where there is (1) unlinked heritable fitness variation (their 1995 paper), or (2) linkage, where fitness-determining sites are randomly scattered along a chromosome (their 1998 paper). Overall, their models are formulated in a quantitative genetics tradition, where the population genetic dynamics at the selected loci are not explicitly modeled (although these links are made more explicitly in their '98 paper). In contrast, in deriving our expressions for temporal autocovariance and variances, we use a population genetic approach, modeling the dynamics at selected sites (though we simplify from the full multilocus treatment, e.g. we assume selected loci experience independent sweeps and we ignore the LD between selected sites). We show that we can reconcile the two approaches, and demonstrate that the temporal autocovariance expressions we develop in our models are implicit in their model. We also work through their expressions for N_e with heritable variance, because it represents a quite useful result but their original presentation was spread across two papers (and a change in notation).

Santiago and Caballero's 1995 and 1998 models for N_e While our goal in the main text of our paper was to develop expressions for the temporal variances and autocovariances in allele frequency change when there is heritable fitness variation in the population, the goal of both the 1995 and 1998 Santiago and Caballero papers is to derive an expression for the long-run N_e when there is heritable variation for fitness in the population. In their 1995 paper, they find the effective population size for large t (see p.

1018, equation 16) to be

$$N_e = \lim_{t\to\infty} \frac{p_0(1-p_0) - \mathrm{Var}(p_{t-1})}{2(\mathrm{Var}(p_t) - \mathrm{Var}(p_{t-1}))} \tag{2.61}$$

$$N_e = \frac{4N}{2 + V_n + Q^2C^2} \tag{2.62}$$

where C^2 is the heritable variation for fitness (V_A in our notation), and V_n is the non-heritable variation in offspring number (i.e. under a Wright–Fisher model, $V_n \approx 2$). For a neutral locus completely unlinked from fitness variation (the situation first considered by Robertson 1961), $Q = 1 + G/2 + (G/2)^2 + (G/2)^3 + \ldots = \sum_{i=0}^{\infty}(G/2)^i = 2/(2-G)$ (Santiago and Caballero 1995, equation 17). Here, G represents the decay rate of the additive genetic variance associated with a particular haplotype. Note that we've simplified their expressions by assuming no assortative mating, and that we try to follow their notation as closely as possible (consequently, the Q here is unrelated to the $Q_{t,s}$ of the main text). Santiago and Caballero (1995) assume that continual artificial selection maintains a constant level C^2 of fitness variation in the population each generation, yet the *particular* fitness backgrounds the neutral allele is stochastically associated only contributes a fraction G in the next generation, G^2 in the generation after, and so on, as selection reduces genetic variation for fitness (note: in their 1998 paper, they use Z instead of G). Similarly, the associations between the neutral and fitness backgrounds decay at a rate $1/2$ due to independent assortment. Note that Robertson (1961) assumed that the fitness backgrounds that become stochastically associated with the neutral allele do not experience any decay in their fitness variation ($G = 1$); in this case, $Q = 2$ as Robertson's work found. With an arbitrary amount of linkage between the focal neutral and fitness backgrounds, Santiago and Caballero (1998) show that only Q is affected, and derive an expression for Q that only depends on G and the size of the genome in Morgans, L (equation 6, 1998).

In our main text, we model the temporal autocovariance created by heritable fitness variation, which also impacts the cumulative variance in allele frequency change $\mathrm{Var}(p_t - p_0)$. To illustrate how our model connects with theirs, below is the cumulative variance in allele frequency change for three generations in their 1995 notation, with the corresponding

changes in allele frequency below,

$$\begin{aligned}\mathrm{Var}(p_3 - p_0) = \mathbb{E}\Bigg(\Bigg(&\underbrace{S_1 + D_1 + H_1}_{\Delta p_1} + \\ &\underbrace{(1-r)GS_1 + S_2 + D_2 + H_2}_{\Delta p_2} + \\ &\underbrace{(1-r)^2G^2S_1 + (1-r)GS_2 + S_3 + D_3 + H_3}_{\Delta p_3}\Bigg)^2\Bigg). \end{aligned} \tag{2.63}$$

Grouping terms by the generation that the initial association was formed, we see how Santiago and Caballero (1995) define the Q_i terms in their notation,

$$\begin{aligned}\mathrm{Var}(p_3 - p_0) = \mathbb{E}\Bigg(\Bigg(&\underbrace{S_1(1 + (1-r)G + (1-r)^2G^2)}_{\text{creation and persistence of generation 1 associations } := S_1Q_3} + D_1 + H_1 + \\ &\underbrace{S_2(1 + (1-r)G)}_{\text{creation and persistence of generation 2 associations } := S_2Q_2} + D_2 + H_2 + \\ &\underbrace{S_3}_{\text{creation of generation 3 associations } := S_3Q_1} + D_3 + H_3\Bigg)^2\Bigg). \end{aligned} \tag{2.64}$$

since the associations created in generation i $(0 < i \leq t)$ persist with probability $(1 - r)^{t-i}$, with proportion G^{t-i} of its original fitness variation in generation t. In general, the cumulative impact of the associations formed i generations ago has coefficient $Q_i = \sum_{j=0}^{i-1}(1-r)^jG^j$. Using these Q_i terms simplifies this equation to

$$\begin{aligned}\mathrm{Var}(p_4 - p_0) = \mathbb{E}\Bigg(\Bigg(&S_1Q_4 + D_1 + H_1 + S_2Q_3 + D_2 + H_2 + \\ &S_3Q_2 + D_3 + H_3 + S_4Q_1 + D_4 + H_4\Bigg)^2\Bigg) \end{aligned} \tag{2.65}$$

or, in general,

$$\mathrm{Var}(p_t - p_0) = \sum_{i=1}^{t} \mathbb{E}(D_i^2) + \mathbb{E}(H_i^2) + Q_{t-i+1}^2 E(S_i^2). \tag{2.66}$$

Then, Santiago and Caballero (1995) note that assuming V_n, C^2, and population size N are constant across generations, the magnitude of all of the effects $\mathbb{E}(D_i^2)$, $\mathbb{E}(H_i^2)$, and $\mathbb{E}(S_i^2)$ are constant across all generations (for all i, so we omit the i subscript for these terms), except for a geometric decay due to drift at a rate $(1 - 1/2N_e)$ per generation that effects all terms. Such that, when we include the decay in the variance due to drift,

$$\mathrm{Var}(p_t - p_0) = \sum_{i=1}^{t} \left(\mathbb{E}(D^2) + \mathbb{E}(H^2) + Q_i^2 E(S^2)\right) \left(1 - \frac{1}{2N_e}\right)^{t-i} \tag{2.67}$$

(cf. p. 1018 of Santiago and Caballero 1995). In the long run, the variance in the neutral allele's frequency change hits a balance. Many copies of the neutral allele segregating in the population are on fitness backgrounds it has recently become stochastically associated with, as segregation and recombination have not broke these associations apart. A few copies of the neutral allele are on fitness backgrounds they became associated with many generations ago, that have by chance survived to remain associated. In all cases, the effect these associations have on present-day allele frequency change is weakened by the fact that natural selection has reduced the genetic variance of these fitness backgrounds. Since the long-run variance in allele frequency under drift in a Wright–Fisher population is

$$\mathrm{Var}(p_t) = p_0(1 - p_0)\left[1 - \left(1 - \frac{1}{2N}\right)^t\right]. \tag{2.68}$$

One can estimate the effective population size N_e using the observed difference in variances $\mathrm{Var}(p_t)$ and $\mathrm{Var}(p_{t-1})$. (Note that this is a different long-run effective population size used by others, $N_e = p_0(1-p_0)t/(2\,\mathrm{Var}(p_t - p_0))$, Crow and Kimura 1970) Santiago and Caballero use Equation (2.68), taking the difference $\mathrm{Var}(p_t) - \mathrm{Var}(p_{t-1})$ and rearranging to end up with the large t estimator of N_e,

$$N_e = \frac{p_0(1 - p_0) - \mathrm{Var}(p_{t-1})}{2(\mathrm{Var}(p_t) - \mathrm{Var}(p_{t-1}))} \tag{2.69}$$

(cf. p. 1018, Santiago and Caballero 1995). Rearranging,

$$
\begin{aligned}
2N_e(\mathrm{Var}(p_t) - \mathrm{Var}(p_{t-1})) &= p_0(1-p_0) - \mathrm{Var}(p_{t-1}) \\
2N_e\,\mathrm{Var}(p_t) - 2N_e\,\mathrm{Var}(p_{t-1}) + \mathrm{Var}(p_{t-1}) &= p_0(1-p_0) \\
2N_e\left(\mathrm{Var}(p_t) - \mathrm{Var}(p_{t-1})\left(1 - \frac{1}{2N_e}\right)\right) &= p_0(1-p_0). \qquad (2.70)
\end{aligned}
$$

This very conveniently simplifies the sum in Equation (2.67), as we can show with the case of $t = 3$,

$$
\begin{aligned}
\mathrm{Var}(p_3) &= \left(\mathbb{E}(D^2) + \mathbb{E}(H^2) + Q_1^2\mathbb{E}(S^2)\right)\left(1 - \frac{1}{2N_e}\right)^2 + \\
&\quad \left(\mathbb{E}(D^2) + \mathbb{E}(H^2) + Q_2^2\mathbb{E}(S^2)\right)\left(1 - \frac{1}{2N_e}\right) + \\
&\quad \mathbb{E}(D^2) + \mathbb{E}(H^2) + Q_3^2\mathbb{E}(S^2) \\
\mathrm{Var}(p_2)\left(1 - \frac{1}{2N_e}\right) &= \left(\mathbb{E}(D^2) + \mathbb{E}(H^2) + Q_1^2\mathbb{E}(S^2)\right)\left(1 - \frac{1}{2N_e}\right)^2 + \\
&\quad \left(\mathbb{E}(D^2) + \mathbb{E}(H^2) + Q_2^2\mathbb{E}(S^2)\right)\left(1 - \frac{1}{2N_e}\right) \\
\mathrm{Var}(p_3) - \mathrm{Var}(p_2)\left(1 - \frac{1}{2N_e}\right) &= \mathbb{E}(D^2) + \mathbb{E}(H^2) + Q_3^2\mathbb{E}(S^2)
\end{aligned}
$$

or, generally,

$$
\mathrm{Var}(p_t) - \mathrm{Var}(p_{t-1})\left(1 - \frac{1}{2N_e}\right) = \mathbb{E}(D^2) + \mathbb{E}(H^2) + Q_t^2\mathbb{E}(S^2) \qquad (2.71)
$$

Inserting this into Equation (2.70), the long-run effective population size can be written as

$$
\begin{aligned}
N_e &= \frac{p_0(1-p_0)}{2\left(\mathrm{Var}(p_t) - \mathrm{Var}(p_{t-1})\left(1 - \frac{1}{2N_e}\right)\right)} \\
&= \frac{p_0(1-p_0)}{2\left(\mathbb{E}(D^2) + \mathbb{E}(H^2) + Q_\infty^2\mathbb{E}(S^2)\right)} \qquad (2.72)
\end{aligned}
$$

where $Q_\infty = 1 + 1/2 + 1/4 + \ldots = 2$ in Robertson's (1961) model, and $Q_\infty = 1/(1-G(1-r))$ in Santiago and Caballero's (1995) model. (Note: r here represents the recombination fraction between fitness variation and neutral sites, which differs from Santiago and Caballero (1995) equation 17, where r represents the correlation between parental fitness).

Then, Santiago and Caballero (1995) show,

$$\mathbb{E}(S^2) = \frac{p_0(1-p_0)}{2N} C^2 \tag{2.73}$$

$$\mathbb{E}(D^2) = \frac{p_0(1-p_0)}{2N} \frac{V_n}{4} \tag{2.74}$$

$$\mathbb{E}(H^2) = \frac{p_0(1-p_0)}{2N} \frac{1}{2} \tag{2.75}$$

(cf. Santiago and Caballero 1995, equation 11). Inserting these into Equation (2.72), we have

$$N_e = \frac{4N}{2 + V_n + 4Q_\infty^2 C^2} \tag{2.76}$$

which is a simplified version of Santiago and Caballero's equation 16, and which further simplifies to $N_e = N$ when $V_n = 2$ and $C^2 = 0$, the effective population size of a Wright–Fisher population of N hermaphroditic individuals.

The covariances caused by fitness associations With an understanding now of the basics of Santiago and Caballero's (1995, 1998) models, how they connect to our notation, and how they reach their expression for the long-run effective population size, we turn now to finding the temporal autocovariances implicit in their model. We start by looking at the variance in allele frequency between generations 0 and 4 (Equation (2.63)), including an additional generation so the pattern is clearer later,

$$\mathrm{Var}(p_4 - p_0) = \mathbb{E}\left(\Big(\underbrace{S_1 + D_1 + H_1}_{\Delta p_1} + \underbrace{(1-r)GS_1 + S_2 + D_2 + H_2}_{\Delta p_2} + \underbrace{(1-r)^2G^2S_1 + (1-r)GS_2 + S_3 + D_3 + H_3}_{\Delta p_3} + \underbrace{(1-r)^3G^3S_1 + (1-r)^2G^2S_2 + (1-r)GS_3 + S_4 + D_4 + H_4}_{\Delta p_4}\Big)^2\right).$$

The cross-terms like $\mathbb{E}(D_1D_2)$, $\mathbb{E}(H_1D_1)$ and $\mathbb{E}(S_1S_2)$ are all expected products of independent random variables, where the expectation of each random variable is zero, and consequently are all zero. The only non-zero cross terms are products of $\mathbb{E}(S_i^2)$. When we look at the covariances with the allele frequency change in the initial generation and a later generation s, $\mathrm{Cov}(\Delta_{_H} p_1, \Delta_{_H} p_s)$,

$$\mathrm{Cov}(\Delta_{_H} p_1, \Delta_{_H} p_1) = \mathrm{Var}(\Delta_{_H} p_1) = \mathbb{E}(S_1^2) \tag{2.77}$$

$$\mathrm{Cov}(\Delta_{_H} p_1, \Delta_{_H} p_2) = \frac{\mathbb{E}(S_1^2)G}{2}(1-r) \tag{2.78}$$

$$\mathrm{Cov}(\Delta_{_H} p_1, \Delta_{_H} p_3) = \frac{\mathbb{E}(S_1^2)G^2}{2}(1-r)^2 \tag{2.79}$$

$$\mathrm{Cov}(\Delta_{_H} p_1, \Delta_{_H} p_4) = \frac{\mathbb{E}(S_1^2)G^3}{2}(1-r)^3 \tag{2.80}$$

where the $1/2$ coefficient comes from the fact that in Santiago and Caballero's work, the $\mathbb{E}(S_1^2)$ products represent *both* the $\mathrm{Cov}(\Delta_{_H} p_t, \Delta_{_H} p_s)$ and $\mathrm{Cov}(\Delta_{_H} p_s, \Delta_{_H} p_t)$ terms, so a single temporal autocovariance in our notation is half their joint covariance term.

However, if our reference generation is different, say 2, the associations from earlier generations that have persisted to that generation can also lead to covariances to later generations. Looking at the covariances

$$\mathrm{Cov}(\Delta_H p_2, \Delta_H p_2) = \frac{\mathbb{E}(S_2^2) + \mathbb{E}(S_1^2)(1-r)G}{2} \tag{2.81}$$

$$\mathrm{Cov}(\Delta_H p_2, \Delta_H p_3) = \frac{\mathbb{E}(S_2^2)G + \mathbb{E}(S_1^2)(1-r)G^2}{2}(1-r) \tag{2.82}$$

$$\mathrm{Cov}(\Delta_H p_2, \Delta_H p_4) = \frac{\mathbb{E}(S_2^2)(1-r)G^2 + \mathbb{E}(S_1^2)(1-r)^2G^3}{2}(1-r)2. \tag{2.83}$$

Likewise, the covariances $\mathrm{Cov}(\Delta_H p_3, \Delta_H p_s)$ include the associations that persist from earlier generations. In general,

$$\mathrm{Cov}(\Delta_H p_t, \Delta_H p_s) = \frac{1}{2}\sum_{i=1}^{t} \mathbb{E}(S_i^2)\left(G(1-r)\right)^{t+s-2i}, \quad \text{for } t \leq s. \tag{2.84}$$

This expression is more complex than our expression for temporal autocovariance because its modeling the LD in generation t as it builds up from generations 1 to t. In contrast, our expressions for covariance incorporate all of this build up of LD as the initial LD term $\mathbb{E}(\mathcal{R}_t)$ (for a single locus case). This expression for autocovariance implied by Santiago and Caballero's (1995) work matches our expression for autocovariance (for a single locus) when the arbitrary first generation is t rather than 1

$$\mathrm{Cov}(\Delta_H p_t, \Delta_H p_s) = \frac{\mathbb{E}(S_t^2)G^{s-t}}{2}(1-r)^{s-t}, \quad \text{for } t \leq s. \tag{2.85}$$

Using the expression for $\mathbb{E}(S_t^2)$ (equivalent to $\mathrm{Var}(\Delta_H p_t)$ in our notation) derived in Appendix Section 2.6.6,

$$\frac{\mathrm{Cov}(\Delta_H p_t, \Delta_H p_s)}{p_t(1-p_t)} = \frac{C^2G^{s-t}}{4N}(1-r)^{s-t}, \quad \text{for } t \leq s. \tag{2.86}$$

This is analogous to Equation (2.8) for a single locus, where C^2G^{s-t} is the additive variation in generation s (equivalent to our $V_a(s)$), and the factor $1/2N$ represents the chance build up of LD between the neutral site and an unlinked fitness background. In our expression, we condition on existing linkage disequilibrium $\mathbb{E}(\mathcal{R}_t^2)$ between the neutral site and its fitness background, whereas they assume a buildup of linkage disequilibria

to a drift-recombination equilibrium. We can see this by returning to the $\Delta_H p_4$ term of Equation (2.63),

$$\mathrm{Var}(\Delta_H p_4) = \mathbb{E}\left((1-r)^3 G^3 S_1 + (1-r)^2 G^2 S_2 + (1-r) G S_3 + S_4 + D_4 + H_4\right)^2 \quad (2.87)$$

$$= (1-r)^5 G^5 \mathbb{E}(S_1^2) + (1-r)^4 G^4 \mathbb{E}(S_2^2) + (1-r)^2 G^2 \mathbb{E}(S_3)^2 + \mathbb{E}(S_4^2) \quad (2.88)$$

where following Santiago and Caballero's (1995, p. 1018) approach, we can replace each $\mathbb{E}(S_i)$ with $\mathbb{E}(S_i^2) = \mathbb{E}(S^2)(1 - 1/2N)^{i-1}$ and let $G = 1$ as we focus on the buildup of LD. This gives us the general equation,

$$\mathrm{Var}(\Delta_H p_t) = \mathbb{E}(S^2) \sum_{i=1}^{t} (1-r)^{2i} \left(1 - \frac{1}{2N}\right)^{i-1} \quad (2.89)$$

and taking this geometric series to infinity converges (since $(1-r)^2(1-1/2N) < 1$) and replacing $\mathbb{E}(S^2)$ with the chance associations that build up gametes sampled into individuals (Equation (2.58)),

$$\begin{aligned}
\mathbb{E}((\Delta_H p_\infty)^2) &= \mathbb{E}(S^2) \sum_{i=1}^{\infty} (1-r)^{2i} \left(1 - \frac{1}{2N}\right)^{i-1} \\
&= \frac{\mathbb{E}(S^2)}{1 - 1/2N} \sum_{i=1}^{\infty} \left((1-r)^2 \left(1 - \frac{1}{2N}\right)\right)^i \\
&= \frac{C^2 p_0 (1-p_0)}{1 - 1/2N} \frac{1}{1 - (1-r)^2(1 - 1/2N)}.
\end{aligned} \quad (2.90)$$

When we assume $r \to 0$ and $1/N \to 0$ and Nr is a constant, this gives us

$$\mathbb{E}(\mathcal{R}^2) = \frac{\mathbb{E}((\Delta_H p_\infty)^2)}{C^2 p_0 (1-p_0)} \approx \frac{1}{1 + 4Nr} \quad (2.91)$$

which is analogous to the $\mathbb{E}(\mathcal{R}^2)$ measure of linkage disequilibrium, standardized to rescale the fitness variation. The right-hand side is identical to Sved's identity by descent equilibrium $\mathbb{E}(\mathcal{R}^2)$ under drift-recombination balance (1971). Note that our expression can

be recovered from Equation (2.84) when the reference generation $t \to \infty$ such that the LD hits its equilibrium level,

$$\frac{\text{Cov}(\Delta_H p_t, \Delta_H p_s)}{p_0(1-p_0)} = \frac{1}{2}\underbrace{C^2 G^{s-t}}_{V_A(s)}\underbrace{\frac{1}{1+4Nr}}_{\mathbb{E}(\mathcal{R}_t^2)}(1-r)^{s-t} \tag{2.92}$$

which is identical to our expression for temporal autocovariance when initial LD is due to a neutral drift-recombination balance, and the change in V_A during selection is modeled as a geometric decay at rate G. Note that the terms in underbraces indicate the corresponding terms in Equation (2.8) for a single locus.

2.6.8 Multilocus simulation details

Targeting an initial level of Additive Genetic Variation We choose θ for the coalescent simulations to target a total number of segregating sites $L + M$, where L is the number of selected sites (a parameter we vary in our multilocus simulations), and at least $M = 200$ randomly placed neutral sites over which we can calculate the temporal autocovariance. Then, the total number of target sites $M + L$ is then inflated by a factor of 1.5 to ensure a sufficient number of sites given the random mutation process. The L selected sites are randomly chosen from the segregating sites, and all remaining mutations are neutral. Thus, using Watterson's expression for the expected number of segregating sites under the coalescent (1975), we have $\theta = 1.5(M+L)/(\gamma + \log(2N))$ where $\gamma \approx 0.577$ is Euler's Gamma. Each of the L selected sites is given a random effect size of $\pm\alpha$ with equal probability, where we choose by targeting a specific level additive genic variation $V_a = 2\alpha^2 \sum_l^L p_l(1-p_l) = \alpha^2 SSH_L$ where $SSH_L = 2\sum_l^L p_l(1-p_l)$ is the sum of site heterozygosity of the L neutrally evolving sites that will be selected once selection begins. Under neutrality, $\mathbb{E}(SSH_L) = \theta_L = L/(\gamma + \log(2N))$. Then, we set $\alpha = \sqrt{V_a/\theta_L}$. We empirically validate that our target genic variation is close to the empirically observed level.

Choosing the simulation parameter range We simulate over a grid of parameter ranges, varying the number of loci L, the target additive genic variation V_a in the region

(by varying α), and the recombination map length of the region R in Morgans. We have varied these parameters over ranges that encompass a wide range likely to be encountered in natural populations. To do this, we found that additive genetic variation for lifetime reproductive success varied over orders of magnitude, from 0 (e.g. in male red deer, Kruuk et al. (2000)) to 1.1 in male red-billed gull (Teplitsky et al. 2009). These values of additive genetic variation are for the entire genome (we write these as $V_{A,GW}$, where GW indicates genome-wide); our simulations model a region of varying map length. We expect most recombination map lengths to be roughly over the scale of $5 - 50$ Morgans in length, and we chose to investigate how temporal autocovariance behaves across a spectrum of recombination, from a completed linked region ($R = 0$), to the scale over which a strong classic hardsweeps could affect diversity (0.5 centiMorgans) to a region where the ends are approximately unlinked (4.5 Morgans), overall giving us a parameter range of $R \in \{0, 0.005, 0.01, 0.05, 0.1, 0.5, 1.5, 4.5\}$. Over this grid of our region recombination map lengths, and the total organism recombination map lengths, we get a rough estimate of the number of regions we would expect with this level of recombination in the organism's total genome, imagining homogeneous recombination rate, by taking G/R. Using this estimate of the number of regions in the genome, we calculate the genetic variation per region over our grid of parameters as ${}^{V_{A,GW}R}/_{G}$, and target a level of additive genic variation per region V_a equal to this regional additive genetic variation V_A. From preliminary simulations, we had found we can not detect much temporal autocovariance below $V_a < 0.001$ with the initial level of linkage disequilibrium from mutation-drift balance, so we ignore parameters less than this value (other than $V_a = 0$ as a control). Additionally, to reduce the number of simulations, we exclude $V_a > 0.1$ as this only excludes a small region of the parameter grid and preliminary simulations demonstrated the behavior of temporal autocovariance with high V_a is evident with the included values. Overall, this gives us a spectrum of target additive genic variation per region of $V_a \in \{0.001, 0.002, 0.005, 0.01, 0.02, 0.05, 0.08, 0.1\}$. Note that to prevent our plots from being too dense, we include only a representative subset of this parameter grid in our figures.

2.6.9 Accounting for allele frequency sampling noise

In practice, one will calculate the temporal variance-covariance matrix on allele frequency trajectories calculated from sampled chromosomes from the population. We assume a binomial sampling process, where n chromosomes are sampled from the population such that $\widetilde{p} = {}^{X}/_{n}$, and $X \sim \text{Binom}(p, n)$. We can then write $\widetilde{p}_t = p_t + \varepsilon_t$, and our covariances can be written as

$$\begin{aligned}\text{Cov}(\Delta\widetilde{p}_t, \Delta\widetilde{p}_s) &= \text{Cov}(\widetilde{p}_{t+1} - \widetilde{p}_t, \widetilde{p}_{s+1} - \widetilde{p}_s) \\ &= \text{Cov}(p_{t+1} + \varepsilon_{t+1} - p_t - \varepsilon_t, p_{s+1} + \varepsilon_{s+1} - p_s - \varepsilon_s). \end{aligned} \tag{2.93}$$

Note this simplifies to

$$\text{Cov}(\Delta\widetilde{p}_t, \Delta\widetilde{p}_s) = \text{Cov}(p_{t+1} - p_t, p_{s+1} - p_s) \text{ if } |t - s| > 1, \tag{2.94}$$

since in these cases, the sampling noise at a timepoint is not shared between the estimated allele frequency changes. However, if $|t - s| = 1$ the sampling noise from timepoint $t + 1$ is shared, biasing the sample estimate of covariance:

$$\begin{aligned}\text{Cov}(\Delta\widetilde{p}_t, \Delta\widetilde{p}_{t+1}) &= \text{Cov}(p_{t+1} + \varepsilon_{t+1} - p_t - \varepsilon_t, p_{t+2} + \varepsilon_{t+2} - p_{t+1} - \varepsilon_{t+1}) \\ &= \text{Cov}(\Delta p_t + \varepsilon_{t+1} - \varepsilon_t, \Delta p_{t+1} + \varepsilon_{t+2} - \varepsilon_{t+1}) \\ &= \text{Cov}(\Delta p_t, \Delta p_{t+1}) - \text{Var}(\varepsilon_{t+1}). \end{aligned} \tag{2.95}$$

Similarly, the variance ($t = s$) is biased, as it is impacted by the binomial sampling noise too,

$$\begin{aligned}\text{Var}(\Delta\widetilde{p}_t) &= \text{Cov}(\Delta p_t + \varepsilon_{t+1} - \varepsilon_t, \Delta p_t + \varepsilon_{t+1} - \varepsilon_t) \\ &= \text{Var}(\Delta p_t) + \text{Var}(\varepsilon_{t+1}) + \text{Var}(\varepsilon_t) \end{aligned} \tag{2.96}$$

In practice, these covariances are calculated over loci in a region or across the entire genome. We assume that the tracked allele has been randomly swapped (e.g. the tracked

allele frequency is not systematically the minor, major, or reference allele), such that $\mathbb{E}(\Delta p_{t,l}) = 0$ for all t and l. Then, the unbiased covariance estimate as calculated over loci is

$$\frac{1}{L}\sum_{l=1}^{L}(\Delta p_{t,l}\Delta p_{t+1,l}) = \frac{1}{L}\sum_{l=1}^{L}\Delta\widetilde{p}_{t,l}\Delta\widetilde{p}_{t+1,l} + \frac{1}{L}\sum_{l=1}^{L}\varepsilon^2_{t+1,l}. \tag{2.97}$$

Then, we can use an unbiased plugin estimate of the frequency sampling variance $\mathbb{E}(\varepsilon^2_{t+1,l}) = \mathrm{V}(\varepsilon_{t+1,l}) = {}^{p_{t+1,l}(1-p_{t+1,l})}/_{(n_{t,l}-1)}$ (Nei 1987, p. 191) to estimate these bias terms, and add or subtract them from the estimator accordingly. Accounting for finite sampling, the unbiased sample variance-covariance matrix now has elements:

$$Q_{t,t+1} = \frac{1}{L}\sum_{l=1}^{L}\Delta\widetilde{p}_{t,l}\Delta\widetilde{p}_{t+1,l} + \frac{1}{L}\sum_{l=1}^{L}\frac{p_{t+1,l}(1-p_{t+1,l})}{n_{t+1,l}-1}, \tag{2.98}$$

and variance

$$Q_{t,t} = \frac{1}{L}\sum_{l=1}^{L}(\Delta\widetilde{p}_{t,l})^2 - \frac{1}{L}\sum_{l=1}^{L}\frac{p_{t,l}(1-p_{t,l})}{n_{t,l}-1} - \frac{1}{L}\sum_{l=1}^{L}\frac{p_{t+1,l}(1-p_{t+1,l})}{n_{t+1,l}-1}. \tag{2.99}$$

In Section 2.2.5, we used population frequencies in introducing the method of moments estimators of $\widehat{V_A(1)}$ and $\widehat{N}$. Here, we discuss the performance of these estimators with sample allele frequencies. Our simulations are identical to those described in Section 2.2.4, except we have increased the target number of neutral sites in each region so it is around $10,000$. We mimic sampling of $n = \{50, 100, 200, 500\}$ chromosomes from the population, and use the bias-corrected sample variance-covariance matrix in the method-of-moments approach described in Section 2.3 to estimate $\widehat{V_A(1)}$ and $\widehat{N}$.

In Figure 2.6.3, we show the performance of our estimators in the case where $n = 100$ chromosomes have been sampled from the population. Overall, there are two important differences compared with Figure 2.5 of the main text. First, while the estimator $\widehat{V_A(1)}$ performs well for high levels around $V_A \sim 0.1$, the variance around the estimator increases significantly as V_A grows weaker. As the covariances are proportional to ${}^{V_A}/_{R}$, sampling

noise grows larger than the theoretical temporal autocovariance as V_A become weaker. Then, one cannot discriminate against the chance covariances formed by the sampling process from the temporal autocovariance created by linked selection without either a large sample size or more timepoints. Second, the approach underestimates $V_A(1)$ for very loose linkage ($R > 1/2$). This is another consequence of the first problem; as sampling noise grows equal, or larger than the magnitude of temporal autocovariance, the estimation procedure performs poorly. As the linkage becomes more loose, the magnitude of temporal autocovariance grows weak relative to the sampling noise, and this noise can be partially absorbed by $\widehat{N}$. This effect can be somewhat ameliorated by calculating the sample variance-covariance matrix over a shorter region of the genome such that R is smaller (as long as SNP density is sufficient), or by increasing the sample size. Finally, the estimation of effective population size shown in Figure 2.6.3 are also affected by V_A, as discussed in Section 2.3 (though the effect is obscured by the sampling noise): high levels of V_A in regions with low recombination generally lead to underestimates of $\widehat{N}$.

To understand how sample size affects the method-of-moments estimators, Figure 2.6.4 depicts median relative error of $\widehat{V_A(1)}$ and $\widehat{N}$ for various sample sizes.

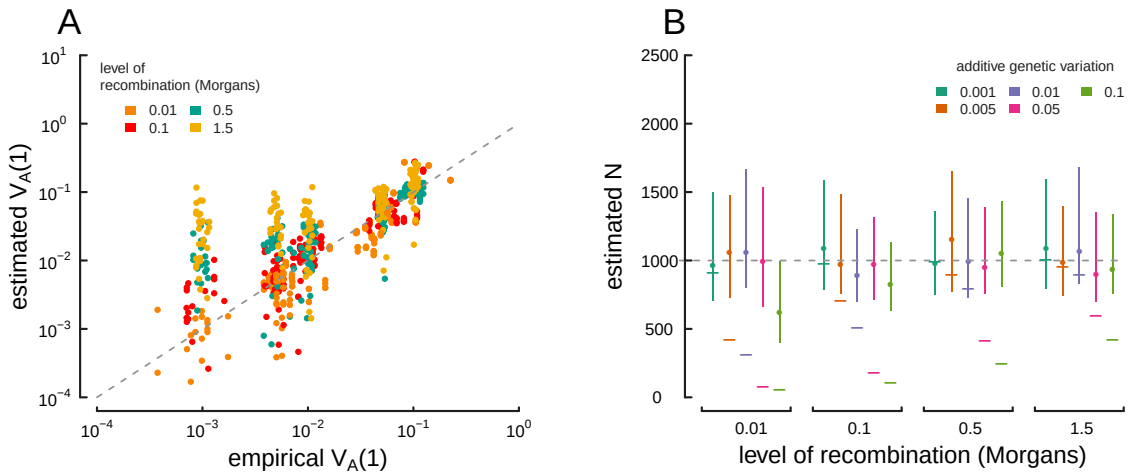

Figure 2.6.3: True parameter values and estimates using the method-of-moments approach on sample ($n = 100$ chromosomes) multilocus simulation data; these figures are analogous to Figure 2.5 in the main text, except the estimators have been calculated on sample, rather than population frequency data. (A) The true $V_A(1)$ (x-axis) and $\widehat{V_A(1)}$ estimated from the sample variance/covariance matrix (y-axis) for each simulation replicate across different levels of recombination (indicated by each point's color). (B) Estimated drift-effective population size ($\widehat{N}$) across a range of simulations with different levels of additive genetic variance and recombination. Each point denotes the median, with lines denoting the interquartile range. A simple temporal estimate of the effective population size, estimated with accounting for the effects of selection, is averaged for each replicate and plotted as a dash. The true value ($N = 1,000$) is shown with the dashed gray line.

2.6.10 Appendix Figures

2.6.10.1 Validation of simulation routine

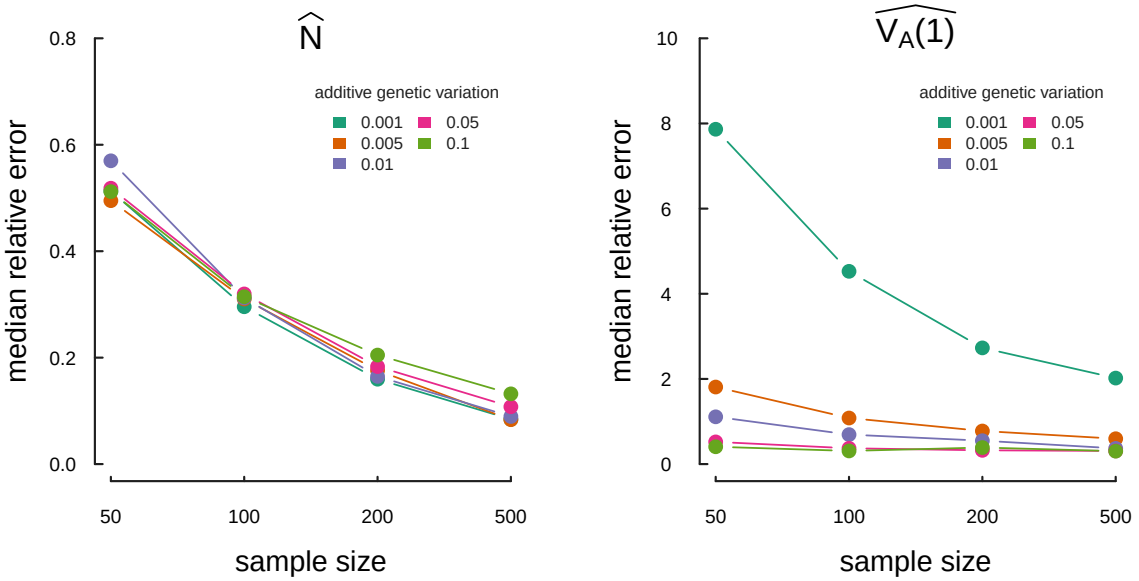

Figure 2.6.4: The median relative estimation error, over 30 replicate simulations, of the method of moments estimator for drift effective population size ($\widehat{N}$) and the initial additive genetic variance ($\widehat{V_A(1)}$).

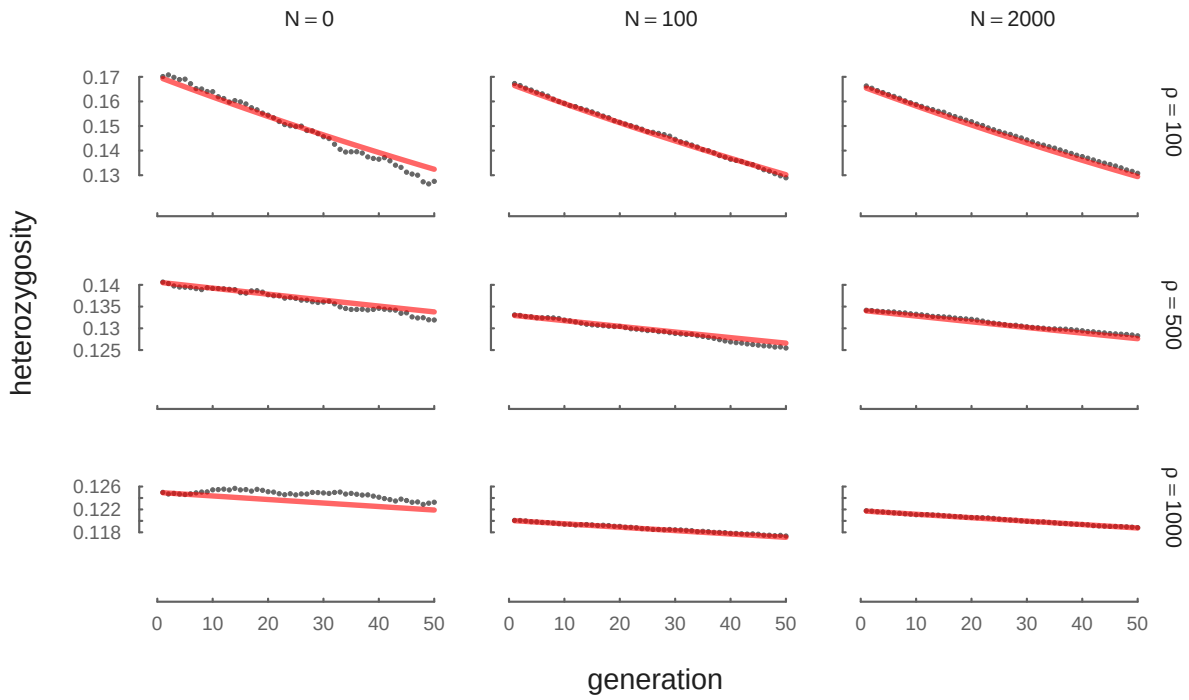

Figure 2.6.5: The neutral decay of heterozygosity due to drift, averaged across 100 replicates and a variety of N and ρ levels. The red line is the theoretical expectation $H_t = H_1(1 - 1/(2N))^{t-1}$.

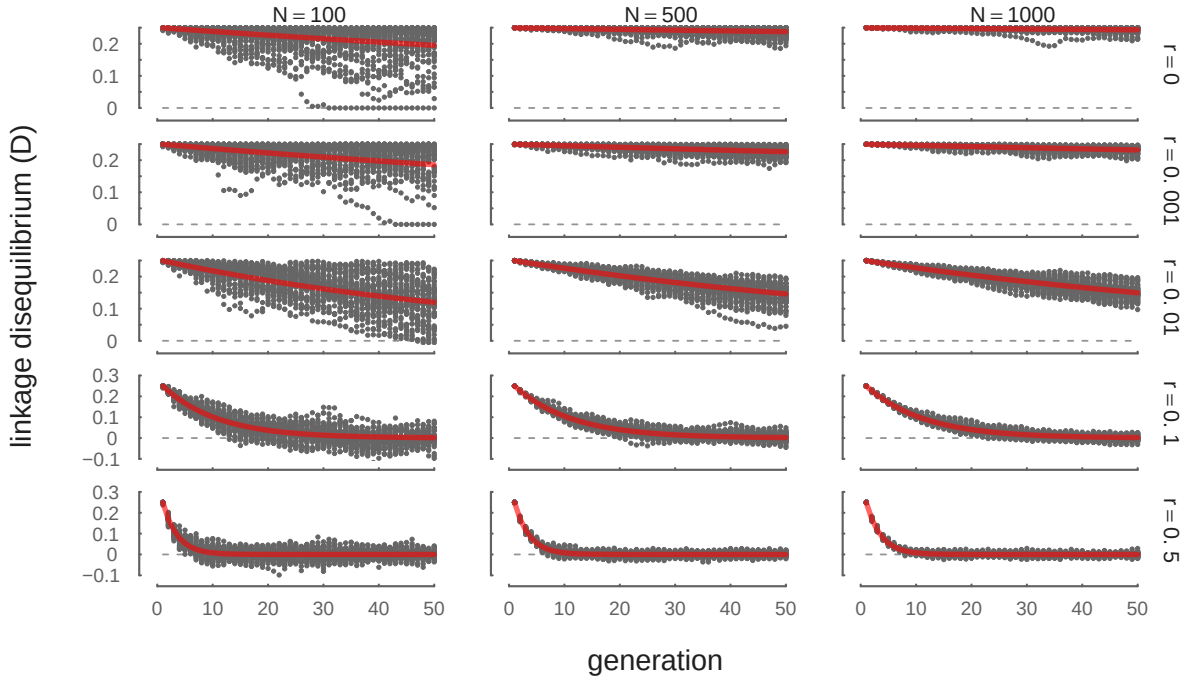

Figure 2.6.6: The decay of LD between neutral sites due to recombination, across 100 replicates and a variety of V_A and R levels. The initial population is created to have an artificial level of initial LD, with half the gametes carrying all derived alleles, and the other half carrying all ancestral alleles. The red line is the theoretical expectation $D_t = D_1(1 - 1/(2N))^{t-1}(1 - r)^{t-1}$.

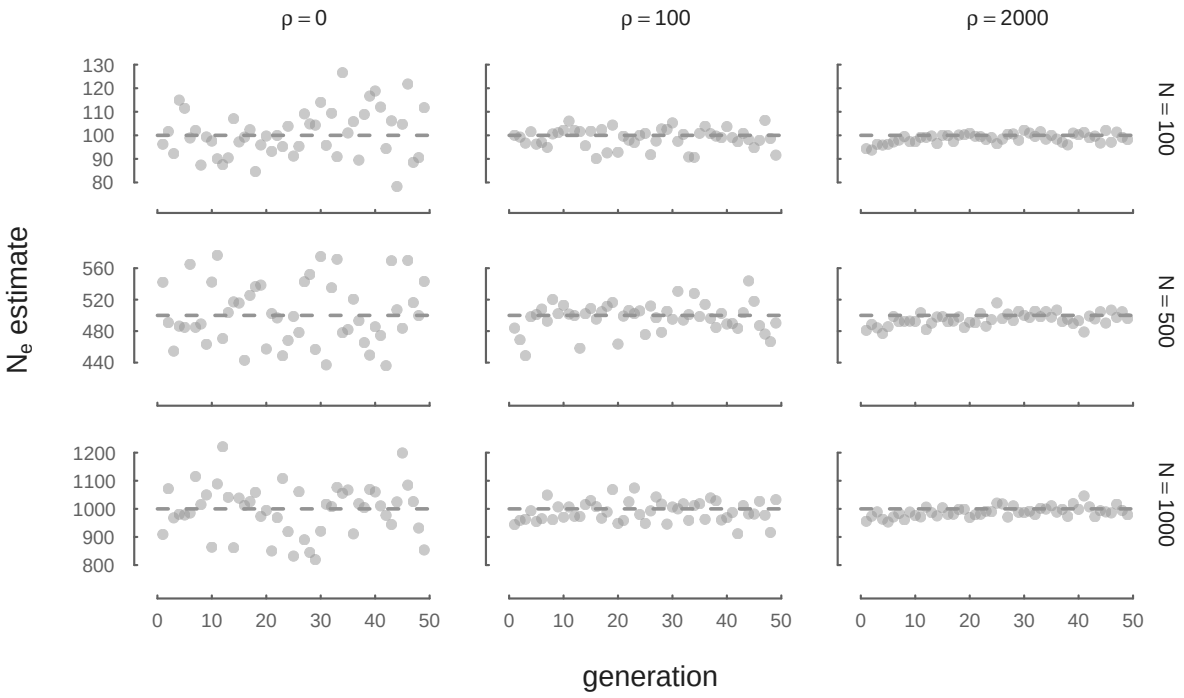

Figure 2.6.7: N_e estimated through time from neutral forward simulations is consistent with true N across a variety of recombination ρ and N parameters. Here, we estimate N_e with $\widehat{N_e} = {}^{p(1-p)}/_{2\,\mathrm{Var}(\Delta p)}$ from neutral allele frequency changes.

2.6.10.2 Dynamics of Variances

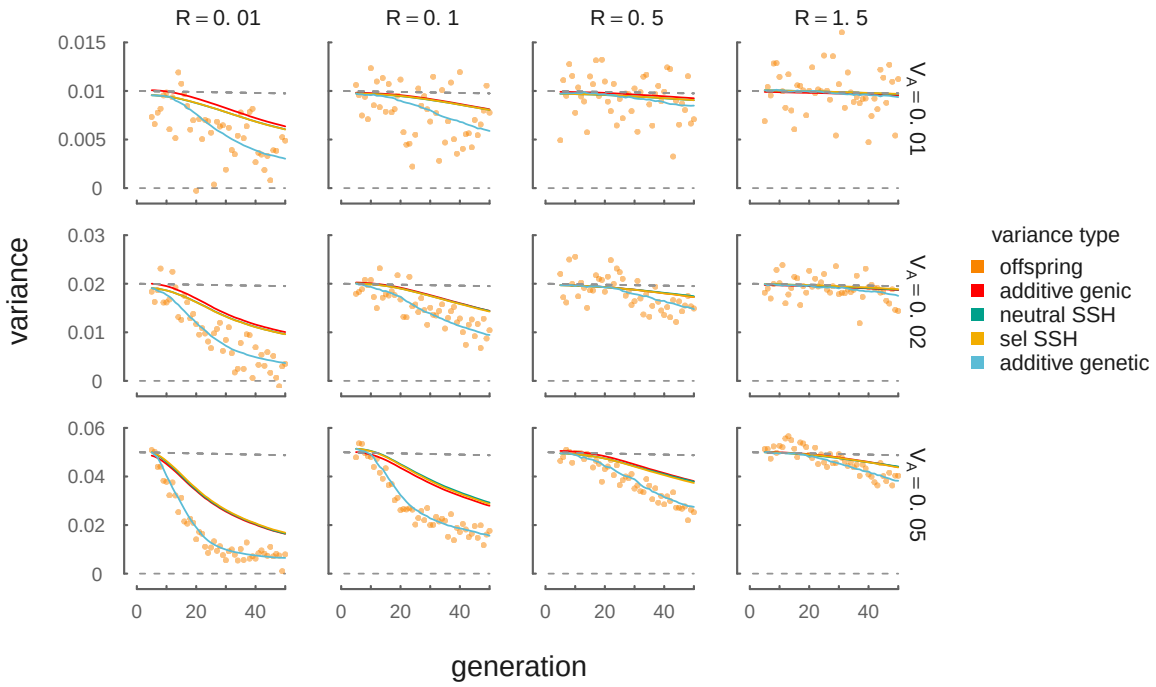

Figure 2.6.8: The dynamics of different variances in our simulations, across a variety of initial target V_A and R levels. Orange points represent the empirical heritable variance in offspring (e.g. with the noise of the Wright–Fisher reproduction process removed). These closely track the additive genetic variance for the trait undergoing directional selection, $V_A = \mathrm{Var}(z)$. The red line shows the dynamics of additive genic variance, $V_a = 2\sum_l \alpha_l^2 p_l(1-p_l)$, which is closely tracked by both the selected (yellow line) and neutral (green line) sum of site heterozygosity proxies described in Section 2.2.3.

2.6.10.3 Supplementary Temporal Autocovariance Figures

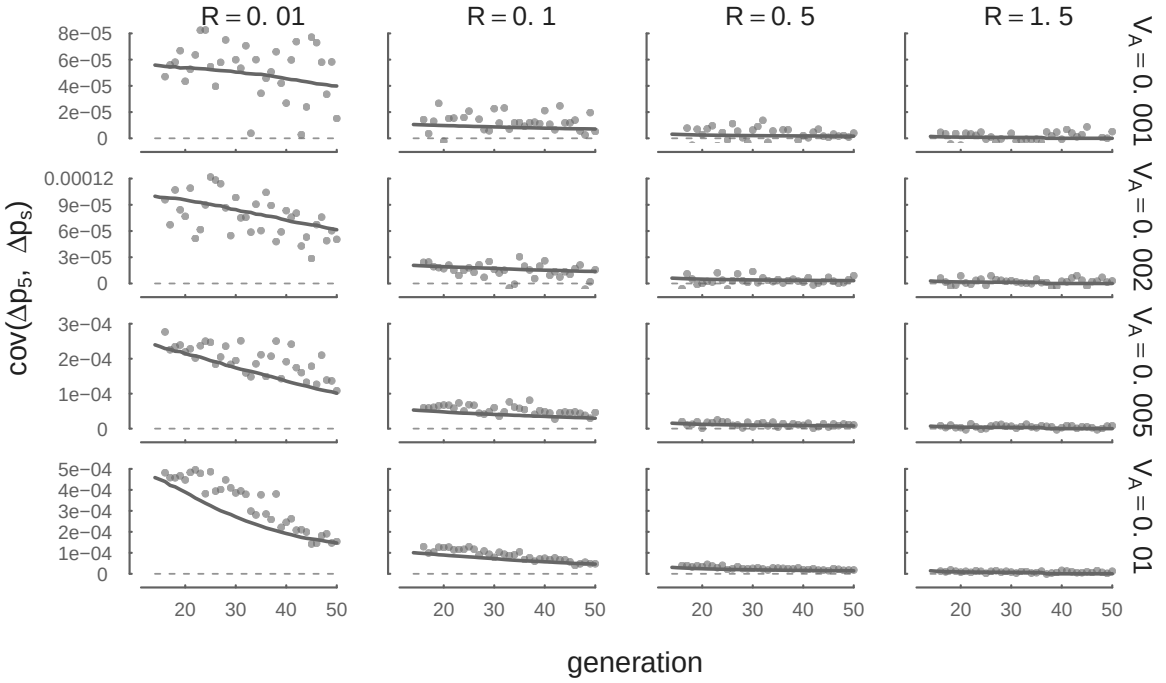

Figure 2.6.9: Each panel shows the temporal autocovariance $\mathrm{Cov}(\Delta p_{13}, \Delta p_s)$ on the y-axis, where s varies along the x-axis. This is analogous to Figure 2.2 with a different reference generation ($t = 13$), and compares the averaged simulation results (points) with the temporal autocovariance predicted by Equation (2.10) using the empirical additive genetic variance (curve). The covariances in these panels are weaker compared to those in Figure 2.2 because by generation 13, additive genetic variance for fitness and the linkage disequilibria between neutral and selected sites has decayed.

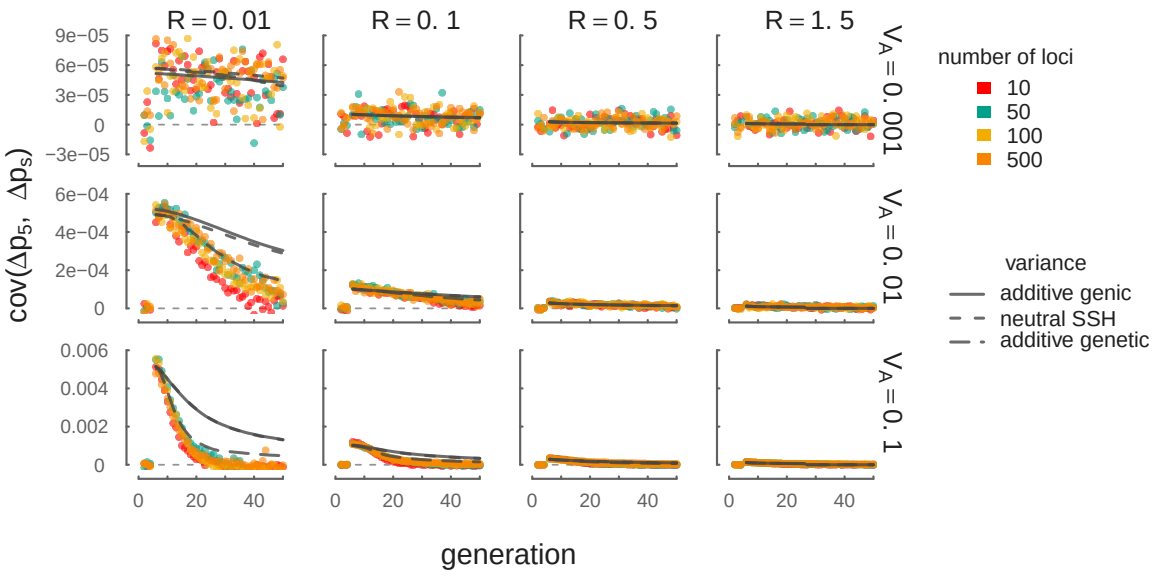

Figure 2.6.10: A version of Figure 2.2 with a subset of V_A parameters used in our simulations that vary over orders of magnitude. This demonstrates that our theory using the empirical additive genic variance (solid gray line), additive genetic variance (long dashed gray line), and the neutral SSH proxy (short dashed gray lines) performs as described in Section 2.2.5 even when V_A varies over orders of magnitude in a region. Higher variance in the empirical covariances with weak selection ($V_A = 0.001$) are due to chance covariances due to drift. The light gray dashed line depicts $\text{Cov}(\Delta p_5, \Delta p_s) = 0$.

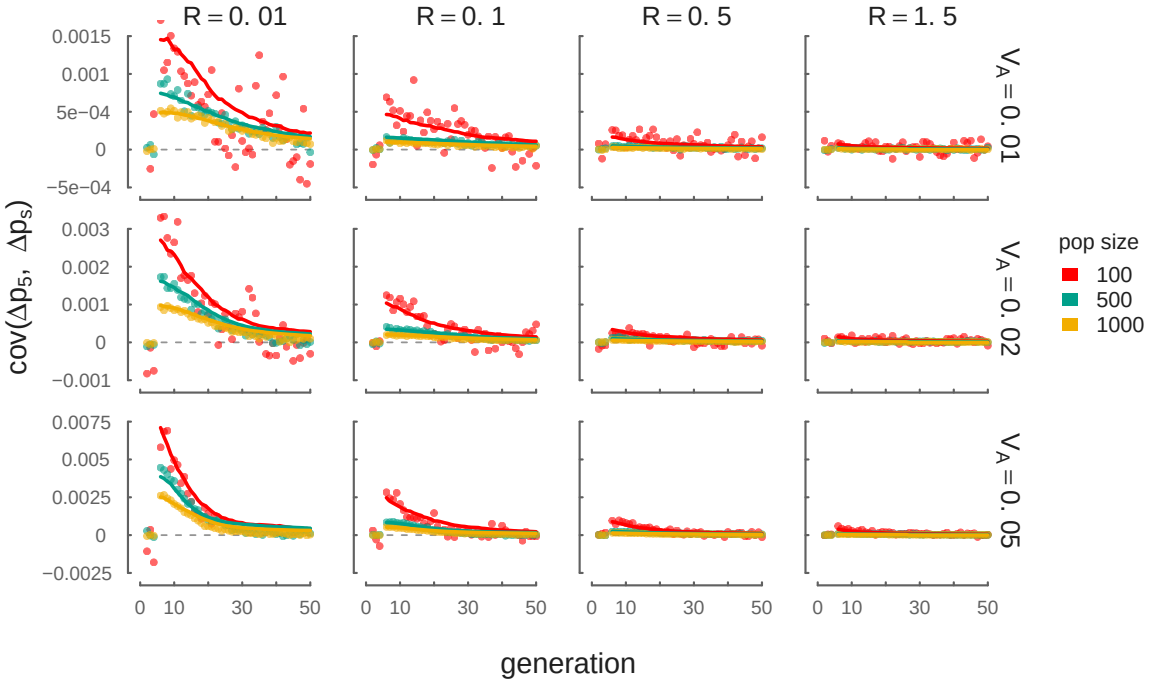

Figure 2.6.11: A version of Figure 2.2 demonstrating temporal autocovariance simulation results and theoretical predictions with varying N. This demonstrates that our theory using the empirical additive genetic variance (lines) fits simulations across a variety of N parameters. The light gray dashed line depicts $\text{Cov}(\Delta p_5, \Delta p_s) = 0$. Note that the initial LD varies due to differing equilibrium levels of LD from our burnin across varying N.

Chapter 3

Estimating the contribution of selection to temporal allele frequency change

3.1 Introduction

A long-standing problem in evolutionary genetics is quantifying the roles of genetic drift and selection in shaping genome-wide allele frequency changes. Selection can both directly and indirectly affect allele frequencies, with the indirect effect coming from the action of selection on correlated loci elsewhere in genome e.g. linked selection (Maynard Smith and Haigh 1974, Charlesworth et al. 1993; Nordborg et al. 1996; see Barton 2000 for a review). Previous work on this question has mostly focused on teasing apart the impacts of drift and selection on genome-wide diversity using population samples from a single contemporary timepoint, often by modeling the correlation between regional recombination rate, gene density, and diversity created in the presence of linked selection (Begun and Aquadro 1992; Elyashiv et al. 2016). This approach has shown linked selection has a major role in shaping patterns of genome-wide diversity across the genomes of some of organisms (Andersen et al. 2012; Begun et al. 2007; Beissinger et al. 2016; Cutter and Choi 2010; Sattath et al. 2011; Williamson et al. 2014), and has allowed us to quantify the relative influence of positive selection (hitchhiking) and negative selection (background selection; Elyashiv et al. 2016; Hernandez et al. 2011; McVicker et al. 2009; Nordborg et al. 2005a.

However, we lack an understanding of how genome-wide linked selection acts over time.

There are numerous examples of rapid phenotypic adaptation (Franks et al. 2007; Grant and Grant 2006, 2011; Reznick et al. 1997) and rapid genomic evolution in asexual populations (Baym et al. 2016; Bennett et al. 1990; Good et al. 2017). Yet the polygenic nature of fitness makes detecting the impact selection on genome-wide variation over short timescales in sexual populations remarkably difficult. This is because the effect of selection on a polygenic trait (such as fitness) is distributed across loci in proportion to their effect sizes. This can lead to subtle allele frequency shifts on standing variation that are difficult to distinguish from background levels of genetic drift and sampling variance. However, increasingly genomic experimental evolution studies with multiple timepoints, and in some cases multiple replicate populations, are being used to detect selected loci (Turner and Miller 2012; Turner et al. 2011) and differentiate modes of selection (Barghi et al. 2019; Burke et al. 2010; Therkildsen et al. 2019). In addition these temporal-genomic studies have begun in wild populations, some with the goal of finding variants that exhibit frequency changes consistent with fluctuating selection (Bergland et al. 2014; Machado et al. 2018). In a previous paper, we proposed that one useful signal for understanding the genome-wide impact of polygenic linked selection detectable from temporal genomic studies is the temporal autocovariance in allele frequency changes (Buffalo and Coop 2019). These covariances are directly estimable from temporal genomic data and are created when the loci that underly heritable fitness variation perturb the frequencies of linked neutral alleles; in contrast, when genetic drift acts alone in a closed population, these covariances are zero in expectation. Mathematically, temporal covariances are useful because it is natural to decompose the total variance in allele frequency change across a set of time intervals into the variances and covariances in allele frequency change among time intervals. Furthermore, biologically, these covariances reflect the extent to which allele frequency changes in one generation predict changes in another due to a shared fitness background and shared selection pressures.

Here, we provide the first empirical analyses to quantify the impact of linked selection acting over short timescales (tens of generations) across two evolve and re-sequence

studies (Barghi et al. 2019; Kelly and Hughes 2019), and one artificial selection experiment (Castro et al. 2019). We repeatedly find a signal of temporal covariance, consistent with linked selection acting to significantly perturb genome-wide allele frequency changes across the genome in a manner that other approaches would not be able differentiate from genetic drift. We estimate the lower bound on the proportion of total variation in allele frequency change caused by linked selection, and the correlation between allele frequency changes between replicate populations caused by response to convergent selection pressures. Overall, we demonstrate that linked selection has a powerful role in shaping genome-wide allele frequency changes over very short timescales.

3.2 Results

Table 3.1: Summary of the studies reanalyzed.

Study	Species	Selection	Replicates	N	Gens.	Timepoints
Kelly and Hughes (2019)	*D. simulans*	lab	3	∼1100	14	2
Barghi et al. (2019)	*D. simulans*	lab	10	∼1000	60	7
Castro et al. (2019)	*M. musculus*	tibiae length	2	32	20	2
		control	1	28		

We first analyzed Barghi et al. (2019), an evolve-and-resequence study with ten replicate populations exposed to a high temperature lab environment and evolved for 60 generations, and sequenced every ten generations. Using the seven timepoints and ten replicate populations, we estimated the genome-wide 6×6 temporal covariance matrix $\mathbf{Q}$ for each of the ten replicates. Each row of these matrices represent the temporal covariance $\mathrm{Cov}(\Delta_{10}p_s, \Delta_{10}p_t)$, between the allele frequency change (in ten-generation intervals, denoted $\Delta_{10}p_t$) in some initial reference generation s (the row of the matrix), and some later timepoint t (the column of the matrix). We corrected these matrices for biases created due to sampling noise, and normalize the entries for heterozygosity (see Supplementary Material Sections 3.5.2 and 3.5.4 for details on the bias correction). The covariances are expected to be zero when only drift is acting in a closed population, as only heritable variation for fitness can create covariance between allele frequency changes (Buffalo and Coop 2019). Averaging across the ten replicate temporal covariances matrices, we find temporal covariances that are statistically significant (95% block bootstraps CIs do not contain zero), consistent with linked selection perturbing genome-wide allele frequency changes over very short time periods. The covariances between all adjacent time intervals are positive and then decay towards zero as we look at more distant time intervals, as expected when directional selection affects linked variants' frequency trajectories until ultimately linkage disequilibrium and the additive genetic variance for fitness associated with neutral alleles decays (Buffalo and Coop 2019). The temporal covariances per replicate are noisier but this general pattern holds; see Supplementary Figures 3.5. Barghi et al. (2019)'s design means that the covariances we see in adjacent time intervals are on average ten generations apart, and given the temporal decay in covariance we see, the covariances on shorter time-scales (e.g. if adjacent generations had been sequenced)

may well be higher yet (see Supplementary Material Section 3.5.5 for more details).

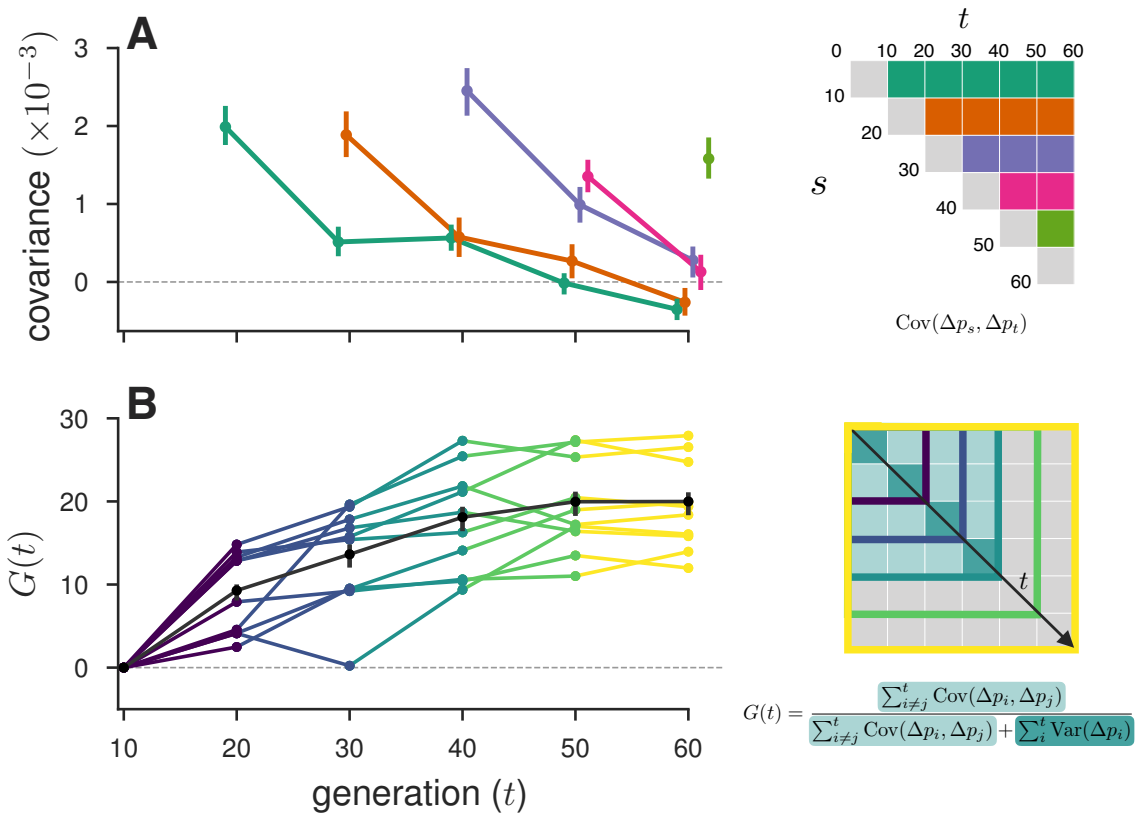

Figure 3.1: A: Temporal covariance, averaged across all ten replicate populations, through time from the Barghi et al. (2019) study. Each line depicts the temporal covariance $\mathrm{Cov}(\Delta p_s, \Delta p_t)$ from some reference generation s to a later time t which varies along the x-axis; each line corresponds to a row of the upper-triangle of the temporal covariance matrix with the same color (upper right). The ranges around each point are 95% block-bootstrap confidence intervals. B: The proportion of the total variance in allele frequency change explained by linked selection, $G(t)$, as it varies through time t along the x-axis. The black line is the $G(t)$ averaged across replicates, with the 95% block-bootstrap confidence interval. The other lines are the $G(t)$ for each individual replicate, with colors indicating what subset of the temporal-covariance matrix to the right is being included in the calculation of $G(t)$.

While the presence of positive temporal covariances is consistent with linked selection affecting allele frequencies over time, this measure not easily interpretable. Additionally, we can quantify the impact of linked selection on allele frequency change as the ratio of total covariance in allele frequency change to the total variance in allele frequency change. We denote the change in allele frequency as $\Delta p_t = p_{t+1} - p_t$, where p_t is the allele frequency in generation t. Since the total variation in allele frequency change can be partitioned into

variance and covariance components, $\mathrm{Var}(p_t - p_0) = \sum_i \mathrm{Var}(\Delta p_i) + \sum_{i \neq j} \mathrm{Cov}(\Delta p_i, \Delta p_j)$, and the covariances are zero when drift acts alone, this is a lower bound on how much of the variance in allele frequency change is caused by linked selection (Buffalo and Coop 2019). We call this measure $G(t)$, defined as

$$G(t) = \frac{\sum_{i \neq j}^{t} \mathrm{Cov}(\Delta p_i, \Delta p_j)}{\mathrm{Var}(p_t - p_0)} \tag{3.1}$$

which estimates the effect of linked selection between the initial generation 0 and some later generation t, which can be varied to see how this quantity grows through time. As with the temporal covariances, the study design of Barghi et al. (2019) leads our measure $G(t)$ to be even more conservative, since the temporal covariances within each ten-generation block between sequenced timepoints are not directly observable, and are not included in the numerator of $G(t)$. Still, we find a remarkably strong signal. Greater than 20% of total variation in allele frequency change over 60 generations is the result of linked selection.

Additionally, we looked for a signal of temporal autocovariance in Bergland et al. (2014), a study that collected *Drosophila melanogaster* through Spring-Fall seasons across three years. With a pattern of genome-wide fluctuating selection, we might expect a pattern of positive covariances between similar seasonal changes, and negative covariances between dissimilar seasonal changes. However, we find no such signal; we discuss this in more depth in Supplementary Materials Section 3.6.5.

The replicate design of Barghi et al. (2019) allows us to quantify another covariance: the covariance in allele frequency change between replicate populations experiencing convergent selection pressures. These between-replicate covariances are created in the same way as temporal covariances: neutral alleles linked to a particular fitness background experience are expected to have allele frequency changes in the same direction if the selection pressures are similar. Intuitively, where temporal covariances reflect that neutral alleles associated with heritable fitness backgrounds are predictive of frequency changes between generations, replicate covariances reflect that heritable fitness backgrounds common to each replicate predict (under the same selection pressures) frequency changes between

replicates. We measure this through a statistic similar to a correlation, which we call the convergent correlation: the ratio of average between-replicate covariance across all pairs to the average standard deviation across all pairs of replicates,

$$\mathrm{cor}(\Delta p_s, \Delta p_t) = \frac{\mathbb{E}_{A \neq B}\left(\mathrm{Cov}(\Delta p_{s,A}, \Delta p_{t,B})\right)}{\mathbb{E}_{A \neq B}\left(\sqrt{\mathrm{Var}(\Delta p_{s,A})\,\mathrm{Var}(\Delta p_{t,B})}\right)} \tag{3.2}$$

where A and B here are two replicate labels, and for the Barghi et al. (2019) data, we use $\Delta_{10} p_t$.

We've calculated the convergent correlation for all rows of the replicate covariance matrices. Like temporal covariances, we visualize these through time (Figure 3.2 A), with each line representing the convergent correlation from a particular reference generation s as it varies with t (shown on the x-axis). In other words, each of the colored lines corresponds to the like-colored row of the convergence correlation matrix (upper left in Figure 3.2 A). We find these convergent covariances are relatively weak, and decay very quickly from an initial value of about 0.1 (95% block bootstrap confidence intervals $[0.094, 0.11]$) to around 0.01 (95% CIs [0.0087, 0.015]) within 20 generations. This seems to confirm a primary finding of the original Barghi et al. (2019) study: that alternative loci contribute to adaptation in different replicates.

A benefit of between-replicate covariances is that unlike temporal covariances, these can be calculated with only two sequenced timepoints and a replicated study design. This allowed us to assess the impact of linked selection in driving convergent patterns of allele frequency change across replicate populations in two other studies. First, we reanalyzed the selection experiment of Kelly and Hughes (2019), which evolved three replicate wild populations of *Drosophila simulans* for 14 generations adapting to a novel laboratory environment. Since each replicate was exposed to the same selection pressure and share linkage disequilibria common to the original natural founding population, we expected each of the three replicate populations to have positive between-replicate covariances. We find all three pairwise between-replicate covariances are positive and statistically significant (95% CIs, [0.0063, 0.0086], [0.0064, 0.0086], [0.0061, 0.0083]). We estimate the

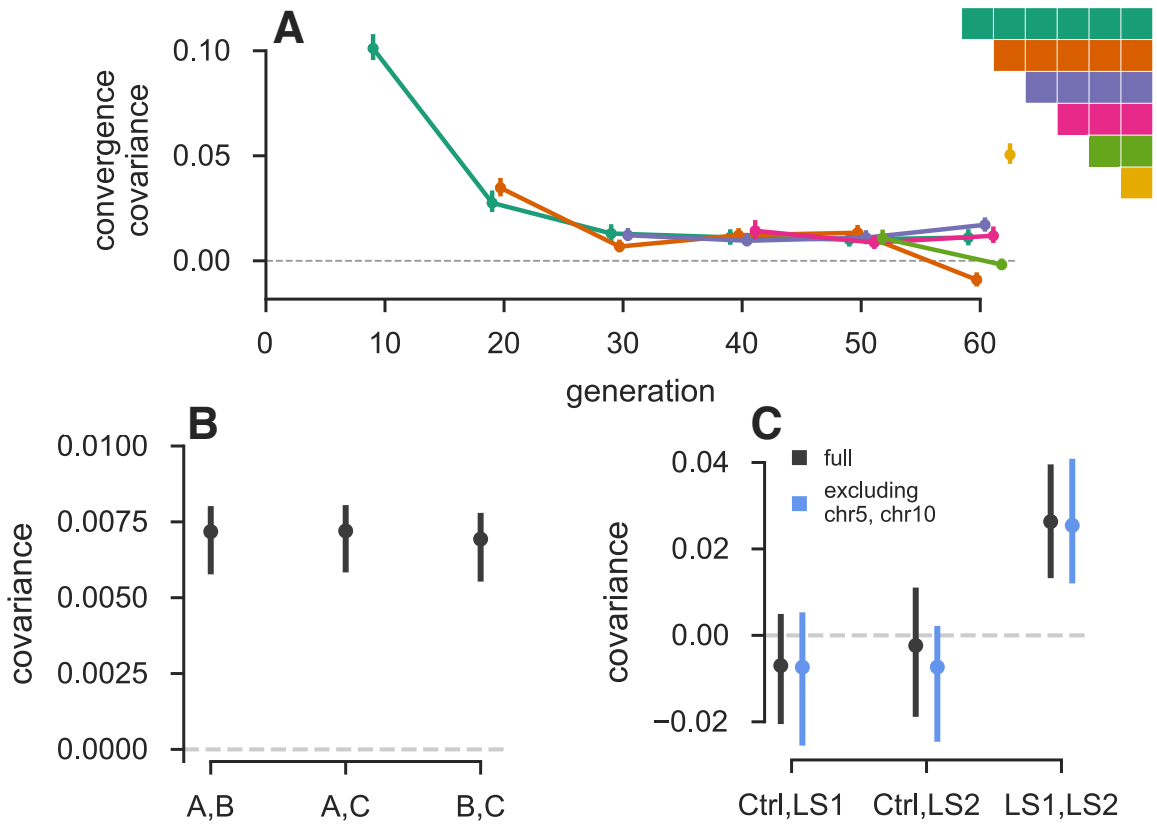

Figure 3.2: **A**: The convergence correlation, averaged across replicate pairs, through time. Each line represents the convergence correlation cor$(\Delta p_s, \Delta p_s)$ from a starting reference generation s to a later time t, which varies along the x-axis; each line corresponds to a row of the temporal convergence correlation matrix depicted to the right. **B**: The convergence covariance between individual pairs of replicates in the Kelly and Hughes (2019) data. **C**: The convergence covariance between individual pairs of replicates in (Castro et al. 2019) data, for the two selection lines (LS1 and LS2) and the control (Ctrl); gray CIs are those using the complete dataset, blue CIs exclude chromosomes 5 and 10 which harbor the two regions Castro et al. (2019) found to have signals of parallel selection between LS1 and LS2.

convergent correlation coefficient across these replicates as 0.36 (95% block-bootstrap confidence interval $[0.31, 0.40]$).

Second, we reanalyzed the Longshanks selection experiment, which selected for longer tibiae length relative to body size in mice, leading to a response to selection of about 5 standard deviations over the course of twenty generations (Castro et al. 2019). This study includes two independent selection lines, Longshanks 1 and 2 (LS1 and LS2), and an unselected control line (Ctrl). Consequently, this selection experiment offers a useful control to test our between-replicate covariances: we expect to see positive between-

replicate covariance in the comparison between the two Longshanks selection lines, but not between the two pairwise comparisons between the control line and the two Longshanks lines. We find that this is the case (gray confidence intervals in Figure 3.2 C), with the two Longshanks comparisons to the control line not being significantly different from zero, while the comparison between the two Longshanks line is statistically significantly different from zero (CIs [0.013, 0.037]).

A major finding in the Longshanks study were two major-effect loci that showed parallel frequency shifts between the two selection lines: a region harboring the gene Nkx3-2 known to be involved in limb development, and another region harboring six other candidate genes. We were curious to what extent our genome-wide covariances were being driven by these two outlier large-effect loci, so we excluded them from the analysis. Since we do not know the extent to which linkage disequilibrium around these large-effect loci affects neighboring loci, we took the conservative precaution of excluding the entire chromosomes these loci reside on (chromosomes 5 and 10), and re-calculating the temporal covariances. We find excluding these large effect loci has little impact on the confidence intervals (blue confidence intervals in Figure 3.2), indicating that these across-replicate covariances are indeed driven by a polygenic signal.

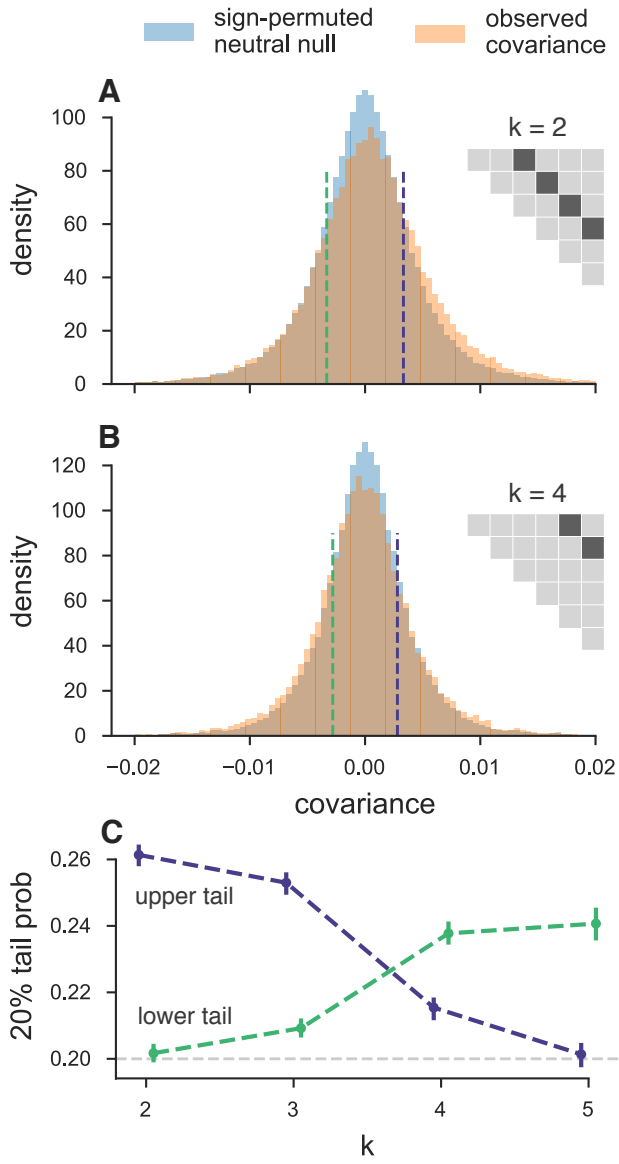

Figure 3.3: **A**, **B**: The distribution of temporal covariances calculated in 100kb genomic windows from the Barghi et al. (2019) study, plotted alongside an empirical neutral null distribution created by recalculating the windowed covariances on a 1,000 sign permutations of allele frequency changes within tiles. The histogram bin number is 88, chosen by cross validation (Supplementary Materials 3.2). In subfigure **A**, windowed covariances $\mathrm{Cov}(\Delta p_t, \Delta p_{t+k})$ are separated by $k = 2 \times 10$ generations and in subfigure **A** the covariances are separated by $k = 4 \times 10$ generations; each k is an off-diagonal from the variance diagonal of the temporal covariance matrix (see cartoon of upper-triangle of covariance matrix in subfigures **A** and **B**, where the first diagonal is the variance, and the dark gray indicates which off-diagonal of the covariance matrix is plotted in the histograms). **C**: The lower and upper tail probabilities of the observed windowed covariances, at 20% and 80% quintiles of the empirical neutral null distribution, for varying time between allele frequency changes (i.e. which off-diagonal k). The confidence intervals are 95% block-bootstrap confidence intervals, and the light gray dashed line indicates the 20% tail probability expected under the neutral null.

Finally, we observed that in the longest study we analyzed (Barghi et al. 2019), some genome-wide temporal covariances become negative at future timepoints (see the first two rows in Figure 3.1 A). This shows that alleles that were on average going up initially are later going down in frequency, i.e. that the average direction of selection experienced by alleles has flipped. This must reflect either a change in the environment or the genetic background, due to epistatic relationships among alleles altered by frequency changes or recombination breaking up selective alleles. Such reversals of selective dynamics could be occurring at other timepoints but the signal of a change in the direction of selection at particular loci may be washed out when we calculate our genome-wide average temporal covariances. To address this limitation, we calculated the distribution of the temporal covariances over 100kb genomic windows (Figure 3.3, pooling across all replicates; see Supplementary Figure 3.4 for individuals replicates). The covariance of each tile will be noisy, due to sampling and genetic drift, and the neutral distribution of the covariance is complicated due to linkage disequilibria (which can occur over long physical distances in E&R and selection studies, Baldwin-Brown et al. 2014; Nuzhdin and Turner 2013). To address this, we have developed a permutation-based procedure that constructs a null distribution by randomly flipping the signs of the allele frequency changes per-genomic window. This destroys the systematic covariances created by linked selection and creates a sampling distribution of the covariances spuriously created by neutral genetic drift while preserving the complex dependencies between adjacent loci created by linkage disequilibrium. This empirical neutral null distribution is conservative in the sense that the variances of the covariances are wider than expected under drift alone as they include the effect of selection on the allele frequency change within a time-interval, just not between time-intervals. We see (Figure 3.3 A and B) that windowed temporal covariances between close timepoints are skewed positive (a heavy right tail), while between more distant timepoints these windowed temporal covariances tend to shift to become more negative (a heavy left tail). We quantified the degree to which the left and right tails are inflated compared to the null distribution as a function of time, and see excesses in both tails in Figure 3.3 C. This finding is also robust to sign-permuting allele frequency changes

on a chromosome-level, the longest extent that gametic linkage disequilibria can extend (Supplementary Figure 3.7). We see a striking pattern that the windowed covariances not only decay towards zero, but in fact become negative through time, consistent with many regions in the genome having had a reversed fitness effect at later timepoints.

3.3 Discussion

Since the seminal analysis of Maynard Smith and Haigh (1974) demonstrating that diversity is reduced at linked neutral variation as an advantageous polymorphism sweeps to fixation, over four decades of theoretical and empirical research has enriched our understanding of linked selection. This work has led to the discovery of selected genes from genomic signals of hitchhiking (Nair et al. 2003; Voight et al. 2006), found genome-wide signals of linked selection (Aguade et al. 1989; Andersen et al. 2012; Begun and Aquadro 1992; Cutter and Choi 2010; Cutter and Payseur 2003) leading to the development of recurrent hitchhiking (Stephan et al. 1992) and background selection (Charlesworth et al. 1993) models that attempt explain this pattern. Since, much attention has focused on quantifying the impact of background selection (McVicker et al. 2009) and developing theoretic machinery (Coop and Ralph 2012) to differentiate the regional reductions in diversity into those caused by full and partial sweeps, and those caused by background selection (Elyashiv et al. 2016). However, as other models of soft sweeps from standing variation emerged (Hermisson and Pennings 2005; Pennings and Hermisson 2006), attention shifted towards detecting other modes of linked selection (Pritchard et al. 2010), a more difficult endeavor (Przeworski et al. 2005) addressed using new coalescent models (Berg and Coop 2015) and machine learning methods (Schrider and Kern 2017). An alternative approach to understanding the genome-wide effects of selection on standing variation, e.g. selection on an infinitesimal polygenic trait, stems from an early quantitative genetic model of linked selection (Robertson 1961) and its later developments (Santiago and Caballero 1995, 1998; see also Barton 2000 for a comparison of these models with classic hitchhiking models). Implicit in these models is that autocovariance between allele frequency change is created when there is heritable fitness variation in the

population, a signal that can be readily detected from temporal genomic data (Buffalo and Coop 2019). Here, we provide the first empirical evidence of linked selection acting on standing variation over very short timescales.

We reanalyzed three published temporal genomic datasets and detected the genome-wide signature of linked selection acting over tens of generations. Furthermore, we find the dynamics of temporal autocovariance are consistent with theory; the temporal covariance in allele frequencies decays as both the fitness variation associated with particular haplotypes and the linkage disequilibria between selected and neutral loci decay through time. In reanalyzing one study (Barghi et al. 2019), we find that after sixty generations, greater than 20% of the variation in allele frequency change is directly due to the action linked selection. Capitalizing on replicated evolve-and-resequence study designs, we characterized the extent to which convergent selection pressures lead to parallel changes in allele frequencies across replicate populations, finding moderate correlations in allele frequency changes.

While we must keep in mind that the studies analyzed here were all laboratory populations and natural selection in the wild will likely differ, overall we have found that linked selection has a remarkably strong effect for such short study durations. Depending on how many loci affect fitness, such a strong effect of linked selection may not be differentiable from genetic drift using only single contemporary population samples. In this way, temporal data allows us to sidestep the key problem of detecting selection from standing variation: that the genomic footprint leaves too soft of a signature to differentiate from a background of genetic drift. In fact we find that the temporal covariance signal is detectable even in the most extremely difficult to detect soft sweep case: polygenic selection on an infinitesimal trait. In our reanalysis of the Castro et al. (2019) data, by showing the covariance signal remains even after excluding the chromosomes containing two large-effect loci, we showed the covariance signal we detect is indeed driven by polygenic fitness variation (and confirm a point in the original study that tibiae length, aside from these two large effect loci, is a highly polygenic trait).

It is worth building some intuition why temporal covariance allows us to detect such

faint signals of polygenic linked selection from temporal genomic data. Each variant is subject to both variance in allele frequency due to drift and two levels of sampling noise (as individuals are sampled from the population and reads are sampled from amplified DNA), which at any locus swamps the temporal covariance signal and creates spurious covariances. However, these spurious covariances do not share a common sign across timepoints whereas the covariances created by linked selection do; consequently, averaging across the entire genome, the temporal signal exceeds sampling noise.

One limitation of these analyses is that none of the studies we reanalyzed estimated linkage disequilibria data for the evolved populations. Our theory of temporal autocovariance tells us that the temporal autocovariances a neutral site experiences is determined by the product of the expected linkage disequilibrium and additive fitness variation that persists through the generations (Buffalo and Coop 2019). This leads to a clear prediction: regions of higher linkage disequilibrium and lower recombination should have greater temporal autocovariance than regions with lower LD and higher recombination. Unfortunately, we lack a high-resolution recombination map for *D. simulans* and while there are LD data for *D. simulans* (Signor et al. 2018) we did not find a relationship between temporal covariance and LD.

We believe this is driven by the idiosyncratic nature of LD in evolve-and-resequence populations (Kelly and Hughes 2019; Nuzhdin and Turner 2013), and that we might find such a relationship if LD data from the evolved population were available. Unfortunately, sequencing multiple timepoints is expensive and the low-coverage and/or pooled-sequencing approaches common in these studies prohibit estimating linkage disequilibrium. Future studies complete with LD data and recombination maps would allow one to disentangle the influence of closely linked sites from more distant sites in causing temporal autocovariance, and allow us to better understand whether sites in high recombination regions are free from the effects of linked selection. Furthermore, such additional data would allow for localizing the effects of temporal covariance, which would allow us to estimate not just the genome-wide fraction of variation in frequency change ($G(t)$), but also the fraction of the genome impacted by linked selection, allowing us to synthesize

the temporal approach with single-timepoint studies like that of Elyashiv et al. (2016).

Thus far, the most comprehensive studies implicating linked selection in affecting genome-wide diversity have been in *Drosophila* (Begun and Aquadro 1992; Elyashiv et al. 2016; Sattath et al. 2011) and *Caenorhabditis* (Andersen et al. 2012; Cutter and Payseur 2003), whereas the evidence for linked selection in plant and yeast species is weak (Cutter and Payseur 2013). Both *Drosophila* and *Caenorhabditis* have short genetic maps (or in the case of selfing *C. elegans*, small effective recombination rates), and large effect population sizes, two factors predicted to increase the degree to which hitchhiking impacts genome-wide diversity (Barton 2000). However, our results here show that even with small effective population sizes (300, 450, and 45 for the Kelly and Hughes (2019), and Castro et al. (2019) studies respectively) and, in the case of mice, moderately-sized genetic maps (around 14 Morgans; Cox et al. 2009), we still see a fairly strong effect of linked selection. This suggests that while these factors may govern the dynamics of classic hitchhiking events, they could perhaps play less of a role in polygenic linked selection. However, with only three cases analyzed, further studies on different taxa are needed.

Finally, in reanalyzing the Barghi et al. (2019) study, we find evidence of complex linked selection dynamics. This is due either to a change in the environment and its consequences for the fitness of regions in the genome, recombination breaking up selected alleles, or epistatic interactions between loci. It is important to note that the original study did not intentionally alter the environment in any way; this signal is attained without intentionally seeking it out. Discerning which of these is creating negative temporal autocovariance is a sizable challenge, requiring sequencing each generation and LD data.

Overall, we hope this will encourage more temporal genomic studies in both laboratory and natural populations. Understanding the dynamics of linked selection over short timescales will help to unite phenotypic studies of rapid adaptation of polygenic adaptations with a detectable genomic signature, to address long-standing questions concerning linked selection, evolutionary quantitative genetics, and the overall impact selection has on genetic variation.

3.4 Appendix

3.5 Estimator Bias Correction

3.5.1 Correcting variance bias with a single depth sampling process

Following Waples (1989), we have that that the variance in allele frequency change at a locus in the initial generation, which is entirely due to the binomial sampling process, is $\mathrm{Var}(p_0) = {}^{p_0(1-p_0)}/_{d_0}$ where d_0 is the number of binomial draws (e.g. read depth). At a later timepoint, the variance in allele frequency is a result of both the binomial sampling process at time t and the evolutionary process. Using the law of total variation we can partition the variation from each process,

$$\mathrm{Var}(\widetilde{p_t}) = \mathbb{E}(\mathrm{Var}(\widetilde{p_t}|p_t)) + \mathrm{Var}(\mathbb{E}(\widetilde{p_t}|p_t)) \tag{3.3}$$

$$= \underbrace{\frac{p_t(1-p_t)}{d_t}}_{\text{generation } t \text{ sampling noise}} + \underbrace{\mathrm{Var}(p_t)}_{\text{variance due to evolutionary process}} . \tag{3.4}$$

Under a drift-only process, $\mathrm{Var}(p_t) = p_0(1-p_0)\left[1 - \left(1 - \frac{1}{2N}\right)^t\right]$. However, with heritable variation in fitness, we need to consider the covariance in allele frequency changes across generations (Buffalo and Coop 2019). We can write

$$V(p_t) = V\left(p_0 + (p_1 - p_0) + (p_2 - p_1) + \ldots + (p_t - p_{t-1})\right) \tag{3.5}$$

$$= V\left(p_0 + \Delta p_0 + \Delta p_1 + \ldots + \Delta p_{t-1}\right) \tag{3.6}$$

$$= V(p_0) + \sum_{i=0}^{t-1} \mathrm{Cov}(p_0, \Delta p_i) + \sum_{i=0}^{t-1} \mathrm{Var}(\Delta p_i) + \sum_{0 \le i < j}^{t-1} \mathrm{Cov}(\Delta p_i, \Delta p_j). \tag{3.7}$$

Each allele frequency change is equally like to be positive as it is to be negative; thus by symmetry this second term is zero. Additionally $V(p_0) = 0$, as we treat p_0 as a fixed initial frequency. We can write,

$$V(p_t) = \sum_{i=0}^{t-1} \mathrm{Var}(\Delta p_i) + \sum_{0 \le i < j}^{t-1} \mathrm{Cov}(\Delta p_i, \Delta p_j). \tag{3.8}$$

The second term, the cumulative impact of variance in allele frequency change can be partitioned into heritable fitness and drift components (Buffalo and Coop 2019; Santiago and Caballero 1995)

$$V(p_t) = \sum_{i=0}^{t-1} \mathrm{Var}(\Delta_{D} p_i) + \sum_{i=0}^{t-1} \mathrm{Var}(\Delta_{H} p_i) + \sum_{0 \le i < j}^{t-1} \mathrm{Cov}(\Delta p_i, \Delta p_j). \tag{3.9}$$

where $\Delta_{H} p_t$ and $\Delta_{D} p_t$ indicate the allele frequency change due to heritable fitness variation and drift respectively. Then, sum of drift variances in allele frequency change is

$$\sum_{i=0}^{t-1} \mathrm{Var}(\Delta_{D} p_i) = \sum_{i=0}^{t-1} \frac{p_i(1-p_i)}{2N} \tag{3.10}$$

replacing the heterozygosity in generation i with its expectation, we have

$$\sum_{i=0}^{t-1} \mathrm{Var}(\Delta_{D} p_i) = p_0(1-p_0) \sum_{i=0}^{t-1} \frac{1}{2N} \left(1 - \frac{1}{2N}\right)^{i} \tag{3.11}$$

$$= p_0(1-p_0) \left[1 - \left(1 - \frac{1}{2N}\right)^{t}\right] \tag{3.12}$$

which is the usual variance in allele frequency change due to drift. Then, the total allele frequency change from generations 0 to t is $\mathrm{Var}(\widetilde{p}_t - \widetilde{p}_0) = \mathrm{Var}(\widetilde{p}_t) + \mathrm{Var}(\widetilde{p}_0) - 2\,\mathrm{Cov}(\widetilde{p}_t, \widetilde{p}_0)$, where the covariance depends on the nature of the sampling plan (see Nei and Tajima 1981; Waples 1989). In the case where there is heritable variation for fitness, and using the fact that $\mathrm{Cov}(\widetilde{p}_t, \widetilde{p}_0) = {}^{p_0(1-p_0)}/_{2N}$ for Plan I sampling procedures (Waples 1989), we write,

$$\mathrm{Var}(\widetilde{p}_t - \widetilde{p}_0) = \mathrm{Var}(\widetilde{p}_t) + \mathrm{Var}(\widetilde{p}_0) - 2C\,\mathrm{Cov}(\widetilde{p}_t, \widetilde{p}_0) \tag{3.13}$$

$$= \frac{p_t(1-p_t)}{d_t} + \frac{p_0(1-p_0)}{d_0} + p_0(1-p_0)\left[1 - \left(1 - \frac{1}{2N}\right)^t\right] + \tag{3.14}$$

$$\sum_{i=0}^{t-1} \mathrm{Var}(\Delta_{_H} p_i) + \sum_{0 \le i < j}^{t-1} \mathrm{Cov}(\Delta p_i, \Delta p_j) - \frac{C p_0(1-p_0)}{2N} \tag{3.15}$$

$$\frac{\mathrm{Var}(\widetilde{p}_t - \widetilde{p}_0)}{p_0(1-p_0)} = 1 + \frac{p_t(1-p_t)}{p_0(1-p_0)d_t} + \frac{1}{d_0} - \left(1 - \frac{1}{2N}\right)^t + \tag{3.16}$$

$$\sum_{i=0}^{t-1} \frac{\mathrm{Var}(\Delta_{_H} p_i)}{p_0(1-p_0)} + \sum_{0 \le i < j}^{t-1} \frac{\mathrm{Cov}(\Delta p_i, \Delta p_j)}{p_0(1-p_0)} - \frac{C}{N} \tag{3.17}$$

where $C = 1$ if Plan I is used, and $C = 0$ if Plan II is used (see Waples 1989, p. 380 and Figure 1 for a description of these sampling procedures; throughout the paper we use sampling Plan II). We move terms creating a bias-corrected estimator for the population variance in allele frequency change, and replace all population heterozygosity terms with the unbiased sample estimators, e.g. $\frac{d_t}{d_t - 1}\widetilde{p}_t(1-\widetilde{p}_t)$,

$$\frac{d_0 - 1}{d_0}\frac{\mathrm{Var}(\widetilde{p}_1 - \widetilde{p}_0)}{\widetilde{p}_0(1-\widetilde{p}_0)} - \frac{(d_0 - 1)}{d_0(d_1 - 1)}\frac{\widetilde{p}_1(1-\widetilde{p}_1)}{\widetilde{p}_0(1-\widetilde{p}_0)} - \frac{1}{d_0} + \frac{C}{N} = \frac{\mathrm{Var}(\Delta_{_H} p_0)}{p_0(1-p_0)} + \frac{1}{2N} \tag{3.18}$$

3.5.2 Correcting variance bias with individual and depth sampling processes

Here, we extend the sampling bias correction described above to handle two binomial sampling processes: one as individuals are binomially sampled from the population, and another as reads are binomially sampled during sequencing. (see also Jónás et al. 2016). Let $X_t \sim \mathrm{Binom}(n_t, p_t)$ where X_t is the count of alleles and n_t is the number of diploids sampled at time t. Then, these individuals are sequenced at a depth of d_t, and $Y_t \sim \mathrm{Binom}(d_t, {}^{X_t}/_{n_t})$ reads have the tracked allele. We let $\widetilde{p}_t = {}^{Y_t}/_{d_t}$ be the observed sample allele frequency. Then, the sampling noise is

$$\mathrm{Var}(\widetilde{p}_t|p_t) = \mathbb{E}(\mathrm{Var}(\widetilde{p}_t|X_t)) + \mathrm{Var}(\mathbb{E}(\widetilde{p}_t|X_t)) \tag{3.19}$$

$$= p_t(1-p_t)\left(\frac{1}{n_t} + \frac{1}{d_t} - \frac{1}{n_t d_t}\right) \tag{3.20}$$

$$\mathrm{Var}(\widetilde{p}_t - \widetilde{p}_0) = p_t(1-p_t)\left(\frac{1}{n_t} + \frac{1}{d_t} - \frac{1}{n_t d_t}\right) + p_0(1-p_0)\left(\frac{1}{n_0} + \frac{1}{d_0} - \frac{1}{n_0 d_0}\right) \tag{3.21}$$

$$- \frac{Cp_0(1-p_0)}{N} + p_0(1-p_0)\left[1 - \left(1 - \frac{1}{2N}\right)^t\right] + \sum_{i=0}^{t-1} \mathrm{Var}(\Delta_{_H} p_i) \tag{3.22}$$

$$+ \sum_{0 \le i < j}^{t-1} \mathrm{Cov}(\Delta p_i, \Delta p_j) \tag{3.23}$$

Through the law of total expectation (see Kolaczkowski et al. 2011 Supplementary File 1 for a sample proof), one can find that an unbiased estimator of the half the heterozygosity is

$$\frac{n_t d_t}{(n_t - 1)(d_t - 1)} \widetilde{p}_t(1 - \widetilde{p}_t). \tag{3.24}$$

Replacing this unbiased estimator for half of the heterozygosity into our expression above, the total sample variance is

$$\mathrm{Var}(\widetilde{p}_t - \widetilde{p}_0) = \frac{n_t d_t \widetilde{p}_t(1-\widetilde{p}_t)}{(n_t-1)(d_t-1)}\left(\frac{1}{n_t} + \frac{1}{d_t} - \frac{1}{n_t d_t}\right) + \frac{n_0 d_0 \widetilde{p}_0(1-\widetilde{p}_0)}{(n_0-1)(d_0-1)}\left(\frac{1}{n_0} + \frac{1}{d_0} - \frac{1}{n_0 d_0}\right) + \tag{3.25}$$

$$\frac{n_0 d_0 \widetilde{p}_0(1-\widetilde{p}_0)}{(n_0-1)(d_0-1)}\left[1 - \left(1 - \frac{1}{2N}\right)^t\right] - \frac{C}{N}\frac{n_0 d_0 \widetilde{p}_0(1-\widetilde{p}_0)}{(n_0-1)(d_0-1)} + \sum_{i=0}^{t-1} \mathrm{Var}(\Delta_{_H} p_i) + \sum_{0 \le i < j}^{t-1} \mathrm{Cov}(\Delta p_i, \Delta p_j). \tag{3.26}$$

As with equation (3.18), we can rearrange this to get a biased-correct estimate of the variance in allele frequency change between adjacent generations, $\mathrm{Var}(\Delta p_t)$.

3.5.3 Covariance Correction

We also need to apply a bias correction to the temporal covariances (and possibly the replicate covariances if the initial sample frequencies are all shared). The basic issue is that $\mathrm{Cov}(\Delta\widetilde{p}_t, \Delta\widetilde{p}_{t+1}) = \mathrm{Cov}(\widetilde{p}_{t+1} - \widetilde{p}_t, \widetilde{p}_{t+2} - \widetilde{p}_{t+1})$, and thus shares the sampling noise of timepoint $t+1$. Thus acts to bias the covariance by subtracting off the noise variance term of $\mathrm{Var}(\widetilde{p}_{t+1})$, so we add the expectation of this bias, derived above, back in. We discuss this in more detail below in deriving the bias correction for the temporal-replicate variance covariance matrix.

3.5.4 Temporal-Replicate Covariance Matrix Correction

In practice, we simultaneously estimate the temporal and replicate covariance matrices for each replicate, which we call the temporal-replicate covariance matrix. This needs a bias correction; we extend the bias corrections for single locus variance and covariance described in Supplementary Material Sections 3.5.1, 3.5.2, and 3.5.3 to multiple sampled loci and the temporal-replicate covariance matrix here. With frequency data collected at $T+1$ timepoints across R replicate populations at L loci, we have multidimensional arrays $\mathbf{F}$ of allele frequencies, $\mathbf{D}$ of sequencing depths, and $\mathbf{N}$ of the number of individuals sequenced, each of dimension $R \times (T+1) \times L$. We calculate the array $\mathbf{\Delta F}$ which contains the allele frequency changes between adjacent generations, and has dimension $R \times T \times L$. The operation $\mathrm{flat}(\mathbf{\Delta F})$ flattens this array to a $(R \cdot T) \times L$ matrix, such that rows are grouped by replicate, e.g. for timepoint t, replicate r, and locus l such that for allele frequencies $p_{t,r,l}$, the frequency change entries are

$$\mathrm{flat}(\mathbf{\Delta F}) = \begin{bmatrix} \Delta p_{1,0,0} & \Delta p_{2,0,0} & \dots & \Delta p_{1,1,0} & \Delta p_{2,1,0} & \dots & \Delta p_{T,R,0} \\ \Delta p_{1,0,1} & \Delta p_{2,0,1} & \dots & \Delta p_{1,1,1} & \Delta p_{2,1,1} & \dots & \Delta p_{T,R,1} \\ \vdots & \vdots & \ddots & \vdots & \vdots & \ddots & \vdots \\ \Delta p_{1,0,L} & \Delta p_{2,0,L} & \dots & \Delta p_{1,1,L} & \Delta p_{2,1,L} & \dots & \Delta p_{T,R,L} \end{bmatrix} \tag{3.27}$$

where each $\Delta p_{t,r,l} = p_{t+1,r,l} - p_{t,r,l}$. Then, the sample temporal-replicate covariance matrix $\mathbf{Q}'$ calculated on $\mathrm{flat}(\mathbf{\Delta F})$ is a $(R \cdot T) \times (R \cdot T)$ matrix, with the R temporal-covariance

block submatrices along the diagonal, and the $R(R-1)$ replicate-covariance submatrices matrices in the upper and lower triangles of the matrix,

$$\mathbf{Q}' = \begin{bmatrix} \mathbf{Q}'_{1,1} & \mathbf{Q}'_{1,2} & \dots & \mathbf{Q}'_{1,R} \\ \mathbf{Q}'_{2,1} & \mathbf{Q}'_{2,2} & \dots & \mathbf{Q}'_{2,R} \\ \vdots & \vdots & \ddots & \vdots \\ \mathbf{Q}'_{R,1} & \mathbf{Q}'_{R,2} & \dots & \mathbf{Q}'_{R,R} \end{bmatrix} \tag{3.28}$$

where each submatrix $\mathbf{Q}'_{i,j}$ $(i \neq j)$ is the $T \times T$ sample replicate covariance matrix for replicates i and j, and the submatrices along the diagonal $\mathbf{Q}'_{r,r}$ are the temporal covariance matrices for replicate r.

Given the bias of the sample covariance of allele frequency changes, we calculated an expected bias matrix $\mathbf{B}$, averaging over loci,

$$\mathbf{B} = \frac{1}{L} \sum_{l=1}^{L} \frac{\mathbf{h}_l}{2} \circ \left(\frac{1}{\mathbf{d}_l} + \frac{1}{2\mathbf{n}_l} + \frac{1}{2\mathbf{d}_l \circ \mathbf{n}_l} \right) \tag{3.29}$$

where $\circ$ denotes elementwise product, and $\mathbf{h}_l$, $\mathbf{d}_l$, and $\mathbf{n}_l$, are rows corresponding to locus l of the unbiased heterozygosity arrays $\mathbf{H}$, depth matrix $\mathbf{D}$, and number of diploids matrix $\mathbf{N}$. The unbiased $R \times (T+1) \times L$ heterozygosity array can be calculated as

$$\mathbf{H} = \frac{2\mathbf{D} \circ \mathbf{N}}{(\mathbf{D}-1) \circ (\mathbf{N}-1)} \circ \mathbf{F} \circ (1-\mathbf{F}) \tag{3.30}$$

where division here is elementwise. Thus, $\mathbf{B}$ is a $R \times (T+1)$ matrix. As explained in Supplementary Material Section 3.5.2 and 3.5.3, the temporal variances and covariances require bias corrections, meaning each temporal covariance submatrix $\mathbf{Q}_{r,r}$ requires two corrections. For an element $Q_{r,t,s} = \mathrm{Cov}(\Delta p_t, \Delta p_s)$ of the temporal covariance submatrix for replicate r, $\mathbf{Q}_{r,r}$, we apply the following correction

$$Q_{r,t,s} = \begin{cases} Q'_{r,t,s} - b_{r,t} - b_{r,t+1}, & \text{if } t = s \\ Q'_{r,t,s} + b_{r,\max(t,s)}, & \text{if } |t-s| = 1 \end{cases} \tag{3.31}$$

where $b_{r,t}$ is element in row r and column t of $\mathbf{B}$.

3.5.5 Barghi et al. (2019) Temporal Covariances

Since each replicate population was sequenced every ten generations, the timepoints $t_0 = 0$ generations, $t_1 = 10$ generations, $t_2 = 20$ generations, etc., lead to observed allele frequency changes across ten generation blocks, $\Delta p_{t_0}, \Delta p_{t_1}, \ldots, \Delta p_{t_6}$. Consequently, the ten temporal covariance matrices for each of the ten replicate populations have off-diagonal elements of the form $\mathrm{Cov}(\Delta p_{t_0}, \Delta p_{t_1}) = \mathrm{Cov}(p_{t_1} - p_{t_0}, p_{t_2} - p_{t_1}) = \sum_{i=0}^{10} \sum_{j=10}^{20} \mathrm{Cov}(\Delta p_i, \Delta p_j)$. Each diagonal element has the form $\mathrm{Var}(\Delta p_{t_0}) = \sum_{i=0}^{t_0} \mathrm{Var}(\Delta p_i) + \sum_{i \neq j}^{t_0} \mathrm{Cov}(\Delta p_i, \Delta p_j)$, and is thus a combination of the effects of drift and selection, as both the variance in allele frequency changes and cumulative temporal autocovariances terms increase the variance in allele frequency. With sampling each generation, one could more accurately partition the total variance in allele frequency change (Buffalo and Coop 2019); while we cannot directly estimate the contribution of linked selection to the variance in allele frequency change here, the presence of a positive observed covariance between allele frequency change can only be caused linked selection.

3.5.6 Block Bootstrap Procedure

To infer the uncertainty of covariance, convergence correlation, and $G(t)$ estimates, we used a block bootstrap procedure. This is a version of the bootstrap that resamples blocks of data points, rather than individual data points, to infer the uncertainty of an statistic in the presence of unknown correlation structure between data. With genome-wide data, linkage disequilibria between sites creates complex and unknown dependencies between variants. The estimators used in this paper are predominantly ratios, e.g. temporal-replicate covariance standardized by half the heterozygosity, $G(t)$ which is the ratio of covariance to total variance, and the convergence correlation (equation (3.2)). In these cases, we can exploit the linearity of the expectation to make the bootstrap procedure more computationally efficient, by pre-calculating the statistics of the ratio's numerator and denominator, $N(\mathbf{x}_i)$ and $D(\mathbf{x}_i)$, on the data $\mathbf{x}_i$ for all blocks $i \in \{1, 2, \ldots, W\}$ in the genome. Then we draw W bootstrap samples with replacement, and compute the estimate for bootstrap sample b with an average weighted by the number of loci in all sampled blocks,

$$\tilde{\theta}_b = \sum_{i=1}^{W} w_i \frac{N(\mathbf{x}_i)}{D(\mathbf{x}_i)} \tag{3.32}$$

Note that computing the ratio of averages rather than the average of a ratio is a practice common for population genetic statistics like F_{ST} (Bhatia et al. 2013). With these B bootstrap estimates, we calculate the $\alpha/2$ and $1 - \alpha/2$ quantiles, which we use to estimate the $1 - \alpha = 95\%$ pivot confidence intervals (p. 33 Wasserman 2006, p. 194 Davison and Hinkley 2013) throughout the paper,

$$C_\alpha = \left(2\widehat{\theta} - q_{1-\alpha/2}, 2\widehat{\theta} - q_{\alpha/2}\right). \tag{3.33}$$

where $\widehat{\theta}$ is the estimate, and q_x is bootstrap quantile for probability x.

3.6 Supplementary Figures

3.6.1 Bias Correction for Barghi et al. (2019)

We have investigated the effectiveness of our correction on real data by exploiting the relationship between sampling depth and the magnitude of the variance and covariance biases, and comparing the observed variances and covariances before and after correction. We plot the variance and covariance (between adjacent timepoints) before and after the bias correction against the average sample depth in 100kb genomic windows in Figure 3.1. Overall, we find the biased-correction procedure removes the relationship between variance and covariance and depth, indicating it is working adequately.

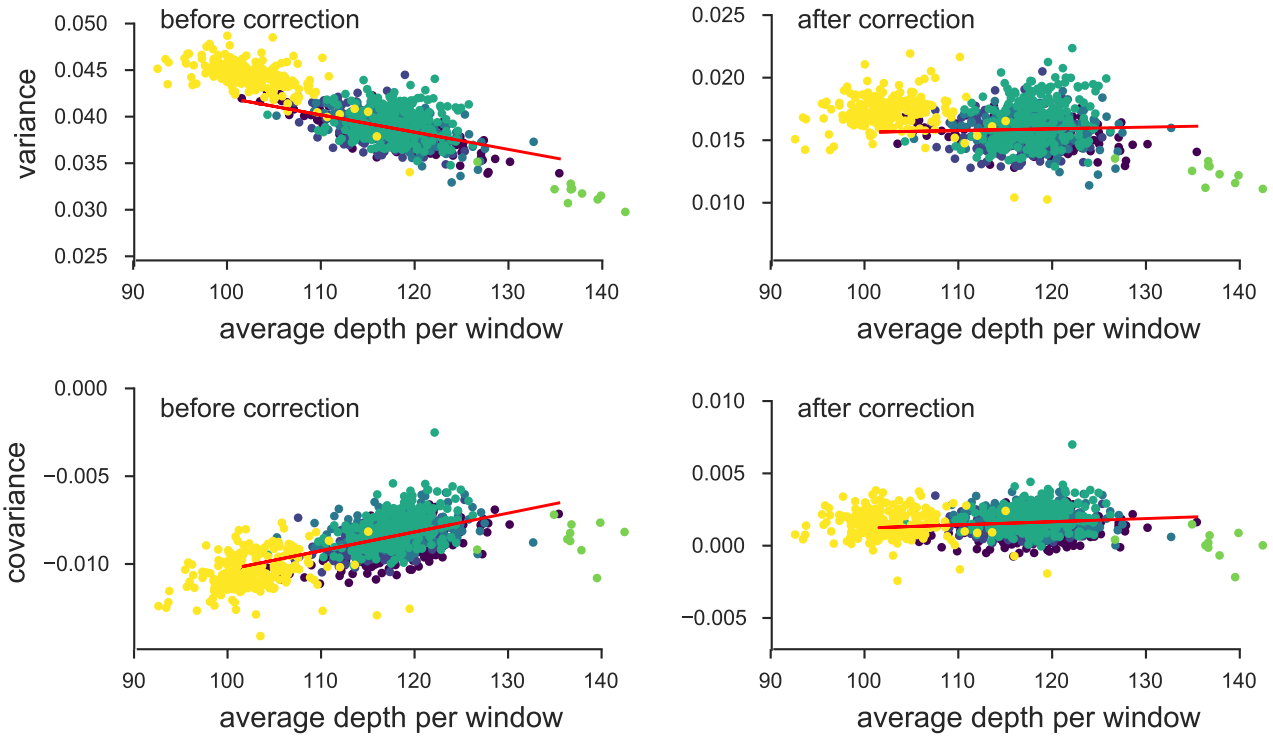

Figure 3.1: The variance and covariances from the Barghi et al. (2019) study, calculated in 100kb genomic windows plotted against average depth in a window before and after bias correction. Each panel has a least-squares estimate between the variance and covariance, and the average depth. Overall, the bias correction corrects sampling bias in both the variance and covariance such that the relationship with depth is constant. Colors indicate the different chromosomes of *D. simulans*; we have excluded the X chromosome (yellow points) and chromosome 4 points (green points to far right) from the regression due to large differences in average coverage.

3.6.2 Barghi et al. (2019) Binsize Cross-Validation

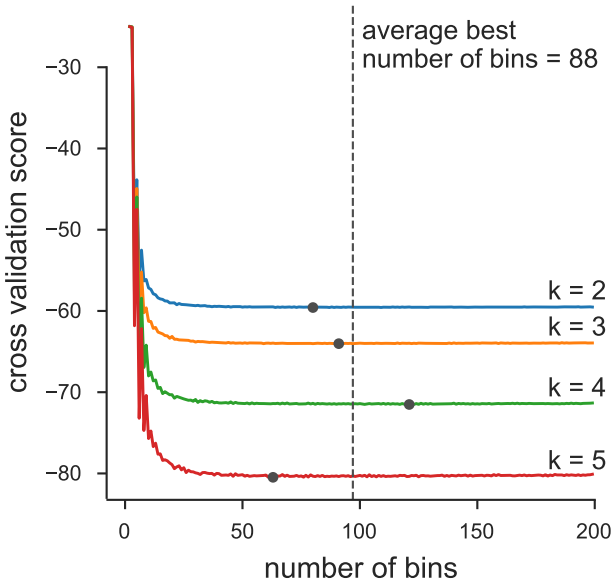

Figure 3.2: We chose number of bins used in the histograms of Figure 3.3 via an analytic expression for the cross-validation risk, based on the equation 6.16 of (Wasserman 2006, p. 129). Above, we plot the cross-validation risk for various numbers of bins, for each of the four off-diagonals of the temporal covariance matrix that we analyze. Overall, because the number of data points is large, oversmoothing is less of a problem, leading the cross-validation risk to be relatively flat across a large number of bins. Each gray point indicates the minimal risk for a particular off-diagonal, and the dashed line indicates the best average binwidth across off-diagonals.

3.6.3 Barghi et al. (2019) Empirical Null and Windowed Covariance Distributions

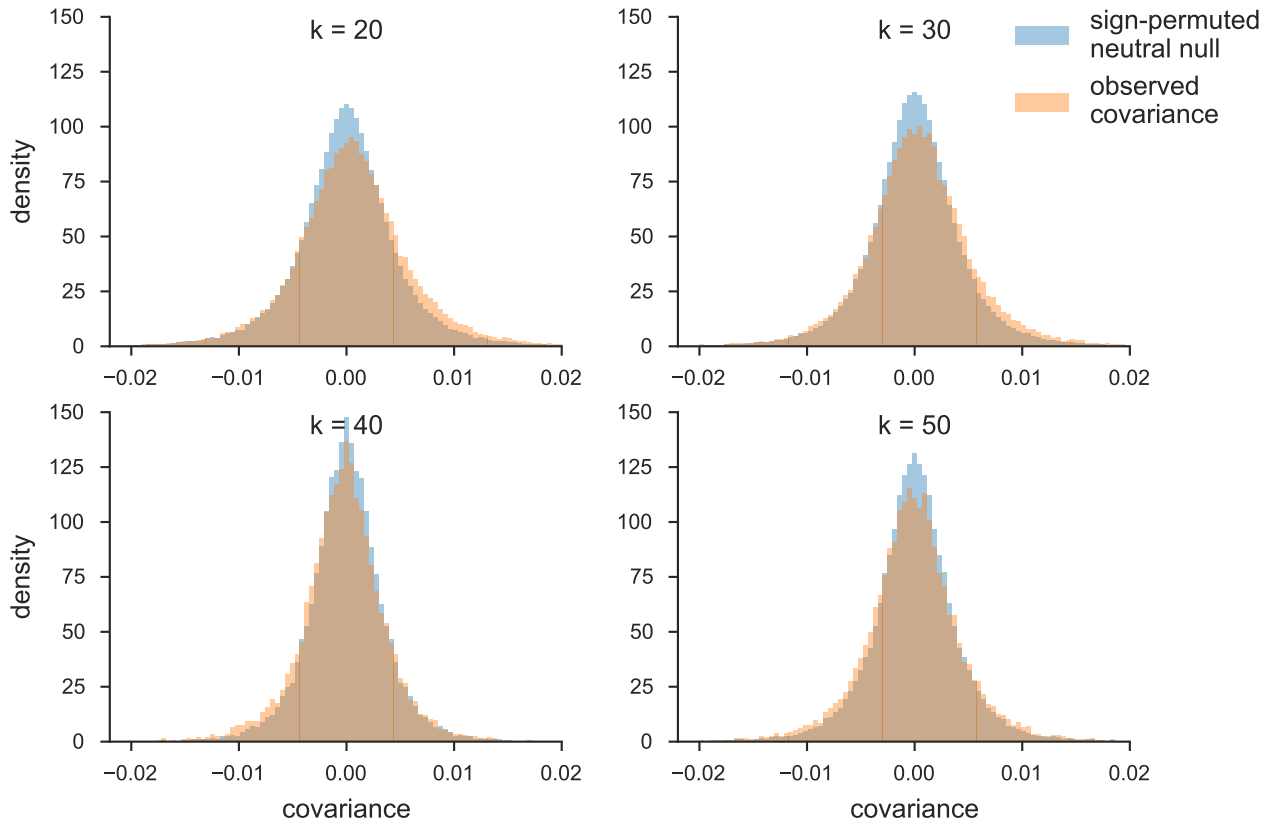

Figure 3.3: The distribution of temporal covariances calculated across 100kb genomic windows from Barghi et al. (2019)'s study (orange) and the block sign permuted empirical neutral null distribution of the windowed covariances (blue). Each panel shows these windowed covariances and the empirical null distribution for covariances $\mathrm{Cov}(\Delta p_t, \Delta p_{t+k})$, k is the number of generations between allele frequency changes.

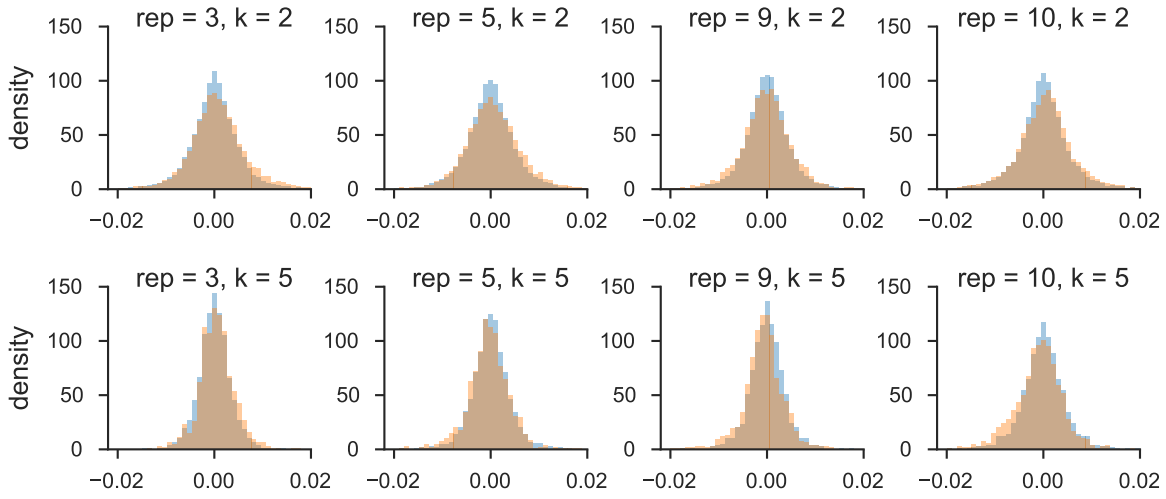

Figure 3.4: The distribution of windowed temporal covariances alongside the empirical neutral null for five randomly sampled replicates (columns), for $k = 2$ (first row) and $k = 5$ (second row). The main figure of the paper pools all replicate window and empirical neutral null covariances; we show here the windowed temporal covariances tend to shift from being positive (a heavier right tail) to become more negative (a heavier left tail) through time within particular replicates.

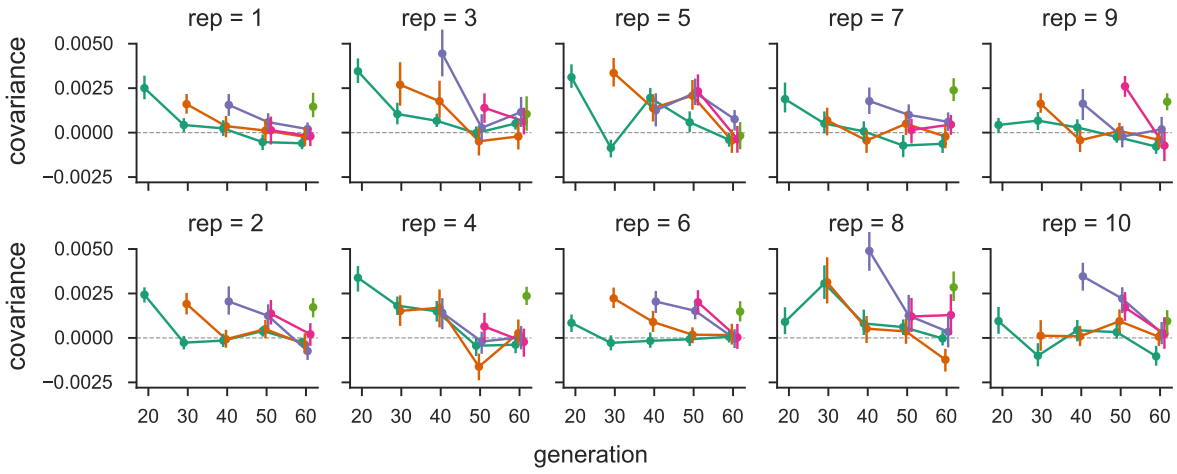

Figure 3.5: The temporal covariances from the Barghi et al. (2019) study, for each replicate individually. As in Figure 3.1, each line follows the temporal covariances from some initial reference generation through time, which represent the rows of temporal covariance matrix.

3.6.4 Barghi et al. (2019) Tail Probabilities for Windowed Covariances Distributions

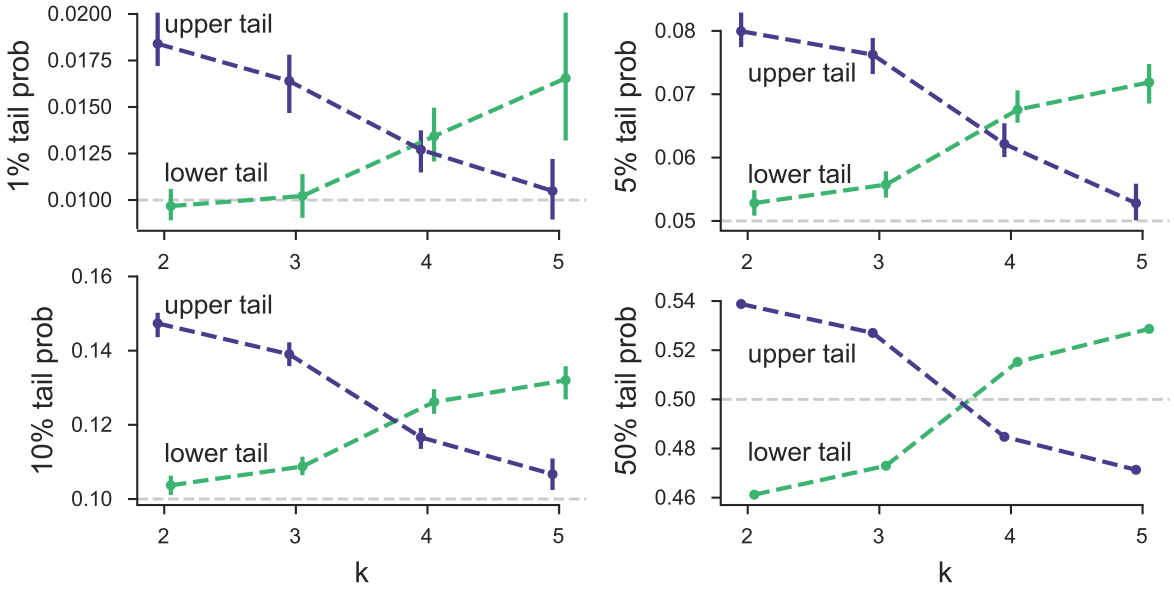

Figure 3.6: Tail probabilities of Barghi et al. (2019) data for various α levels

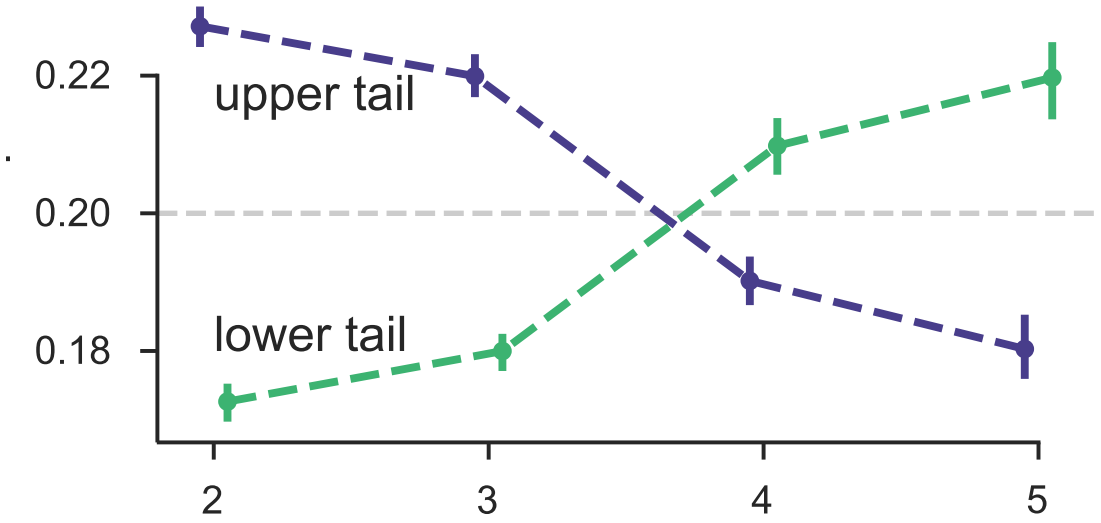

Figure 3.7: The 20% lower and upper tail probabilities for the observed windowed covariances from the Barghi et al. (2019) study, based on sign-permuting at the chromosome level. This permutation empirical null is robust to long-range linkage disequilibrium acting over entire chromosomes.

3.6.5 Bergland et al. (2014) Re-Analysis

We also applied our temporal covariance approach to Bergland et al. (2014), which found evidence of genome-wide fluctuating selection between Spring and Fall seasons across three years in *Drosophila melanogaster*. As described in Buffalo and Coop (2019), we might expect positive covariances between like seasons changes (i.e. Spring 2010 to Fall 2010 and Spring 2011 to Fall 2011), and negative covariances between dislike seasonal changes (i.e. Fall 2009 to Spring 2010 and Fall 2010 to Spring 2011) when fluctuating selection is strong and acts genome-wide, as the original study found. However, while we find temporal covariances that are non-zero, we find only weak support for a seasonal fluctuating model driving these covariances. In Supplementary Figure 3.11, we show the temporal covariances from varying reference generations, across seasonal transitions that are alike (e.g. the covariance between the allele frequency changes between Fall 2009 and Spring 2009, and frequency changes between Fall 2010 and Spring 2010), and dislike (e.g. the covariance between the allele frequency change between Fall 2009 and Spring 2009, and the frequency changes between Spring 2010 and Fall 2009). The first row of temporal covariance matrix is consistent with fluctuating selection operating for two timepoints, as the first covariance is negative, and the second is positive, and later covariances are not statistically differentiable from zero (which could occur if LD and additive genetic variance decay). However, the all other temporal covariances do not fit the pattern we would expect under genome-wide fluctuating selection.

We wanted to establish that our temporal-covariance matrix bias correction was working correctly. We find that it corrects the relationship between depth and both variance and covariance (Supplementary Figure 3.10) as expected.

It is unclear how strong the fluctuations would have to be to generate a genome-wide average signal of fluctuating selection from temporal covariances. For example, many loci could still show a signal of fluctuating selection, but the average signal could be overwhelmed by other signals of other selection. To investigate whether there was an genome-wide excess of loci showing evidence of fluctuating selection we reanalyzed the data of (Bergland et al. 2014) using the same seasonal fluctuating model as the original

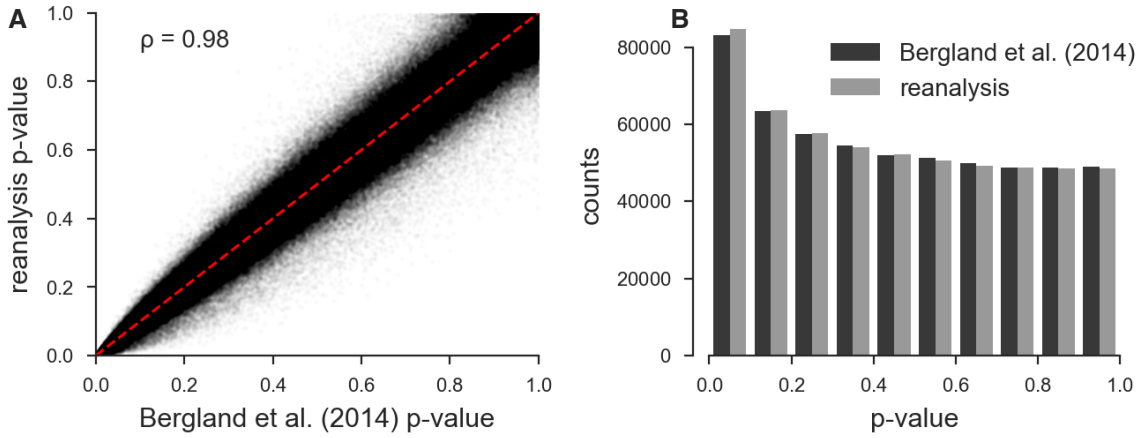

Figure 3.8: A: Scatterplot of the original unadjusted p-values from Bergland et al. (2014) and the p-values from our reanalysis of the same data using the same statistical methods; the minor discrepancy is likely due to software version differences. B: The histograms of the p-values of our reanalysis and the original Bergland et al. (2014) data; again the minor discrepancy is likely due to software differences. Overall, our implementation of Bergland et al.'s statistical methods produces results very close to the original analysis.

paper. This model is a Binomial logit-linked GLM fit per-locus, where the Spring/Fall seasons are encoded as a dummy variable, and are regressed on the frequency data. We use the same binomial weighting procedure as Bergland et al. (2014), where the weights are determined by the effective number of chromosomes, $N_{eff} = (2n_t d_t - 1)/(2n_t + d_t)$ (n_t and d_t are the number of diploid individuals and the read depth at timepoint t, respectively). We fit this model on all loci marked as used in the VCF provided with the Bergland et al. (2014) study (doi:10.5061/dryad.v883p). Overall, our p-values for the Wald test for each locus closely match those of the original paper (Pearson correlation coefficient 0.98, p-value $< 2.2 \times 10^{-16}$; see Supplementary Figure 3.8 A), and the histograms of the p-values are nearly identical (Supplementary Figure 3.8 B). Bergland et al. (2014) find loci with a significant association with season after a Benjamini and Hochberg FDR p-value adjustment (Benjamini and Hochberg 1995), however, the null hypothesis of the Wald test does not give us an idea of the expected number of variants that may spuriously fit the pattern of seasonal fluctuating selection.

To investigate whether there is a genome-wide evidence of an enrichment of fluctuating selection we created an empirical null distribution by randomly permuting the season

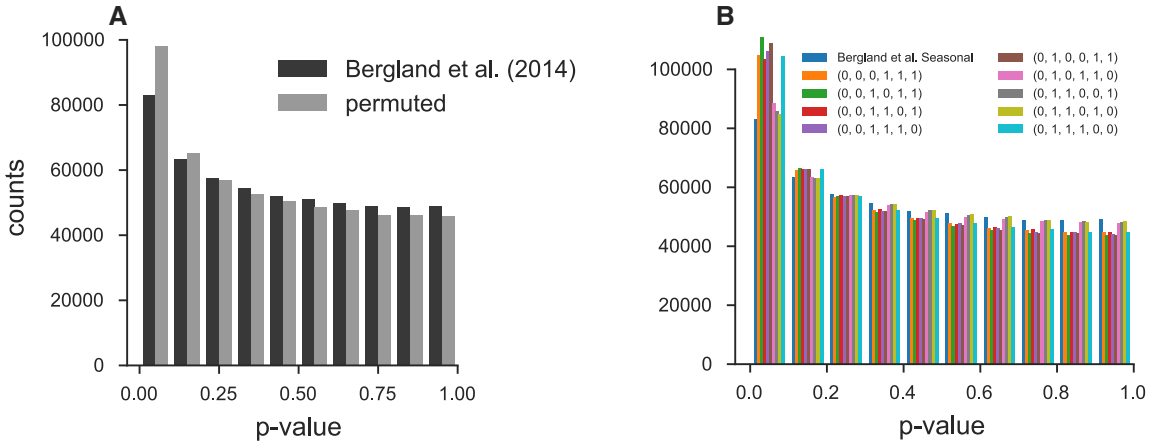

Figure 3.9: Distribution of p-values from the Bergland et al. (2014) study alongside permutation p-values at the loci level (A) and for each possible unique permutation (B).

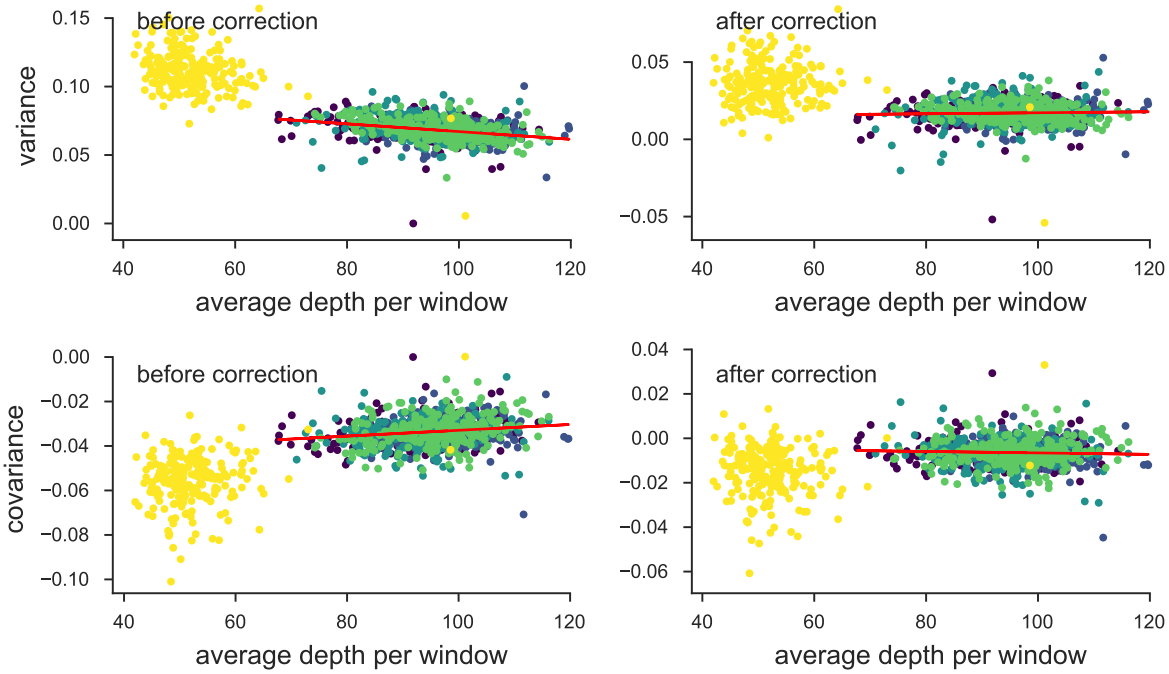

Figure 3.10: The variance and covariances from the Bergland et al. (2014) study, calculated in 100kb genomic windows plotted against average depth in a window before and after bias correction. Each panel has a least-squares estimate between the variance and covariance, and the average depth. The bias correction procedure is correcting sampling bias in both the variance and covariance such that the relationship with depth is constant. Colors indicate the different chromosomes of *D. melanogaster*; we have excluded the X chromosome (yellow points; chromosome 4 was not in the original study) from the regression due to large differences in average coverage.

labels and re-running the per-locus seasonal GLM model, as proposed by Machado et al. (2018). We find, regardless of whether we permute at the locus-level or the permutation replicate-level, that the observed seasonal p-value distribution Bergland et al. (2014) is not enriched for significant p-values beyond what we would expect from the permutation null. In fact, there appears there is more enrichment for low p-values when seasonal labels are randomly permuted (Supplementary Figure 3.9, suggesting by random chance we might expect more variants with a seasonal fluctuating pattern than found in the original Bergland et al. (2014) study. While surprising, this could be explained by the presence of temporal structure across the samples not consistent with seasonal fluctuating selection. Some fraction of the permutations happen to fit this structure well, leading to an enrichment of small p-values. This non-seasonal temporal structure is also evident in our temporal covariances (Supplementary Figure 3.11), where we see strong evidence of selection (non-zero temporal covariances), yet the pattern does not follow that of seasonal fluctuating selection.

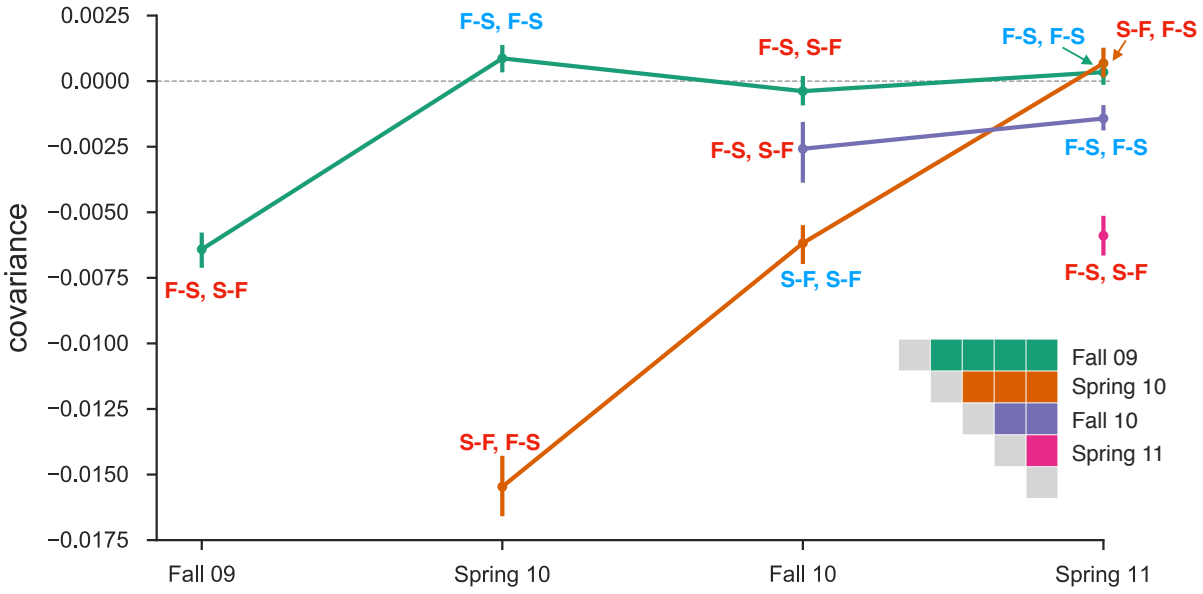

Figure 3.11: Temporal covariances from the Bergland et al. (2014) study, from varying reference generations (e.g. rows along the temporal covariance matrix). Each covariance is labeled indicating whether the covariance is between two like seasonal transitions (e.g. the covariance between allele frequency changes from fall to spring in one year, and fall to spring in another or two dislike seasons (e.g. the covariance between fall to spring in one year, and spring to fall in another year). Covariances between like transitions are expected to be positive when there is a genome-wide effect of fluctuating selection (and these labels are colored blue), while covariances between dislike transitions are expected to be negative (and these labels are colored red). 95% confidence intervals were constructed by a block-bootstrapping procedure where the blocks are megabase tiles.

Bibliography

Aguade, M, N Miyashita, and C H Langley (1989). "Reduced variation in the yellow-achaete-scute region in natural populations of Drosophila melanogaster". en. In: *Genetics* 122.3, pp. 607–615.

Andersen, Erik C et al. (2012). "Chromosome-scale selective sweeps shape Caenorhabditis elegans genomic diversity". en. In: *Nat. Genet.* 44.3, pp. 285–290.

Baca, Mateusz, Karolina Doan, Maciej Sobczyk, Anna Stankovic, and Piotr Węgleński (2012). "Ancient DNA reveals kinship burial patterns of a pre-Columbian Andean community". In: *BMC Genetics* 13.1, p. 1.

Balding, David J and Richard A Nichols (1994). "DNA profile match probability calculation: how to allow for population stratification, relatedness, database selection and single bands". In: *Forensic Science International* 64.2-3, pp. 125–140.

Baldwin-Brown, J G, A D Long, and K R Thornton (2014). "The Power to Detect Quantitative Trait Loci Using Resequenced, Experimentally Evolved Populations of Diploid, Sexual Organisms". In: *Mol. Biol. Evol.* 31.4, pp. 1040–1055.

Barghi, Neda et al. (2019). "Genetic redundancy fuels polygenic adaptation in Drosophila". en. In: *PLoS Biol.* 17.2, e3000128.

Barton, N H (2000). "Genetic hitchhiking". In: *Proceedings of the Royal Society of London B: Biological Sciences* 355.1403, pp. 1553–1562.

Barton, N H and Sarah P Otto (2005). "Evolution of recombination due to random drift". en. In: *Genetics* 169.4, pp. 2353–2370.

Barton, N H and M Turelli (1987). "Adaptive landscapes, genetic distance and the evolution of quantitative characters". en. In: *Genet. Res.* 49.2, pp. 157–173.

— (1991). "Natural and sexual selection on many loci". In: *Genetics* 127.1, pp. 229–255.

Barton, Nicholas H and Alison M Etheridge (2011). "The Relation Between Reproductive Value and Genetic Contribution". In: *Genetics* 188.4, pp. 953–973.

Basin, S. L. (1963). "The Fibonacci sequence as it appears in nature". In: *Fibonacci Quarterly* 1.1, pp. 53–56.

Baym, Michael et al. (2016). "Spatiotemporal microbial evolution on antibiotic landscapes". en. In: *Science* 353.6304, pp. 1147–1151.

Begun, D J and C F Aquadro (1992). "Levels of naturally occurring DNA polymorphism correlate with recombination rates in D. melanogaster". en. In: *Nature* 356.6369, pp. 519–520.

Begun, David J et al. (2007). "Population genomics: whole-genome analysis of polymorphism and divergence in Drosophila simulans". en. In: *PLoS Biol.* 5.11, e310.

Beissinger, Timothy M et al. (2016). "Recent demography drives changes in linked selection across the maize genome". en. In: *Nat Plants* 2, p. 16084.

Belin, Thomas R, David W Gjertson, and Ming-Yi Hu (1997). "Summarizing DNA evidence when relatives are possible suspects". In: *Journal of the American Statistical Association* 92.438, pp. 706–716.

Benjamini, Yoav and Yosef Hochberg (1995). "Controlling the False Discovery Rate: A Practical and Powerful Approach to Multiple Testing". In: *J. R. Stat. Soc. Series B Stat. Methodol.* 57.1, pp. 289–300.

Bennett, A F, K M Dao, and R E Lenski (1990). "Rapid evolution in response to high-temperature selection". en. In: *Nature* 346.6279, pp. 79–81.

Berg, Jeremy J and Graham Coop (2015). "A Coalescent Model for a Sweep of a Unique Standing Variant". en. In: *Genetics* 201.2, pp. 707–725.

Bergland, Alan O, Emily L Behrman, Katherine R O'Brien, Paul S Schmidt, and Dmitri A Petrov (2014). "Genomic Evidence of Rapid and Stable Adaptive Oscillations over Seasonal Time Scales in Drosophila". In: *PLoS Genet.* 10.11, e1004775–19.

Bhatia, Gaurav, Nick Patterson, Sriram Sankararaman, and Alkes L Price (2013). "Estimating and interpreting FST: the impact of rare variants". en. In: *Genome Res.* 23.9, pp. 1514–1521.

Bryc, Katarzyna et al. (2010). "Genome-wide patterns of population structure and admixture in West Africans and African Americans". In: *Proceedings of the National Academy of Sciences* 107.2, pp. 786–791.
Buffalo, Vince and Graham Coop (2019). "The Linked Selection Signature of Rapid Adaptation in Temporal Genomic Data". en.
Bulik-Sullivan, Brendan K et al. (2015). "LD Score regression distinguishes confounding from polygenicity in genome-wide association studies". en. In: *Nat. Genet.* 47.3, pp. 291–295.
Bulmer, M G (1971). "The Effect of Selection on Genetic Variability". In: *Am. Nat.* 105.943, pp. 201–211.
Bulmer, Michael George (1980). *The Mathematical Theory of Quantitative Genetics*. Clarendon Press.
Bürger, R (2000). *The Mathematical Theory of Selection, Recombination, and Mutation*. John Wiley & Sons.
Burke, Molly K et al. (2010). "Genome-wide analysis of a long-term evolution experiment with Drosophila". In: *Nature* 467.7315, pp. 587–590.
Burri, Reto (2017). "Interpreting differentiation landscapes in the light of long-term linked selection: Differentiation And Long-Term Linked Selection". In: *Evolution Letters* 1.3, pp. 118–131.
Burt, Austin (1995). "The Evolution of Fitness". en. In: *Evolution* 49.1, pp. 1–8.
Bustamante, C D and S Ramachandran (2009). "Evaluating signatures of sex-specific processes in the human genome". In: *Nature Genetics* 41.1, pp. 8–10.
Cannings, C (1974). "The latent roots of certain Markov chains arising in genetics: a new approach, I. Haploid models". In: *Adv. Appl. Probab.*, pp. 260–290.
Castro, João Pl et al. (2019). "An integrative genomic analysis of the Longshanks selection experiment for longer limbs in mice". en. In: *Elife* 8.
Chang, Joseph T (1999). "Recent common ancestors of all present-day individuals". In: *Advances in Applied Probability*, pp. 1002–1026.
Charlesworth, Brian (2009). "Fundamental concepts in genetics: effective population size and patterns of molecular evolution and variation". In: *Nature Publishing Group* 10.3, pp. 195–205.
— (2015). "Causes of natural variation in fitness: evidence from studies of Drosophila populations". en. In: *Proc. Natl. Acad. Sci. U. S. A.* 112.6, pp. 1662–1669.
Charlesworth, Brian, M T Morgan, and D Charlesworth (1993). "The effect of deleterious mutations on neutral molecular variation". In: *Genetics* 134.4, pp. 1289–1303.
Chevin, Luis-Miguel and Frédéric Hospital (2008). "Selective sweep at a quantitative trait locus in the presence of background genetic variation". en. In: *Genetics* 180.3, pp. 1645–1660.
Christensen, Ronald (2011). *Plane Answers to Complex Questions | SpringerLink*. Springer Science & Business Media.
Coop, Graham (2016). *Does linked selection explain the narrow range of genetic diversity across species?* Tech. rep. Cold Spring Harbor Labs Journals.
Coop, Graham and Peter Ralph (2012). "Patterns of neutral diversity under general models of selective sweeps". In: *Genetics* 192.1, pp. 205–224.
Corbett-Detig, Russell B, Daniel L Hartl, and Timothy B Sackton (2015). "Natural Selection Constrains Neutral Diversity across A Wide Range of Species". In: *PLoS Biol.* 13.4, e1002112–25.
Cox, Allison et al. (2009). "A new standard genetic map for the laboratory mouse". en. In: *Genetics* 182.4, pp. 1335–1344.
Crouch, Daniel J M (2017). "Statistical aspects of evolution under natural selection, with implications for the advantage of sexual reproduction". en. In: *J. Theor. Biol.* 431, pp. 79–86.
Crow, James Franklin and Motoo Kimura (1970). *An Introduction to Population Genetics Theory*. New York, Evanston and London: Harper & Row, Publishers.

Cutter, A D and J Y Choi (2010). "Natural selection shapes nucleotide polymorphism across the genome of the nematode Caenorhabditis briggsae". In: *Genome Res.* 20.8, pp. 1103–1111.
Cutter, Asher D and Bret A Payseur (2003). "Selection at linked sites in the partial selfer Caenorhabditis elegans". en. In: *Mol. Biol. Evol.* 20.5, pp. 665–673.
— (2013). "Genomic signatures of selection at linked sites: unifying the disparity among species". In: *Nature Publishing Group* 14.4, pp. 262–274.
Davison, A C and D V Hinkley (2013). *Bootstrap Methods and Their Application*. New York, NY, USA: Cambridge University Press.
Dobzhansky, Theodosius (1943). "Genetics of Natural Populations IX. Temporal Changes in the Composition of Populations of Drosophila Pseudoobscura". In: *Genetics* 28.2, pp. 162–186.
— (1971). "Evolutionary Oscillations in Drosophila pseudoobscura". In: *Ecological Genetics and Evolution*. Boston, MA: Springer US, pp. 109–133.
Donnelly, K P (1983). "The probability that related individuals share some section of genome identical by descent". In: *Theoretical Population Biology* 23.1, pp. 34–63.
Durand, Eric Y, Chuong B Do, Joanna L Mountain, and J. Michael Macpherson (2014). "Ancestry Composition: A Novel, Efficient Pipeline for Ancestry Deconvolution". In: *bioRxiv*. DOI: 10.1101/010512. eprint: http://biorxiv.org/content/early/2014/10/18/010512.full.pdf. URL: http://biorxiv.org/content/early/2014/10/18/010512.
Edmonds, Christopher A, Anita S Lillie, and L Luca Cavalli-Sforza (2004). "Mutations arising in the wave front of an expanding population". en. In: *Proc. Natl. Acad. Sci. U. S. A.* 101.4, pp. 975–979.
Elyashiv, Eyal et al. (2016). "A Genomic Map of the Effects of Linked Selection in Drosophila". In: *PLoS Genet.* 12.8, e1006130–24.
Endler, John A (1986). *Natural selection in the wild*. Princeton University Press.
Epstein, M P, W L Duren, and M Boehnke (2000). "Improved inference of relationship for pairs of individuals". In: *The American Journal of Human Genetics* 67.5, pp. 1219–1231.
Excoffier, Laurent and Nicolas Ray (2008). "Surfing during population expansions promotes genetic revolutions and structuration". en. In: *Trends Ecol. Evol.* 23.7, pp. 347–351.
Feder, A F, S Kryazhimskiy, and J B Plotkin (2014). "Identifying signatures of selection in genetic time series". In: *Genetics*.
Feller, Willliam (1950). *An Introduction to Probability Theory and its Applications*. Vol. 1. John Wiley & Sons.
Fisher, R A and E B Ford (1947). "The spread of a gene in natural conditions in a colony of the moth Panaxia dominula". In: *Heredity* 1, pp. 143–174.
Fisher, Ronald Aylmer et al. (1949). "The theory of inbreeding." In: *Edinburgh: Oliver & Boyd.*
— (1954). "A fuller theory of 'junctions' in inbreeding". In: *Heredity* 8, pp. 187–197.
Fox, M, R Sear, and J Beise (2009). "Grandma plays favourites: X-chromosome relatedness and sex-specific childhood mortality". In: *Proceedings of the Royal Society B*.
Franks, Steven J, Sheina Sim, and Arthur E Weis (2007). "Rapid evolution of flowering time by an annual plant in response to a climate fluctuation". In: *Proceedings of the National Academy of Sciences* 104.4, pp. 1278–1282.
Franssen, S U, R Kofler, and C Schlötterer (2017). "Uncovering the genetic signature of quantitative trait evolution with replicated time series data". en. In: *Heredity* 118.1, pp. 42–51.
Fu, Qiaomei et al. (2015). "An early modern human from Romania with a recent Neanderthal ancestor". In: *Nature* 524.7564, pp. 216–219.
Fu, Qiaomei et al. (2016). "The genetic history of Ice Age Europe". en. In: *Nature* 534.7606, pp. 200–205.

Gillespie, J H (2000). "Genetic drift in an infinite population. The pseudohitchhiking model". en. In: *Genetics* 155.2, pp. 909–919.
Gillespie, John H (2001). "Is the population size of a species relevant to its evolution?" In: *Evolution* 55.11, pp. 2161–2169.
Gingerich, P D (1983). "Rates of evolution: effects of time and temporal scaling". en. In: *Science* 222.4620, pp. 159–161.
Glaubitz, Jeffrey C, O Eugene Rhodes, and J Andrew DeWoody (2003). "Prospects for inferring pairwise relationships with single nucleotide polymorphisms". In: *Molecular Ecology* 12.4, pp. 1039–1047.
Goldberg, Amy and Noah A Rosenberg (2015). "Beyond 2/3 and 1/3: The Complex Signatures of Sex-Biased Admixture on the X Chromosome." In: *Genetics* 201.1, pp. 263–279.
Good, Benjamin H, Michael J McDonald, Jeffrey E Barrick, Richard E Lenski, and Michael M Desai (2017). "The dynamics of molecular evolution over 60,000 generations". en. In: *Nature* 551.7678, pp. 45–50.
Good, Benjamin H, Aleksandra M Walczak, Richard A Neher, and Michael M Desai (2014). "Genetic Diversity in the Interference Selection Limit". In: *PLoS Genet.* 10.3, e1004222.
Grant, Peter R and B Rosemary Grant (2006). "Evolution of Character Displacement in Darwin's Finches". In: *Science* 313.5784, pp. 224–226.
— (2011). "Causes of lifetime fitness of Darwin's finches in a fluctuating environment". en. In: *Proc. Natl. Acad. Sci. U. S. A.* 108.2, pp. 674–679.
Gravel, Simon (2012). "Population genetics models of local ancestry." In: *Genetics* 191.2, pp. 607–619.
Gusev, Alexander et al. (2009). "Whole population, genome-wide mapping of hidden relatedness". In: *Genome Research* 19.2, pp. 318–326.
Haak, Wolfgang et al. (2008). "Ancient DNA, Strontium isotopes, and osteological analyses shed light on social and kinship organization of the Later Stone Age". In: *Proceedings of the National Academy of Sciences* 105.47, pp. 18226–18231.
Haldane, J B S (1919). "The combination of linkage values and the calculation of distances between the loci of linked factors". In: *J. Genet.* 8.29, pp. 299–309.
Hallatschek, Oskar and David R Nelson (2008). "Gene surfing in expanding populations". en. In: *Theor. Popul. Biol.* 73.1, pp. 158–170.
Hansen, Lars Peter (1982). "Large Sample Properties of Generalized Method of Moments Estimators". In: *Econometrica* 50.4, pp. 1029–1054.
Hassold, TJ, SL Sherman, D Pettay, DC Page, and PA Jacobs (1991). "XY chromosome nondisjunction in man is associated with diminished recombination in the pseudoautosomal region." In: *American journal of human genetics* 49.2, p. 253.
Hendry, A P and M T Kinnison (1999). "Perspective: the pace of modern life: measuring rates of contemporary microevolution". In: *Evolution* 53.6, p. 1637.
Hendry, Andrew P, Daniel J Schoen, Matthew E Wolak, and Jane M Reid (2018). "The Contemporary Evolution of Fitness". en. In: *Annu. Rev. Ecol. Evol. Syst.*
Henn, Brenna M et al. (2012). "Cryptic Distant Relatives Are Common in Both Isolated and Cosmopolitan Genetic Samples". In: *PLoS One* 7.4, e34267–13.
Hermisson, J and P S Pennings (2005). "Soft sweeps: Molecular population genetics of adaptation from standing genetic variation". In: *Genetics*.
Hernandez, R D, J L Kelley, E Elyashiv, and S C Melton (2011). "Classic selective sweeps were rare in recent human evolution". In: *Science*.
Heyer, Evelyne, Alexandre Sibert, and Frédéric Austerlitz (2005). "Cultural transmission of fitness: genes take the fast lane". en. In: *Trends Genet.* 21.4, pp. 234–239.
Hill, W G and Alan Robertson (1966). "The effect of linkage on limits to artificial selection". In: *Genet. Res.* 8.03, pp. 269–294.
— (1968). "Linkage disequilibrium in finite populations". In: *Theor. Appl. Genet.* 38.6, pp. 226–231.

Höllinger, Ilse, Pleuni S Pennings, and Joachim Hermisson (2019). "Polygenic adaptation: From sweeps to subtle frequency shifts". en. In: *PLoS Genet.* 15.3, e1008035.
Hudson, R R (1994). "How can the low levels of DNA sequence variation in regions of the drosophila genome with low recombination rates be explained?" en. In: *Proc. Natl. Acad. Sci. U. S. A.* 91.15, pp. 6815–6818.
Hudson, R R and N L Kaplan (1995). "Deleterious background selection with recombination". In: *Genetics* 141.4, pp. 1605–1617.
Huff, Chad D et al. (2011). "Maximum-likelihood estimation of recent shared ancestry (ERSA)". In: *Genome Research* 21.5, pp. 768–774.
Ihaka, Ross, Paul Murrell, Kurt Hornik, and Achim Zeileis (2008). "Colorspace: color space manipulation". In: *R package version*, pp. 1–.
J A Woolliams, N R Wray, R Thompson (2008). "Prediction of long-term contributions and inbreeding in populations undergoing mass selection". In: 62, pp. 231–242.
Jain, Kavita and Wolfgang Stephan (2015). "Response of Polygenic Traits Under Stabilizing Selection and Mutation When Loci Have Unequal Effects". en. In: *G3* 5.6, pp. 1065–1074.
— (2017). "Rapid Adaptation of a Polygenic Trait After a Sudden Environmental Shift". In: *Genetics* 206.1, pp. 389–406.
Johansson, Anna M, Mats E Pettersson, Paul B Siegel, and Örjan Carlborg (2010). "Genome-Wide Effects of Long-Term Divergent Selection". In: *PLoS Genet.* 6.11, e1001188–12.
Jónás, Á, T Taus, C Kosiol, and C Schlötterer (2016). "Estimating the Effective Population Size from Temporal Allele Frequency Changes in Experimental Evolution". In: *Genetics*.
Kaplan, N L, R R Hudson, and C H Langley (1989). "The" hitchhiking effect" revisited". In: *Genetics*.
Keinan, Alon and David Reich (2010). "Human population differentiation is strongly correlated with local recombination rate". en. In: *PLoS Genet.* 6.3, e1000886.
Kelleher, Jerome, Alison M Etheridge, and Gilean McVean (2016). "Efficient Coalescent Simulation and Genealogical Analysis for Large Sample Sizes". en. In: *PLoS Comput. Biol.* 12.5, e1004842.
Kelly, John K and Kimberly A Hughes (2019). "Pervasive Linked Selection and Intermediate-Frequency Alleles Are Implicated in an Evolve-and-Resequencing Experiment of Drosophila simulans". en. In: *Genetics* 211.3, pp. 943–961.
Kendall, Maurice, Alan Stuart, J Keith Ord, and A O'Hagan (1994). "Kendall's advanced theory of statistics, volume 1: Distribution theory". In: *Arnold, sixth edition edition*.
Kettlewell, H B D (1958). *A survey of the frequencies of Biston betularia (L.)(Lep.) and its melanic forms in Great Britain*. Vol. 12. Heredity. Nature Publishing Group.
— (1961). "The phenomenon of industrial melanism in Lepidoptera". In: *Annu. Rev. Entomol.*
Keyser-Tracqui, Christine, Eric Crubezy, and Bertrand Ludes (2003). "Nuclear and mitochondrial DNA analysis of a 2,000-year-old necropolis in the Egyin Gol Valley of Mongolia". In: *The American Journal of Human Genetics* 73.2, pp. 247–260.
Kinnison, M T and A P Hendry (2001). "The pace of modern life II: from rates of contemporary microevolution to pattern and process". en. In: *Genetica* 112-113, pp. 145–164.
Kirkpatrick, Mark, Toby Johnson, and Nick Barton (2002). "General Models of Multilocus Evolution". In: *Genetics* 161.4, pp. 1727–1750.
Kolaczkowski, Bryan, Andrew D Kern, Alisha K Holloway, and David J Begun (2011). "Genomic differentiation between temperate and tropical Australian populations of Drosophila melanogaster". en. In: *Genetics* 187.1, pp. 245–260.
Koller, P Ch and CD Darlington (1934). "The genetical and mechanical properties of the sex-chromosomes". In: *Journal of Genetics* 29.2, pp. 159–173.

Kopp, Michael and Joachim Hermisson (2007). "Adaptation of a quantitative trait to a moving optimum". In: *Genetics* 176.1, pp. 715–719.
— (2009a). "The genetic basis of phenotypic adaptation I: fixation of beneficial mutations in the moving optimum model". en. In: *Genetics* 182.1, pp. 233–249.
— (2009b). "The genetic basis of phenotypic adaptation II: the distribution of adaptive substitutions in the moving optimum model". en. In: *Genetics* 183.4, pp. 1453–1476.
Krimbas, C B and S Tsakas (1971). "The genetics of Dacus oleae. V. Changes of esterase polymorphism in a natural population following insecticide control-selection or drift?" In: *Evolution* 25.3, p. 454.
Kruuk, Loeske E B (2004). "Estimating genetic parameters in natural populations using the 'animal model'". In: *Philos. Trans. R. Soc. Lond. B Biol. Sci.* 359.1446, pp. 873–890.
Kruuk, Loeske E B et al. (2000). "Heritability of fitness in a wild mammal population". In: *Proceedings of the National Academy of Sciences* 97.2, pp. 698–703.
Lande, R (1979). "Quantitative genetic analysis of multivariate evolution, applied to brain: body size allometry". In: *Evolution* 33.1, p. 402.
Laughlin, Harry H (1920). "Calculating Ancestral Influence in Man: A Mathematical Measure of the Facts of Bisexual Heredity". In: *Genetics* 5.5, p. 435.
Leffler, Ellen M et al. (2012). "Revisiting an Old Riddle: What Determines Genetic Diversity Levels within Species?" In: *PLoS Biol.* 10.9, e1001388–9.
Lewontin, Richard C (1974). *The genetic basis of evolutionary change*. Vol. 560. Columbia University Press New York.
Liang, Mason and Rasmus Nielsen (2014). "The lengths of admixture tracts". In: *Genetics* 197.3, pp. 953–967.
Lynch, Michael, Bruce Walsh, et al. (1998). *Genetics and analysis of quantitative traits*. Vol. 1. Sinauer Sunderland, MA.
Machado, Heather E et al. (2018). "Broad geographic sampling reveals predictable and pervasive seasonal adaptation in Drosophila". en.
Malaspinas, A S, O Malaspinas, and S N Evans (2012). "Estimating allele age and selection coefficient from time-serial data". In: *Genetics*.
Mathieson, I and G McVean (2013). "Estimating selection coefficients in spatially structured populations from time series data of allele frequencies". In: *Genetics*.
Mathieson, Iain et al. (2015). "Genome-wide patterns of selection in 230 ancient Eurasians". In: *Nature* 528.7583, pp. 499–503.
Maynard Smith, John and John Haigh (1974). "The hitch-hiking effect of a favourable gene". In: *Genet. Res.* 23.01, pp. 23–35.
McVicker, Graham, David Gordon, Colleen Davis, and Phil Green (2009). "Widespread Genomic Signatures of Natural Selection in Hominid Evolution". In: *PLoS Genet.* 5.5, e1000471–16.
Messer, Philipp W, Stephen P Ellner, and Nelson G Hairston Jr (2016). "Can Population Genetics Adapt to Rapid Evolution?" In: *Trends Genet.*, pp. 1–11.
Morley, F H W (1954). "Selection for economic characters in Australian Merino sheep". In: *Aust. J. Agric. Res.* 5.2, pp. 305–316.
Mousseau, T A and D A Roff (1987). "Natural selection and the heritability of fitness components". In: *Heredity*.
Mueller, L D, B A Wilcox, P R Ehrlich, and D G Heckel (1985a). "A direct assessment of the role of genetic drift in determining allele frequency variation in populations of Euphydryas editha". In: *Heredity*.
Mueller, Laurence D, Lorraine G Barr, and Francisco J Ayala (1985b). "Natural selection vs. random drift: evidence from temporal variation in allele frequencies in nature". In: *Genetics* 111.3, pp. 517–554.
Nachman, Michael W and Bret A Payseur (2012). "Recombination rate variation and speciation: theoretical predictions and empirical results from rabbits and mice". en. In: *Philos. Trans. R. Soc. Lond. B Biol. Sci.* 367.1587, pp. 409–421.

Nair, Shalini et al. (2003). "A selective sweep driven by pyrimethamine treatment in southeast asian malaria parasites". In: *Mol. Biol. Evol.* 20.9, pp. 1526–1536.
Neher, R A and B I Shraiman (2011). "Genetic draft and quasi-neutrality in large facultatively sexual populations". en. In: *Genetics* 188.4, pp. 975–996.
Neher, Richard A (2013). "Genetic Draft, Selective Interference, and Population Genetics of Rapid Adaptation". In: *Annu. Rev. Ecol. Evol. Syst.* 44.1, pp. 195–215.
Nei, Masatoshi (1987). *Molecular Evolutionary Genetics*. en. Columbia University Press.
Nei, Masatoshi and Fumio Tajima (1981). "Genetic Drift And Estimation Of Effective Population Size". In: *Genetics* 98.3, pp. 625–640.
Nordborg, Magnus, Brian Charlesworth, and Deborah Charlesworth (1996). "The effect of recombination on background selection*". In: *Genet. Res.* 67.02, pp. 159–174.
Nordborg, Magnus et al. (2005a). "The Pattern of Polymorphism in Arabidopsis thaliana". In: *PLoS Biol.* 3.7, e196–11.
— (2005b). "The pattern of polymorphism in Arabidopsis thaliana". en. In: *PLoS Biol.* 3.7, e196.
Nuzhdin, Sergey V and Thomas L Turner (2013). "Promises and limitations of hitchhiking mapping". en. In: *Curr. Opin. Genet. Dev.* 23.6, pp. 694–699.
Ohta, T and M Kimura (1969). "Linkage disequilibrium at steady state determined by random genetic drift and recurrent mutation". en. In: *Genetics* 63.1, pp. 229–238.
Orozco-terWengel, Pablo et al. (2012). "Adaptation of Drosophilato a novel laboratory environment reveals temporally heterogeneous trajectories of selected alleles". In: *Mol. Ecol.* 21.20, pp. 4931–4941.
Palamara, Pier Francesco, Todd Lencz, Ariel Darvasi, and Itsik Pe'er (2012). "Length distributions of identity by descent reveal fine-scale demographic history". In: *The American Journal of Human Genetics* 91.5, pp. 809–822.
Pennings, Pleuni S and Joachim Hermisson (2006). "Soft Sweeps II—Molecular Population Genetics of Adaptation from Recurrent Mutation or Migration". In: *Mol. Biol. Evol.* 23.5, pp. 1076–1084.
Pinto, Nádia, Leonor Gusmão, and António Amorim (2011). "X-chromosome markers in kinship testing: a generalisation of the IBD approach identifying situations where their contribution is crucial". In: *Forensic Science International: Genetics* 5.1, pp. 27–32.
Pinto, Nádia, Pedro V Silva, and António Amorim (2012). "A general method to assess the utility of the X-chromosomal markers in kinship testing". In: *Forensic Science International: Genetics* 6.2, pp. 198–207.
Pollak, Edward (1983). "A New Method For Estimating The Effective Population Size From Allele Frequency Changes". In: *Genetics* 104.3, pp. 531–548.
Pool, John E and Rasmus Nielsen (2007). "Population size changes reshape genomic patterns of diversity". In: *Evolution* 61.12, pp. 3001–3006.
— (2009). "Inference of historical changes in migration rate from the lengths of migrant tracts". In: *Genetics* 181.2, pp. 711–719.
Price, G R (1970). "Selection and covariance". In: *Nature*.
Pritchard, Jonathan K, Joseph K Pickrell, and Graham Coop (2010). "The Genetics of Human Adaptation: Hard Review Sweeps, Soft Sweeps, and Polygenic Adaptation". In: *Curr. Biol.* 20.4, R208–R215.
Prout, T (1954). "Genetic Drift in Irradiated Experimental Populations of Drosophila Melanogaster". en. In: *Genetics* 39.4, pp. 529–545.
Przeworski, Molly, Graham Coop, and Jeffrey D Wall (2005). "The signature of positive selection on standing genetic variation". en. In: *Evolution* 59.11, pp. 2312–2323.
R Core Team (2015). *R: A Language and Environment for Statistical Computing*. R Foundation for Statistical Computing. Vienna, Austria. URL: `https://www.R-project.org/`.
Rajpurohit, Subhash et al. (2018). "Spatiotemporal dynamics and genome-wide association analysis of desiccation tolerance in Drosophila melanogaster". In: *Mol. Ecol.*

Ralph, Peter and Graham Coop (2013). "The Geography of Recent Genetic Ancestry across Europe". In: *PLoS Biology* 11.5, e1001555. DOI: 10.1371/journal.pbio.1001555. URL: http://dx.doi.org/10.1371%2Fjournal.pbio.1001555.

Ram, Karthik and Hadley Wickham (2015). *wesanderson: A Wes Anderson Palette Generator*. R package version 0.3.2. URL: http://CRAN.R-project.org/package=wesanderson.

Ramachandran, Sohini, Noah A Rosenberg, Marcus W Feldman, and John Wakeley (2008). "Population differentiation and migration: coalescence times in a two-sex island model for autosomal and X-linked loci". In: *Theoretical Population Biology* 74.4, pp. 291–301.

Ramachandran, Sohini, Noah A Rosenberg, Lev A Zhivotovsky, and Marcus W Feldman (2004). "Robustness of the inference of human population structure: a comparison of X-chromosomal and autosomal microsatellites". In: *Human genomics* 1.2, p. 1.

Reznick, David N, Frank H Shaw, F Helen Rodd, and Ruth G Shaw (1997). "Evaluation of the Rate of Evolution in Natural Populations of Guppies (Poecilia reticulata)". In: *Science* 275.5308, pp. 1934–1937.

Rice, William R, Sergey Gavrilets, and Urban Friberg (2008). "Sexually antagonistic "zygotic drive" of the sex chromosomes". In: *PLoS Genetics* 4.12, e1000313.

Robertson, A (1970). "A Theory of Limits in Artificial Selection with Many Linked Loci". In: *Mathematical Topics in Population Genetics*. Ed. by Ken-Ichi Kojima. Berlin, Heidelberg: Springer Berlin Heidelberg, pp. 246–288.

Robertson, Alan (1961). "Inbreeding in artificial selection programmes". In: *Genet. Res.* 2.02, pp. 189–194.

— (1966). "A mathematical model of the culling process in dairy cattle". In: *Anim. Sci.* 8.1, pp. 95–108.

— (1976). "Artificial selection with a large number of linked loci". In: *Proceedings of the International Conference on Quantitative Genetics*. Ed. by Edward Pollak, Oscar Kempthorne, and Theodore B Bailey. Iowa State University Press, pp. 307–322.

Rockman, Matthew V, Sonja S Skrovanek, and Leonid Kruglyak (2010). "Selection at linked sites shapes heritable phenotypic variation in C. elegans". en. In: *Science* 330.6002, pp. 372–376.

Rohde, DLT, S Olson, and J T Chang (2004). "Modelling the recent common ancestry of all living humans". In: *Nature*.

Rosenberg, Noah A. (2016). "Admixture Models and the Breeding Systems of H. S. Jennings: A GENETICS Connection". In: *Genetics* 202.1, pp. 9–13. ISSN: 0016-6731. DOI: 10.1534/genetics.115.181057. eprint: http://genetics.org/content/202/1/9.full.pdf. URL: http://genetics.org/content/202/1/9.

Rosser, Z H, P Balaresque, and M A Jobling (2009). "Gene conversion between the X chromosome and the male-specific region of the Y chromosome at a translocation hotspot". In: *The American Journal of Human Genetics*.

Rossum, Guido (1995). *Python Reference Manual*. Tech. rep. Amsterdam, The Netherlands, The Netherlands.

Royal, Charmaine D et al. (2010). "Inferring genetic ancestry: opportunities, challenges, and implications". In: *The American Journal of Human Genetics* 86.5, pp. 661–673.

Santiago, Enrique and Armando Caballero (1995). "Effective size of populations under selection". In: *Genetics* 139.2, pp. 1013–1030.

— (1998). "Effective Size and Polymorphism of Linked Neutral Loci in Populations Under Directional Selection". In: *Genetics* 149.4, pp. 2105–2117.

Sattath, Shmuel, Eyal Elyashiv, Oren Kolodny, Yosef Rinott, and Guy Sella (2011). "Pervasive adaptive protein evolution apparent in diversity patterns around amino acid substitutions in Drosophila simulans". en. In: *PLoS Genet.* 7.2, e1001302.

Schmid, Karl J, Sebastian Ramos-Onsins, Henriette Ringys-Beckstein, Bernd Weisshaar, and Thomas Mitchell-Olds (2005). "A multilocus sequence survey in Arabidopsis

thaliana reveals a genome-wide departure from a neutral model of DNA sequence polymorphism". en. In: *Genetics* 169.3, pp. 1601–1615.
Schrider, Daniel R and Andrew D Kern (2017). "Soft Sweeps Are the Dominant Mode of Adaptation in the Human Genome". en. In: *Mol. Biol. Evol.* 34.8, pp. 1863–1877.
Sella, Guy, Dmitri A Petrov, Molly Przeworski, and Peter Andolfatto (2009). "Pervasive Natural Selection in the Drosophila Genome?" In: *PLoS Genet.* 5.6, e1000495.
Shaw, R G and F H Shaw (2013). "Quantitative genetic study of the adaptive process". In: *Heredity* 112.1, pp. 13–20.
Shringarpure, Suyash S., Carlos D. Bustamante, Kenneth L. Lange, and David H. Alexander (2016). "Efficient analysis of large datasets and sex bias with ADMIXTURE". In: *bioRxiv*. DOI: 10.1101/039347. eprint: http://biorxiv.org/content/early/2016/02/10/039347.full.pdf. URL: http://biorxiv.org/content/early/2016/02/10/039347.
Signor, Sarah A, Felicia N New, and Sergey Nuzhdin (2018). "A Large Panel of Drosophila simulans Reveals an Abundance of Common Variants". en. In: *Genome Biol. Evol.* 10.1, pp. 189–206.
Simson, Robert (1753). "An Explication of an Obscure Passage in Albert Girard's Commentary upon Simon Stevin's Works (Vide Les Oeuvres Mathem. de Simon Stevin, à Leyde, 1634, p. 169, 170); By Mr. Simson, Professor of Mathematics at the University of Glasgow: Communicated by the Right Honourable Philip Earl Stanhope". In: *Philosophical Transactions (1683-1775)*, pp. 368–377.
Sjerps, Marjan and Ate D Kloosterman (1999). "On the consequences of DNA profile mismatches for close relatives of an excluded suspect". In: *International Journal of Legal Medicine* 112.3, pp. 176–180.
Sloane, N.J.A. (2010). "Online Encyclopaedia of Integer Sequences". In: *Published electronically at http://www.oeis.org*.
Stephan, W, The Wiehe, and M W Lenz (1992). "The effect of strongly selected substitutions on neutral polymorphism: analytical results based on diffusion theory". In: *Theor. Popul. Biol.*
Stephan, Wolfgang, Yun S Song, and Charles H Langley (2006). "The hitchhiking effect on linkage disequilibrium between linked neutral loci". en. In: *Genetics* 172.4, pp. 2647–2663.
Sun, Lei, Kenneth Wilder, and Mary Sara McPeek (2002). "Enhanced pedigree error detection". In: *Human Heredity* 54.2, pp. 99–110.
Sved, J A (1971). *Linkage Disequilibrium and Homozygosity of Chromosome Segments in Finite Populations*. Vol. 2. Theoretical Population Biology. Elsevier.
Teotónio, Henrique, Ivo M Chelo, Martina Bradić, Michael R Rose, and Anthony D Long (2009). "Experimental evolution reveals natural selection on standing genetic variation". In: *Nat. Genet.* 41.2, pp. 251–257.
Teplitsky, Céline, James A Mills, John W Yarrall, and Juha Merilä (2009). "Heritability of fitness components in a wild bird population". en. In: *Evolution* 63.3, pp. 716–726.
Terhorst, Jonathan, Christian Schlötterer, and Yun S Song (2015). "Multi-locus Analysis of Genomic Time Series Data from Experimental Evolution". In: *PLoS Genet.* 11.4, e1005069–29.
Therkildsen, Nina O et al. (2019). "Contrasting genomic shifts underlie parallel phenotypic evolution in response to fishing". en. In: *Science* 365.6452, pp. 487–490.
Thomas, Alun, Nicola J Camp, James M Farnham, Kristina Allen-Brady, and Lisa A Cannon-Albright (2008). "Shared genomic segment analysis. Mapping disease predisposition genes in extended pedigrees using SNP genotype assays". In: *Annals of Human Genetics* 72.2, pp. 279–287.
Thomas, Alun, Mark H Skolnick, and Cathryn M Lewis (1994). "Genomic mismatch scanning in pedigrees". In: *Mathematical Medicine and Biology* 11.1, pp. 1–16.
Thompson, Elizabeth A (2013). "Identity by descent: variation in meiosis, across genomes, and in populations". In: *Genetics* 194.2, pp. 301–326.

Thornton, Kevin R (2018). "Polygenic adaptation to an environmental shift: temporal dynamics of variation under Gaussian stabilizing selection and additive effects on a single trait".
Tomoko Ohta, Motoo Kimura (1971). "Linkage Disequilibrium between Two Segregating Nucleotide Sites under the Steady Flux of Mutations in a Finite Population". In: *Genetics* 68.4, pp. 571–580.
Turelli, M (1988). *Population genetic models for polygenic variation and evolution*. Proceedings of the Second International Conference On Quantitative Genetics.
Turelli, M and N H Barton (1990). "Dynamics of polygenic characters under selection". In: *Theor. Popul. Biol.* 38.1, pp. 1–57.
— (1994). "Genetic and statistical analyses of strong selection on polygenic traits: what, me normal?" In: *Genetics* 138.3, pp. 913–941.
Turner, T L and P M Miller (2012). "Investigating Natural Variation in Drosophila Courtship Song by the Evolve and Resequence Approach". In: *Genetics* 191.2, pp. 633–642.
Turner, Thomas L, Andrew D Stewart, Andrew T Fields, William R Rice, and Aaron M Tarone (2011). "Population-Based Resequencing of Experimentally Evolved Populations Reveals the Genetic Basis of Body Size Variation in Drosophila melanogaster". In: *PLoS Genet.* 7.3, e1001336–10.
Voight, B F, S Kudaravalli, X Wen, and J K Pritchard (2006). "A map of recent positive selection in the human genome". In: *PLoS Biol.*
Wachter, Kenneth W, Eugene A Hammel, and Peter Laslett (1979). *Statistical Studies of Historical Social Structure*. Academic Press Inc.
Wallace, Bruce (1956). "Studies on irradiated populations ofDrosophila melanogaster". en. In: *J. Genet.* 54.2, pp. 280–293.
Walsh, Bruce and Michael Lynch (2018). *Evolution and Selection of Quantitative Traits*. en. Oxford University Press.
Wang, Jinliang and Michael C Whitlock (2003). "Estimating effective population size and migration rates from genetic samples over space and time". en. In: *Genetics* 163.1, pp. 429–446.
Waples, R S (1989). "A generalized approach for estimating effective population size from temporal changes in allele frequency". In: *Genetics* 121.2, pp. 379–391.
Wasserman, Larry (2006). *All of Nonparametric Statistics*. en. Springer Science & Business Media.
Watterson, G A (1975). "On the number of segregating sites in genetical models without recombination". In: *Theor. Popul. Biol.* 7.2, pp. 256–276.
Weir, Bruce S (1996). *Genetic Data Analysis II: Methods for discrete population genetic data*. Sinauer Associates.
Wickham, Hadley (2009). *ggplot2: Elegant Graphics for Data Analysis*. Springer-Verlag New York. ISBN: 978-0-387-98140-6. URL: http://had.co.nz/ggplot2/book.
— (2016a). *purrr: Functional Programming Tools*. R package version 0.2.0. URL: http://CRAN.R-project.org/package=purrr.
— (2016b). *tidyr: Easily Tidy Data with 'spread()' and 'gather()' Functions*. R package version 0.4.0. URL: http://CRAN.R-project.org/package=tidyr.
Wickham, Hadley and Romain Francois (2015). *dplyr: A Grammar of Data Manipulation*. R package version 0.4.3. URL: http://CRAN.R-project.org/package=dplyr.
Wiehe, T H and W Stephan (1993). "Analysis of a genetic hitchhiking model, and its application to DNA polymorphism data from Drosophila melanogaster". en. In: *Mol. Biol. Evol.* 10.4, pp. 842–854.
Wilf, Herbert S (2013). *generatingfunctionology*. Elsevier.
Williamson, Robert J et al. (2014). "Evidence for widespread positive and negative selection in coding and conserved noncoding regions of Capsella grandiflora". en. In: *PLoS Genet.* 10.9, e1004622.

Wray, Naomi R and Robin Thompson (1990). "Prediction of rates of inbreeding in selected populations". In: *Genet. Res.* 55.01, pp. 41–54.
Wright, Sewall (1922). "Coefficients of inbreeding and relationship". In: *The American Naturalist* 56.645, pp. 330–338.
— (1931). "Evolution in Mendelian populations". In: *Genetics* 16.2, p. 97.
— (1934). "The method of path coefficients". In: *The Annals of Mathematical Statistics* 5.3, pp. 161–215.
— (1938). "Size of population and breeding structure in relation to evolution". In: *Science* 87.2263, pp. 430–431.